2015

Dynamic optimization based reactive power planning for improving short-term voltage performance

Magesh Kumar Paramasivam
Iowa State University

Dynamic optimization based reactive power planning for improving short-term voltage performance

by

Magesh Paramasivam

A dissertation submitted to the graduate faculty

in partial fulfillment of the requirements for the degree of

DOCTOR OF PHILOSOPHY

Major: Electrical Engineering

Program of Study Committee:

Venkataramana Ajjarapu, Major Professor

Ian Dobson

Manimaran Govindarasu

Umesh Vaidya

Lizhi Wang

Iowa State University

Ames, Iowa

2015

TABLE OF CONTENTS

LIST OF TABLES

LIST OF FIGURES

ACKNOWLEDGEMENTS

I would like to express my sincere appreciation and gratitude to my advisor Prof. Venkataramana Ajjarapu for his valuable guidance and support throughout the course of my doctoral studies. His insights and words of encouragement have often inspired and motivated me to do quality research. My deepest gratitude is due to my POS committee members for their valuable time and comments.

I wish to express my special thanks to my parents and brother for their amazing support and sacrifices. Words cannot express how grateful I am to them for all their sacrifices.

A special thanks to my fellow students in the voltage stability group for their discussions and suggestions in preparing this thesis. I would also like to express my thanks to all of my friends at ISU for truly making this whole graduate school experience a memorable one.

ABSTRACT

Short term voltage stability in the form of delayed voltage recovery (FIDVR) poses a significant threat to system stability and reliability. This work examines the voltage instability issue in a power system with dense concentration of induction motor loads and applies dynamic VAR injection as a counter-measure to ensure short term voltage stability following a large disturbance. The dynamic behavior of motor loads, such as decelerating and stalling, is considered as the major cause of FIDVR incidents especially during summer peak load conditions in areas where low inertia single-phase air conditioning (A/C) motors comprise a significant portion of the load. If system dynamics are not taken into account properly, the proposed control solution may be an expensive over design or an under design which is not capable of mitigating FIDVR problems completely. This work aims to provide a comprehensive dynamic VAR planning strategy for handling short term voltage stability problems by proper consideration of system dynamics, multiple contingencies, multiple scenarios and operating conditions. In addition, this approach aims to provide valuable system insights such as behavior of different contingencies and dynamic voltage control areas. Contingencies are clustered together according to their behavioral similarity with respect to voltage performance using an entropy based metric called Kullback-Liebler (KL) measure. Using the information of contingency clusters, a new concept called dynamic voltage control areas is derived. The concept of dynamic voltage control area will address the importance of the location of dynamic reactive reserves. Control vector parameterization (CVP), a dynamic optimization based approach is used to identify the optimal locations and amount of dynamic VARs required to mitigate short term voltage problems. The main idea of CVP approach is to solve the system dynamics separately and utilize the system dynamics results in the constraints evaluation during optimization routine. Also this method is applicable to large scale systems because of the utilization of commercial power system and large scale optimization solvers. Simulations have been carried out on mod-

ified IEEE 162 bus system to show the working of contingency clustering, dynamic voltage control area identification and CVP method for single contingency case. The CVP method has also been tested on a large scale realistic power system to show the scalability of the proposed approach.

CHAPTER 1. OVERVIEW

1.1 Introduction

CIGRE and IEEE task force [1] provided the classification of power system stability as shown in Fig.1.1. Based on the physical nature of the instability, size of the disturbance and time frame of interest the power system stability problem is broadly classified into three groups namely rotor angle stability, frequency stability and voltage stability. Voltage stability is defined as the ability of the system to maintain steady voltages at all buses in the system following a disturbance. Voltage instability could lead to progressive rise or fall of voltages at different buses. Voltage collapse is the process by which the sequence of events accompanying voltage instability leading to a blackout condition or abnormally low voltages in a significant portion of the power system. Based on the type of disturbance, the voltage stability problem can be classified as small and large disturbance stability problem. Large disturbance voltage stability refers to the ability of system to maintain steady voltages when subjected to large disturbances such as three phase faults, loss of generators etc.

Small disturbance voltage stability refers to the system's ability to maintain steady voltages when subjected to small perturbations such as incremental changes in the system load. Further, based on the time frame of interest, the voltage stability problem is classified as short-term and long-term stability problem. The study period of interest for short-term voltage stability problem is in the order of several seconds, and for long term voltage stability the study period may extend to several minutes. With growing demand for electric power, and limitations in construction of generation and transmission services, the problem of maintaining voltage stability will remain a challenge in the foreseeable future. Many occurrences of system blackout have been linked to the problem of maintaining voltage stability and inadequate reactive power

supply is a major contributor to this challenge. The consequences of voltage instability include loss of load in an area, tripping of transmission lines and other elements leading to cascading outages.

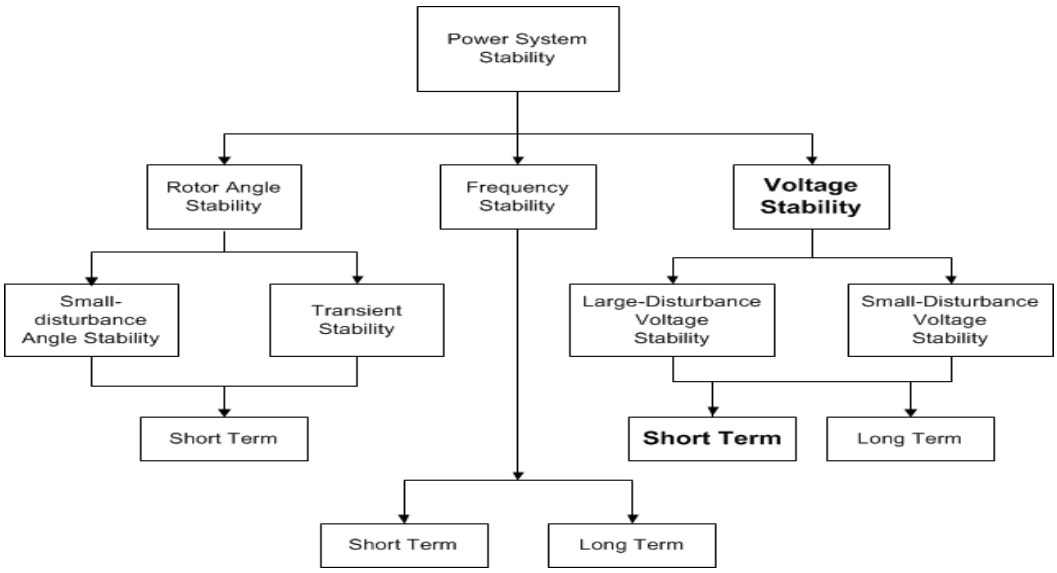

Figure 1.1: Classification of power system stability [1]

The short-term voltage stability is characterized by the interactions of fast acting dynamics of power system components such as induction motors, excitation system of generators, synchronous condensers, static var compensator (SVC), voltage dependent loads, flexible AC transmission system (FACTS), HVDC links etc following a disturbance. The short term voltage stability problem can manifest in one of the two forms - delayed voltage recovery and voltage collapse. According to North American Electric Reliability Corporation (NERC) definition, Fault Induced Delayed Voltage Recovery (FIDVR) is a phenomenon whereby system voltages remain at significantly reduced levels for several seconds after a fault in transmission, sub-transmission or distribution level has been cleared [2]. The NERC transmission issues subcommittee (TIS) provides the following characterization of FIDVR,

- Stalling of induction motors
- Initial recovery of voltage after fault clearing is less than 90% of the pre-contingency voltage level

- Slow voltage recovery of more than 2 seconds to the expected post-contingency steady state voltage level.

FIDVR has gained increased attention in the literature since incidents of slow voltage recovery associated with induction motor dynamics have been reported in summer peaking load areas, where low inertia single phase A/C motors comprise a significant portion of the load. Figure 1.2 shows a typical FIDVR fault that happened in Southern California Edison (SCE) system following a 230 kV transmission fault. In this case, the recovery of voltage is delayed due to stalling of induction motors, which were eventually disconnected by thermal protection switch. After 20 seconds, the voltage overshoots because of the presence of capacitors when sufficient loads are disconnected. Then the capacitors are switched off to reduce the voltage level. During the period where the voltage is returning to its normal value, air conditioner (AC) loads started coming back into the system. Since there is insufficient reactive support due to switched off capacitors, sudden reactive demand lead to exposure to another under voltage event.

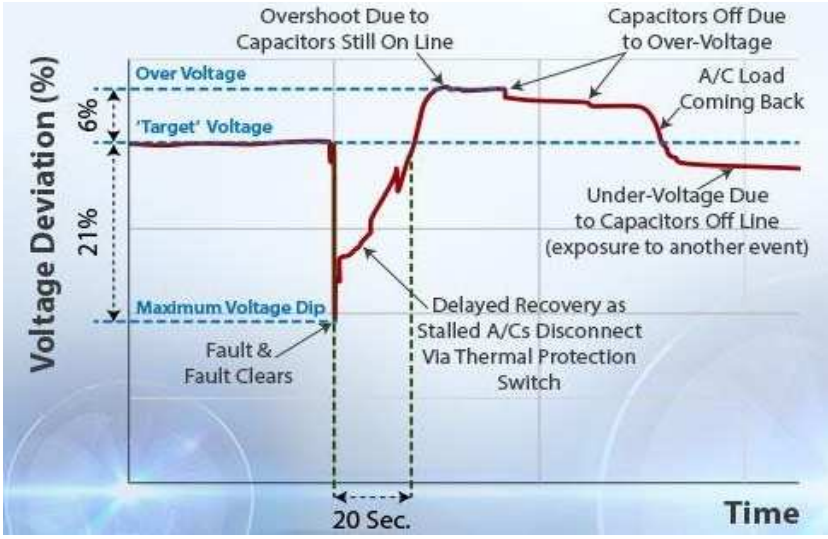

Figure 1.2: A typical FIDVR following a 230 kV transmission fault at SCE system [2].

Faults in areas with high penetration of residential A/C can provoke FIDVR events. The stalling behavior of induction motors, especially single phase residential A/C motors, is one of the major causes of FIDVR events. To gain a better understanding of the role of induction motor stalling in FIDVR events and to guide modeling efforts, more than 25 A/C units were

tested in the SCE and BPA laboratories. Based on the test results, the typical real and reactive power characteristics of an A/C unit when exposed to FIDVR events is shown in fig. 1.3. The following inferences can be made about the characteristic behavior of induction motors.

- Under NORMAL conditions, there is no significant change in the real power requirements when the voltage is reduced until the stall voltage is reached. The reactive power requirements reduces proportionally as the voltage decreases till 85% and then exhibits an inverse proportional characteristics until the stall voltage is reached.

- When the stall voltage is reached, the real and reactive power requirements jumps to higher levels. In fig.1.3, the real power increased from 4000 watts (for 80 F) to as high as 12000 watts when stalled. Similarly, the reactive power increased from 900 vars to 12000 vars under stalled state. In general, when an induction motor stalls following a severe disturbance, it may draw 5 to 8 times its normal reactive power requirement[7],[8].

- In the stalled condition, the real and reactive power requirements are directly proportional to the applied voltage. The higher the applied voltage, the higher the real and reactive power requirements. This behavior continues until the A/C unit is disconnected by a protection unit.

The sudden increase in the reactive power requirement may prevent voltage recovery and may lead to tripping of loads and rapid collapse of an area power system. Although the phenomenon of FIDVR can occur at any voltage level, the impact is adverse when such events happen due to faults at Bulk Energy System (BES). Such events pose the risk of being cascaded into larger area. The consequence of such event could be detrimental as it can lead to blackouts or power plant tripping. Investigation of FIDVR phenomenon requires special emphasis on modeling issues related to induction motor loads as well as on optimal allocation of reactive power resources to ensure adequate voltage recovery following disturbances.

The white paper published by NERC[2] has descriptions about the causes, sequence of events happening during FIDVR incidents and potential solutions to mitigate FIDVR events. Control solutions to mitigate slow voltage recovery problem can be classified into unit-level and system-level solutions. One of the unit level solution is to add a relay that disconnect A/C compressor

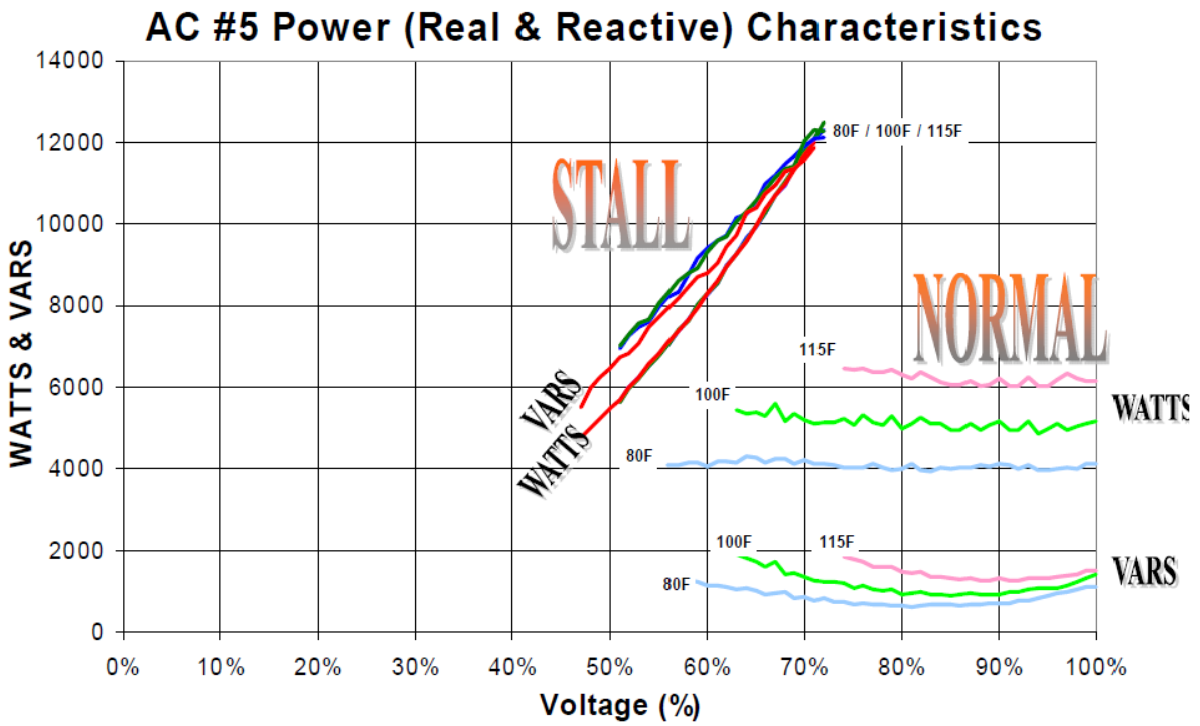

Figure 1.3: Typical A/C real and reactive power characteristics for three different outdoor temperatures [3]

motors when there is a reliable detection of impeding stall condition. Currently, the necessary standards required to achieve this goal is non-existent and retrofit of existing A/C units is even more difficult to accomplish. The use of system level solutions will be necessary until the threat of induction motor loads stalling can be reduced to a significant level. The system level solutions can be further classified into two types: demand-side solutions and supply-side solutions.

Demand side solutions use protection system to rapidly disconnect motor loads at system level during periods of low voltage. Different strategies include use of special protection schemes (SPS), under-voltage load shedding (UVLS) to limit the amount of load affected by low voltage problem. Limiting the impacted load through demand side solutions may not prevent the recurrence of FIDVR events. The system exposure to delayed voltage recovery can be a symptom of a larger issue - inadequate dynamic reactive support. Supply side solutions use dynamic reactive resources to provide dynamic VAR support to the system. Dynamic reactive resources are automatically controlled reactive resources that has the capability to voltage deviations

in a rapid manner. Synchronous generators, synchronous condensers, FACT devices such as static var compensator (SVC), static compensator (STATCOMs) are some examples for dynamic reactive resources. But, large-scale installation of these devices is expensive, and their cost increases with size (capacity). The effectiveness of dynamic support is very dependent on its location. Therefore, it is necessary to develop dynamic VAR placement strategies that enhance short term voltage stability and at the same time remain cost effective solutions.

1.2 Literature Review

In this section, first incidents of FIDVR happened in the utility system have been summarized. Second, the characteristics and role of induction motors in FIDVR events are provided. Third, the efforts to quantify FIDVR events have been discussed. Finally, the approaches that discusses the placement of dynamic reactive resources and their short-comings have been discussed.

Incidents of FIDVR: Various U.S. utilities have reported experiencing delayed voltage recovery events on their systems. FIDVR events have been observed in Southern California, Arizona, Texas, Florida, and the southeastern part of US [9],[10]. Numerous FIDVR events have occurred in the past resulting in a significant loss of load. Some of the major FIDVR that have been reported in the literature are provided in Table 1.1

More recent FIDVR events are not reported in journal articles, but they have been presented at conferences and workshops. Southern California Edison (SCE) has observed 37 FIDVR events in 2006 and six events during 2007. The large number of events during 2006 was attributed to use of high AC load because of hot and humid weather conditions [11]. SCE continues to observe FIDVR events, especially during summer monsoonal season. In [FDC], FIDVR events captured using power quality records in SCE's valley sub-transmission network has been reported.

Induction motor characteristics: The load characteristics of air conditioners and other motor driven compressor loads play a significant role in causing a FIDVR event. When the reciprocating compressors drives pistons, it increases the mechanical load faced by an induction

Table 1.1: Practical FIDVR Incidents

Date	Event/ Utility	Recovery Time	Interrupted Load	Remarks	Ref.
June, 1990	SCE desert region, SCE	Several seconds	-	Major FIDVR event	[9]
August, 1997	Hesperia, SCE	20-25 s	3500 MW	Lugo plane crash accident	[11]
30 July,1999	Union City,Southern Company	15 s	1900 MW	Load tripped by induction motor protection	[10]
28 July, 2003	Hassayampa 500 kV Fault, APS	Several seconds	440 MW	90,000 customers affected	[12]
1 July, 2003	Pinncacle Peak Capacitor Fault, APS	9 s	1000 MW	48,000 customers affected	[12]
29 July, 1995	Phoenix,APS	20 s	2100 MW		[12]
August, 1988	Miami, FPL	10 s	825 MW	Load loss due to device protection	[8]
August, 1987	Memphis,TVA	15s	1265 MW		[2]
SCE- Southern California Edison, APS -Arizona Public Service, FPL- Florida Power and Light company, TVA- Tennessee Valley Authority					

motor. Similarly, for scroll type compressors the mechanical load increases when the compressor turns a scroll to compress the gas.

Figure 1.4 shows a typical torque-speed characteristics for an induction motor. The x-axis represents the normalized motor speed, where 0 corresponds to blocked rotor condition and 1 corresponds to synchronous speed. The low mechanical load torque (blue) represents the situation where the compressor is turning on after several minutes of inaction. The high mechanical load torque (red) represents the normal operating load under compression. The high load torque line intersects the zero-speed axis at a point higher than the starting torque capability of the motor. If the motor were to stall in response to low voltages, then it would not be able to restart. The stalled motors draw significant current which depresses the voltage.

Typically, residential air conditioner motors are equipped with two types of protection, (a) Contactors that disconnect when the voltage drops below 40% (b) inverse-time characteristic current relay (thermal protection). If the stalled voltage is greater than the 40% threshold,

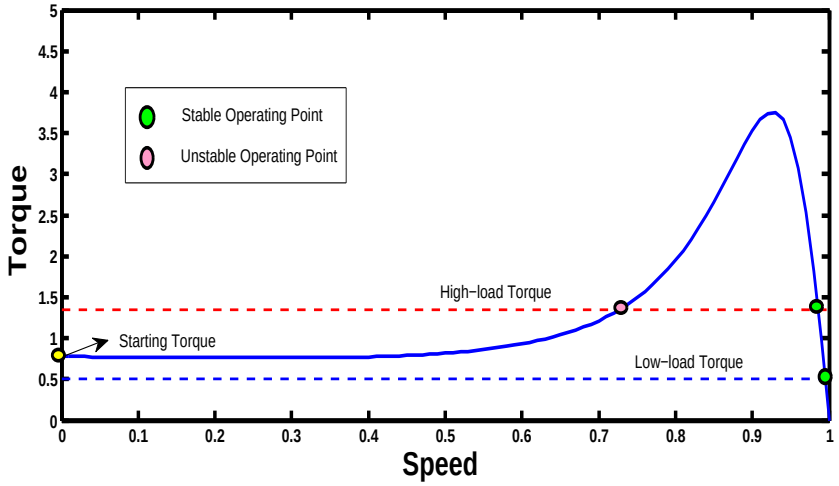

Figure 1.4: Torque-speed characteristics of small induction motors.

then the stalled motors remain connected to the grid. These stalled motors are eventually disconnected by thermal protection within a time span of 3-15 seconds. As the motors are tripped off, the voltage recovers gradually. The gradual recovery in voltage is due to the fact that all motors are not tripped off simultaneously. The motor remains offline until the compressor pressure equilibriates and then the motor can restart.

The earlier papers that dealt with the description of FIDVR phenomenon have represented the mechanical load driven by induction motors using a constant load torque characteristics. However, the more recent model development and testing conducted by WECC have found out the following two significant deficiencies with respect to the earlier modeling efforts

1. The torque of the mechanical load driven by induction motor is not constant. The load torque is position dependent as the motor drives pistons (reciprocating) or turns the off-center scroll.

2. The inertia of the compressor is over-estimated

The WECC Load Model Task Force has been actively involved in the development of improved load models for simulating FIDVR phenomenon. Two U.S Department of Energy Workshops on FIDVR[12],[13] recognized the growing concerns of utilities to the occurrence of such events. FIDVR is also considered to be a national issue due to the increasing penetration

of residential AC loads. From the presentations made at the DOE workshops, it is clear that FIDVR events can be consequential, they persist, and they pose a challenge to the reliable operation of the power grid.

Recent trends in load modeling research include probabilistic load modeling where parameter uncertainties in the aggregated induction motor model and the problem of cascading stall are considered. The stalling of induction motors due to low voltage is a cascading process in which stalled motors tend to reduce the bus voltage and in turn make other induction motors to stall. The typical aggregated induction motors used in time-domain analysis do not capture the cascading stall. A quasi-static modeling and simulation of cascading induction motors stall is presented in [14]. In [15], the induction motor loads variations and uncertainty are modeled in a probabilistic way. To estimate the probabilities of the number of induction motors stalled, an analytic method to estimate the parameters of a model of cascading failure from system parameters is derived. This work studies the influence of system parameters on cascading stall of induction motors.

Characterization of FIDVR events: Next, a review of the methods used to identify and characterize the FIDVR phenomenon has been provided. The enhanced voltage instability predictor (VIP) method is used in [11] to identify FIDVR and short term voltage stability problems. The VIP method is used to discriminate voltage stable cases (FIDVR is treated as voltage stable) from unstable ones. The VIP method represents the power system using a Thevenin equivalent and the parameters are recursively estimated at the rate which the PMU data are measured. Then the relationship between the apparent impedance at the local bus where the measurements are made and the Thevenin impedance is monitored. When the apparent impedance is less than the Thevenin impedance it signifies a short term voltage instability and for stable cases the apparent impedance is greater than the estimated Thevenin impedance.

In the enhanced VIP method, the calculated ΔQ margin is used to identify the FIDVR events. The Q-margin is computed and tracked in real time and it provides the amount of reactive power that can be pulled out of the bus. During FIDVR events, the Q-margin is

reduced considerably as motors are pulling reactive power from the system. This method works on the basis that the Thevenin impedance remains constant between successive estimations, but the Thevenin and load impedance are not constant during varying system conditions.

Slope based techniques and integral error based methods are the two broad categories used to quantify FIDVR. In [16, 17], slope based voltage recovery calculation is used to predict FIDVR events. Successive voltage measurements are used to calculate the slope of the voltage recovery trajectory. Using this slope the expected voltage recovery for the future time is predicted. The predicted voltage recovery is compared with the specified transient voltage recovery criteria for identifying FIDVR events. For the identification of FIDVR using steady state screening of buses, MVA-Volt index is proposed in [18]. The MVA-volt index is summation over all system buses of load MVA times voltage depression from the nominal value during a three phase fault at any bus.

Integral error based measure could not differentiate between two different voltage trajectories - one showing moderate recovery, the other showing fast recovery over a small period of time. On the other hand, any measure based on the slope or the derivative of the voltage trajectory will suffer in case of oscillations or sudden almost discontinuous changes in the voltage magnitude.

Dynamic VAR planning methods: In the following sections, the methods that are used for dynamic VAR planning has been reviewed. Choosing the optimal location and size of reactive power injection devices has been considered a challenging multi-objective optimization problem. This problem has been approached with a range of methodologies of various complexity levels. The available methods can be broadly classified under steady state based techniques and dynamic analysis based methods.

Traditionally the problem of dynamic VAR allocation has been approached using steady state techniques like OPF to identify the optimal locations and amount and time domain simulation is used for checking transient voltage performance. OPF is used to identify reactive deficient locations and if the number of locations identified by OPF analysis is large, they are clustered into small groups due to economic and site related limitations. Certain key bus loca-

tions are chosen among the clustered groups for reactive compensation and the compensation amount is refined to match the steady state requirements. Then time domain simulations are performed to identify the right mix of static and dynamic VArs needed to the meet the specified performance criteria.

In the ERCOT CREZ reactive power compensation study, conducted by ABB, the size and location of dynamic reactive compensation have been identified using steady state analyses techniques like optimal power flow, PV, QV analysis in combination with dynamic simulations [19]. A summary of tools and methodologies to perform comprehensive voltage stability studies for the identification of reactive power requirements is provided in [20] and [21]. The process involved in identifying the reactive requirements and the criteria used for fixing the problem in Entergy system is presented in [22].

Steady state based techniques works on the basis that the reactive deficient locations found using OPF methods are more prone to FIDVR problems. Therefore, these reactive deficient locations can serve as good locations for dynamic VAr installation. However it is possible that there are no problems (reactive deficiency) in the steady state analysis, but still the problem of FIDVR occurs in the time domain analysis. It is due to the fact that the problem of FIDVR is mainly influenced by the high concentration of induction motor loads and its dynamics. Without proper consideration of the load dynamics, it is not possible to detect FIDVR events. This necessitates the need for systematic dynamic analysis methods while dealing with FIDVR problems. Time domain simulation with proper representation of appropriate load models plays a crucial role in dynamic VAR planning studies.

In [23] a time continuation single phase quadratized power flow method is used to find the location and amount of static and dynamic VAR resource needed to alleviate the risk of short term voltage instability problem. This method uses a quasi steady state load models coupled with quasi-dynamic models of generators. Trajectory sensitivity methods are then used to linearize the non linear optimization problem which in turn is solved using linear programming techniques. This method is better than the steady state based approaches but still it cannot capture the full dynamics of the system because it uses only a quasi steady state model of

generators and loads. Also this approach uses linear programming to find the required VAR amount it may not be the same optimal amount obtained by solving a non linear optimization problem.

In [24] the problem is formulated as mixed integer linear optimization and is solved iteratively. Instead of using power flow and dynamic power system models, linear sensitivities are used to formulate the constraints and to find the optimal VAR amount. The LP problem is formulated based on the sensitivities of voltage dip time duration to SVC capacity limit. Margin sensitivities are used to identify the change in voltage stability margin (VSM), which in turn is used to rank order the severe contingencies and identification of potential candidate locations. This screening process is capable of identifying steady state issues, but not the transient issues. For identifying transient voltage problems, the information from steady state screening process combined with prior knowledge of the system and engineering judgement is used to identify critical contingencies and potential candidate locations for placing dynamic VAR sources. The behavior of voltage during fast voltage collapse is highly non-linear and this raises the question whether use of LP formulation is sufficient for solving dynamic VAR placement problem? Also, is there a systematic way to gain knowledge about the system for identifying critical contingencies and potential candidate locations?

In [25], the concept of trajectory sensitivity index (TSI) is proposed to identify the most efficient candidate locations for providing dynamic VAR support for a single contingency case. TSI of a particular bus measures the change in voltage levels at all the buses for an injection of dynamic VAR at the bus where TSI is calculated. The buses that have higher values of TSI are selected as the best candidate locations for the placement of dynamic VAR sources. This method does not provide how much amount to be placed at the chosen candidate locations. Also, the value of TSI is calculated by considering VAR injection at only one location at a time. This method does not consider the effects of VAR injections at multiple locations at the same time.

In [26] dynamic VAR allocation problem is formulated as mixed integer dynamic optimization problem and is solved by converting the optimization problem into a mixed integer non

linear problem (NLP). The conversion to mixed integer non linear program is done by full discretization of state and control variables. An algorithm based upon trajectory sensitivity analysis is used to select candidate VAR locations. Although this method finds the optimal amount and location of dynamic VAR resources needed to ensure acceptable transient voltage performance, the size of optimization problem increases dramatically as the system size increases. Even though mixed integer dynamic optimization described in [26] provides a systematic way of finding the optimal amount of dynamic VAR resource needed to solve fast voltage collapse and slow voltage recovery problems, it suffers from the problem of solving large dimension non linear optimization problem as the power system size increases. This curse of dimensionality makes it difficult to implement this method for large scale realistic power system. Also, implementing the advancement in modeling and solving power system DAEs is quite complicated and tedious because of unavailability of proprietary legacy source codes.

The use of dynamic optimization is very limited in power system due to its computational complexity. However, increasing trends are observed that more researchers are working on migrating power system applications to dynamic optimization formulation for its compact form in mathematics, especially when concerning dynamics of power systems. Research efforts have been made to use dynamic optimization methods to solve other power system power systems problems like stability constrained optimal power flow (SCOPF). Direct discretization methods [8], [9] and constraint transformation methods [10] are considered as the two main approaches in the existing literature to deal with DAEs in SCOPF problems. The direct discretization method attracts more research efforts for its flexibility and the utilization of state of the art NLP techniques. However, conventional direct method based on interior point method (IPM) as NLP optimizing algorithm usually suffers from low computational efficiency as well as huge memory consumption, especially for large-scale problems and multiple contingencies. As a countermeasure, reduced-space IPM (RIPM) is proposed as an important extensions of IPM to accelerate the process of solving primal-dual system in a mathematically equivalent way.

1.3 Thesis Objective

The objective of this work is to develop a comprehensive methodology which can determine the optimized dynamic reactive power compensation (location and level) that is needed to maintain the system short term voltage stability, following a large disturbance. This approach should be valid for a range of operating conditions and contingencies. In contrast to previous approaches, this work evaluates the reactive power needs dynamically and in the transient time frame. The focus is on developing study methodology, procedures and tools to support transmission operators and planners in predicting potential large-disturbance/short-term voltage instability fast voltage collapse or slow voltage recovery incidents, and in planning for and managing the reactive power resources to address such incidents.

1.4 Organization of Thesis

This dissertation includes three major parts - (a) dynamic VAR planning using dynamic optimization, (b) behavioral classification of contingencies and scenarios, (c) identification of dynamic voltage control area. The rest of this dissertation is organized as follows:

Chapter 2 describes a dynamic optimization based approach to optimize the location and amount of dynamic reactive power required to mitigate FIDVR problems for a single contingency. The formulation and implementation of a dynamic optimization method are provided. The method has been tested on the IEEE 162 bus system and a large realistic system in the U.S. and the simulation results have been discussed in detail. The role of trajectory sensitivities, singular value decomposition, linear programming based solutions in improving the solution efficiency of the dynamic optimization are also discussed in this chapter.

Chapter 3 discusses a novel entropy based Kullback-Liebler (KL) measure for the quantification of voltage recoveries. Utilizing the KL measure, contingencies are grouped into different clusters according to their behavioral similarity using a spectral clustering algorithm. The contingency clustering provides representative contingencies that covers wide range of similar contingencies under various operating conditions. Simulation results have been performed on the modified IEEE 162 bus system to test and validate the proposed method.

Chapter 4 describes a new concept named dynamic voltage control areas (DVCAs). The concept of DVCA identifies groups of weak buses vulnerable to short-term voltage problems under a given set of contingencies and also the most effective control locations to provide dynamic reactive support to achieve satisfactory dynamic voltage performance. DVCA identification involves the process of contingency clustering and a mixed inter linear programming (MILP) routine.

Chapter 5 discusses an improved dynamic optimization formulation using KL measure to refine the amount of dynamic VARs required to avoid short-term problems within each DVCA. The dynamic optimization framework discussed in chapter 2 is modified and extended to overcome the curse of dimensionality while handling multiple contingencies under various operating conditions. All concepts have been tested and validated using simulations based on the modified IEEE 162 bus system.

Chapter 6 presents conclusions and significant contributions of this work, and discusses possible future works.

CHAPTER 2. DYNAMIC OPTIMIZATION USING VOLTAGE TIME SERIES

2.1 Introduction

In this chapter, the optimal amount and locations for installing dynamic reactive resources to mitigate slow voltage recovery problems, for a single contingency, are found by dynamic optimization approach. Control vector parameterization (CVP), a dynamic optimization approach, is used to formulate the dynamic reactive resource allocation problem. The dynamic optimization ensures satisfactory performance in system voltages during the transient period. The CVP approach considers the dynamics of the system while performing the optimization. In the CVP approach, the process of finding the power system differential and algebraic equations (DAE) is decoupled from the optimization routine and communications of results between these two modules enables to arrive at the optimal solution. This feature of CVP enables us to utilize the commercial grade DAE software and commercial grade non-linear programming (NLP) solvers for finding the optimal solution of the dynamic reactive resource planning problem. With an integration of commercial grade DAE solver and optimization solver, large scale problems can be solved efficiently. The formulation and implementation details of CVP based dynamic VAR planning for a single contingency are discussed in this chapter. The CVP based dynamic optimization approach is tested on the IEEE 162 bus system and on a realistic power system in the U.S. First, the study results based on IEEE 162 system with detailed air-conditioning model is presented to show the need for the dynamic optimization approach. Next the scalability of the proposed approach is demonstrated by applying this method to a realistic power system in the U.S.

2.2 Motivation and Proposal

The challenging task of choosing the optimal location and amount of reactive resource has been explored in the literature using many methodologies, but the research in this area is far from being perfect. Most of the methods use time domain simulation as a means to check the performance of voltages during dynamic analysis. Dynamic analysis is not considered explicitly during the process of identifying the optimal locations and amount, mainly because of the computational difficulties involved in such procedure. But time domain simulation with proper representation of appropriate load models plays a crucial role in dynamic VAR planning studies. If system dynamics are not taken into account properly, the proposed control solution may be an expensive over design or an under design which is not capable of mitigating FIDVR problems completely. This brings out the need for the use of dynamic optimization in dynamic VAR planning studies.

Direct simultaneous based dynamic optimization has been used in the literature for dynamic VAR planning. However, this method suffers from the curse of dimensionality as the power system size increase. To overcome this issue, a direct sequential based dynamic optimization formulation has been proposed in this work. The main motivation behind using this method is to separate the dynamics of power system from optimization problem part and utilize commercial grade software to solve power system dynamics and optimization. This approach considers the dynamics part during the optimization procedure, but performing dynamics simulations are clearly separated from the optimization procedure. This feature of this approach will help to easily extend this method for large scale power system.

The following section provides background material related to various dynamic optimization methods. .

2.2.1 Dynamic optimization - background information

Dynamic optimization is a class of optimization problems where the optimal solution is obtained by considering the dynamics of the system. Mathematically, the dynamic VAR allocation problem can be modeled as a dynamic optimization problem. Dynamic Optimization [27] is an

optimal control problem (OCP), where the optimum values for control and parameters which minimize a certain performance measure are identified. The optimal control should satisfy the dynamics of the system and also the path constraints on system variables. If the objective function has integer variables, then the OCP becomes a mixed integer dynamic optimization (MIDO) problem. In general the OCP is defined as given in (2.1).

$$
\begin{aligned}
&\underset{t_{\text{final}},u,p}{\text{minimize}}\ J = \phi(t_{\text{final}},u,p,z) + \int_{t_0}^{t_{\text{final}}} L(x,u,t,p,z)dt \\
&\text{Subject to} \\
&\dot{x} = F(x,u,p) \\
&0 = G(x,u,p) \\
&c_i(x,u,p) \leq 0 \\
&t \in [t_0, t_{\text{final}}]\,,\ z_i \in [0,1] \\
&x \in \mathbb{R}^{n_x},\ u \in \mathbb{R}^{n_u},\ p \in \mathbb{R}^{n_p}
\end{aligned}
\tag{2.1}
$$

The objective function of the general OCP problem is given by J and it has two parts - (a) Mayer type, which depends upon final time (t_{final}) constraints and (b) Lagrangian type, which is given by the function L. In OCP, the variables are separated into two classes namely the state variables (x) and control variables (u). The evolution of state variables is dictated by the control variables, via a set of differential and algebraic equations (DAE), which are specified by functions F and G in (2.1). Further, the control and state variables are subjected to performance constraints give by C_i. The parameters and binary variables in the system are denoted by p and z respectively. The number of state variables, control variables and parameters are given by n_x, n_u and n_p respectively.

Numerous analytical and numerical based methods are available to solve the OCP, which are broadly classified into indirect and direct methods. Indirect methods such as Bellman's optimality principle and Pontryagin's maximum principle are analytical methods and they are based on the principle of variations[28]. The application of this method to VAR allocation problem is very difficult because of the complexity and size of the problem.

Direct methods are based on the principle of discretizing the optimal control problem and then applying the non-linear programming (NLP) techniques to the resulting optimization problem. These methods take the advantage of the state of the art NLP solvers. Also, these methods can be applied to system described by ODE (ordinary differential equations), DAE and PDAE (partial differential and algebraic equations) models [4]. The three main variants of direct method of solving optimal control problems are direct simultaneous approach, direct sequential approach and multiple shooting methods [29].

Direct simultaneous approach transforms the OCP problem by discretizing the constraint differential and algebraic equations (DAEs) into a set of algebraic equations at every simulating time steps. This method is also referred as state vector parameterization (SVP) or full discretization method or orthogonal collocation method. There are various discretization schemes such as Implicit Euler method, Trapezoidal method and Radau collocation on finite elements to transform the dynamic optimization problem into a non-linear programming problem. The full discretization method tries to satisfy the dynamic equations and optimality conditions together. As the size of the power system increases, the resulting NLP size will increase and obtaining a solution will be difficult due to convergence problems. Besides the curse of dimensionality, due to the close coupling between model and optimization in the discretization process, detailed dynamic models are difficult to embed into dynamic optimization.

The direct sequential method translates the optimal control problem into an NLP by only discretizing the control variables. The system dynamics are still embedded in the NLP problem, but are handled separately by a numerical integrator. This method is also referred as control vector parametrization (CVP). The NLP algorithm adjusts the control variables based on violation of constraints on state variables generated by system dynamics solver and the gradient information. The gradient information provides details on how the objective function and constraints vary for a change in the control variables. With this approach, large scale dynamic optimization problems can be handled in a better way compared to simultaneous approach.

2.3 Formulation of the Dynamic Optimization Problem

Of the dynamic optimization methods available in the literature, CVP is well suited for dynamic VAR allocation problem because of its decoupling feature that separates the power system dynamics solution procedure from the optimization routine.

2.3.1 Objective function:

The objective function of the dynamic VAr allocation problem is to minimize the number of locations and the maximum amount of dynamic VAR at the chosen locations. Equation (2.2) provides the mathematical formulation of the objective function. $B_{svc,i}^{max}$ denotes the maximum susceptance of SVC placed at location, $'i'$ and W_i denotes the importance (weight) of choosing location i. The locations of the SVCs are integer variables, denoted as z_i, which makes this optimization a mixed integer dynamic optimization (MIDO), a highly computationally intense optimization problem.

$$\begin{aligned} &\underset{B_{svc,i}^{max}}{\text{minimize}}\ f = \phi = \sum_{i=1}^{m} z_i W_i B_{svc,i}^{max} \\ &z_i \in [0,1],\ W_i \in \mathbb{R} \end{aligned} \tag{2.2}$$

2.3.2 Constraints

2.3.2.1 Power system dynamics

Power system grid planning and operating decisions rely on simulations of dynamic behavior of the system. For ensuring reliable and safe operation of the power system, appropriate and realistic models have to be used in the simulation studies. A power system model consists of generation, transmission and load models. The individual models of the generator, automatic voltage regulator (AVR), governor and system loads are given by the differential and algebraic equations (DAE). The transmission network is modeled using algebraic equations.

$$\begin{aligned} \dot{x} &= f(x,y) \\ 0 &= g(x,y) \end{aligned} \tag{2.3}$$

Equation (2.3) represents the set of DAE equations that represent the power system dynamics. The differential and algebraic states are denoted by x and y respectively. f and g represents the set of differential and algebraic functions respectively.

2.3.2.2 Load modeling

In general, for dynamic simulation studies, loads were represented with static characteristics with constant current for active power and constant impedance for reactive power. WECC Modeling and Validation Group (MVWG) has developed a composite load model for dynamic simulation studies. This composite model is represented as CMLD model in PSSE [4] and CMPLDW in GE PSLF [30]). Figure 2.1 shows the representation of CMLD composite load model. This model simulates the dynamic behavior of an aggregate of three phase induction motors, single phase air conditioner motor, electronic loads and static loads connected to a low voltage load bus. The composite load models has the capacity to represent three different types of three phase induction motor loads namely three phase motors driving constant torque loads, torque speed-squared loads with high inertia and torque speed squared loads with low inertia. A single phase air conditioning load is also included in the composite load model structure. This is a grid level model representing an aggregation of a large set of single-phase air conditioners. These motors stall when voltage drops below certain set value and a portion of these motors restart when voltage recovers. In addition to representing the mix of loads at the low voltage bus, this model also includes an equivalent circuit of distribution transformer, substation compensation (Bss), and distribution feeder equivalent (R + jX) and feeder compensation (B1 and B2). The composite load model has under-voltage and under-frequency load shedding protection, which trips a portion or entire load. The dynamic response is reflected at the high voltage system bus.

The following description of model structure and characteristics is an adoption from [3].

Distribution system equivalent represented with a π model captures the voltage drop, real and reactive power losses in primary distribution circuits, distribution transformers and secondary distribution circuits. Typical distribution feeder equivalent data have 4-6% voltage drop, $\frac{R}{X}$ ratio of 0.8, shunt compensation at feeder end is 75% and end use utilization voltage is

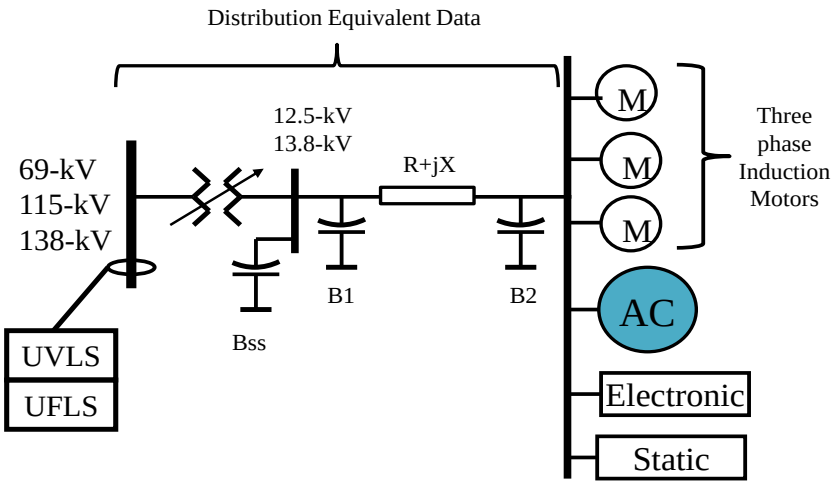

Figure 2.1: CMLD composite load model structure [4]

assumed to be greater than 95%. One of the limitations of this equivalent feeder representation is that it assumes balanced load response of all three phases, since this model is part of a positive sequence program.

Three phase induction motors are represented by CIM6 models from PSSE standard model library. The CIM6 models have detailed representation of electromagnetic dynamics of the motor and rotating load dynamics. In CIM6 type of models, both single-cage and double-cage induction motors are represented using the equivalent circuit impedances. The equivalent circuit of the induction motor can be represented using either Type 1 or Type 2 model as shown in fig.2.2. The equivalent circuit parameters are translated into transient parameters corresponding to flux linkage components for use in the actual model calculations.

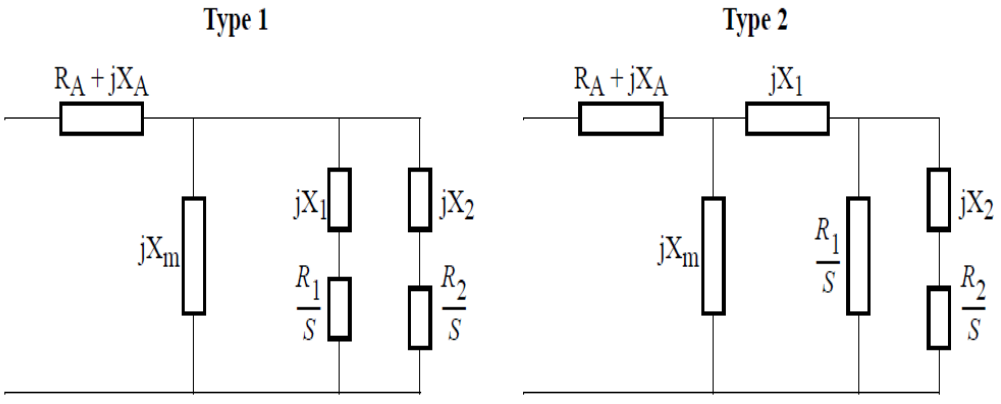

Figure 2.2: Induction Motor Equivalent Circuit [4]

In the CIM6 type models, the mechanical load torque,T_{load}, is represented using (2.4)

$$\begin{aligned} T_{\text{load}} &= T_0(A\omega^2 + B\omega + C_0 + D\omega^{\epsilon}) \\ C_0 &= 1 - A\omega_0^2 - B\omega_0 - D\omega_0^{\epsilon} \\ \omega_0 &= 1 + \Delta\omega \end{aligned} \tag{2.4}$$

The parameter D represent the load damping factor. The variables T_{nom} corresponds to motor load torque at synchronous speed, ω is the current motor speed, ω_0 is the initial motor speed and $\Delta\omega$ correspond to per unit slip.

During initialization of the model, first the total power for the specified load is obtained from the powerflow data. Along with the equivalent circuit impedance and bus voltage, this value is used to calculate the initial slip and actual reactive power consumption of the motor. If there is reactive power difference between the specified load Q and the calculated Q, then it is adjusted by the assignment of a hidden shunt at the corresponding load bus. Based on the motor load and the initial slip, then model then calculates T_{nom} in order to balance the electrical and load torque in the steady state. The inertial time constant of the small induction motor has a direct effect on the electrical dynamics of the motor.

Single phase AC motor model has the representation of compressor motor, compressor motor thermal relay, under-voltage relays and contactors. A schematic diagram of this single phase AC motor performance model is shown in figure 2.3. Motor A and Motor B represents the two categories of aggregated compressor motors. Depending upon the input voltage, the motor operates either in 'running' or 'stalled' state. Motor A will not restart once it enters the stall state, whereas motor B has the capability to restart. The stalled motors corresponding to type A category are eventually tripped by thermal relays. K_{thA} and K_{thB} represent the fraction of motor A and motor B loads that are not tripped by thermal relay. K_{UV} and K_{CON} represent the fractions of motor load that are not tripped by under-voltage relay and contactors. respectively.

Equation (2.5) and (2.6) relates the voltage to real and reactive power of the single phase AC motor under running and stalled conditions respectively. The parameters $a_1 - a_4$ and $b_1 - b_4$ are temperature dependent and are represented by expressions $a(T)$ and $b(T)$ in (2.5).

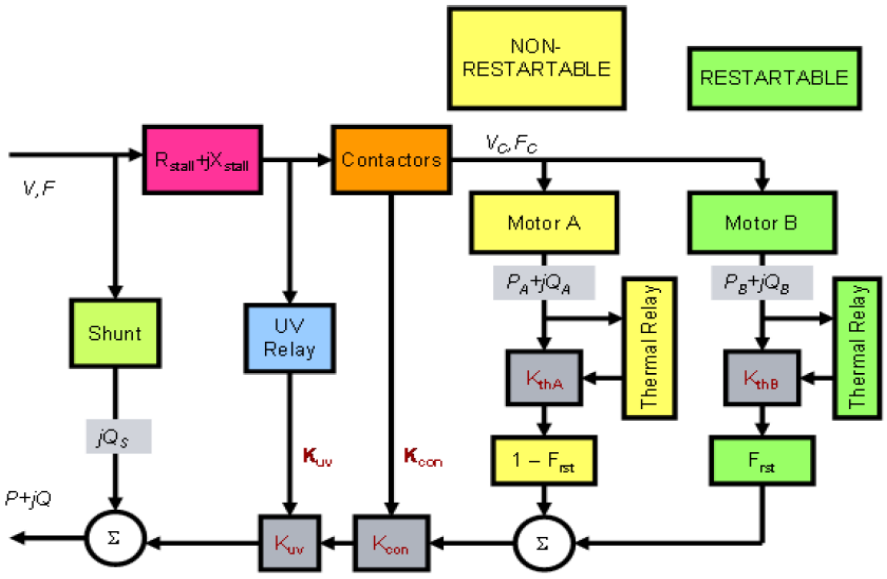

Figure 2.3: Performance model of single phase induction motor model [4]

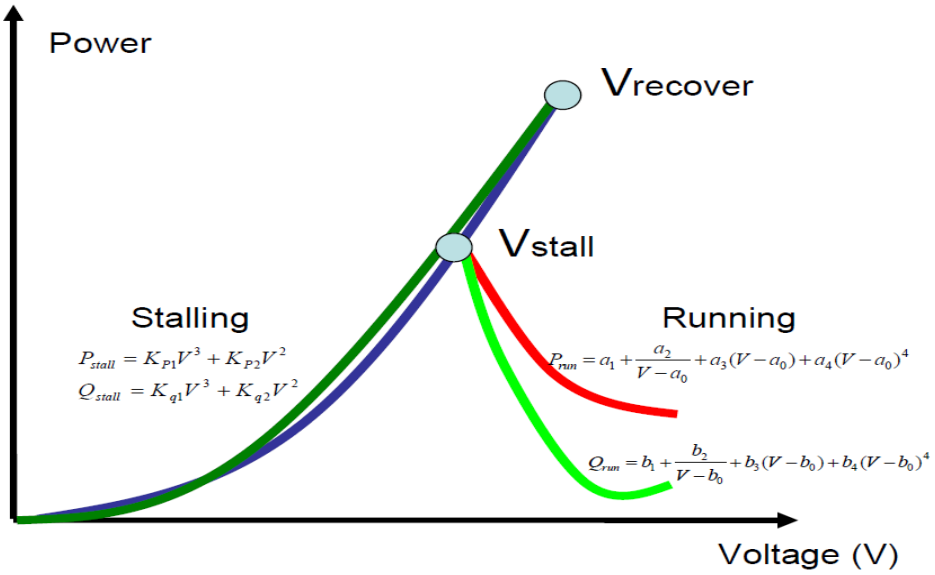

Figure 2.4: Performance model characteristics of compressor motors [4]

$$
\begin{aligned}
P_{run} &= a_1 + \frac{a_2}{V - a_0} + a_3(V - a_0) + a_4(V - a_0)^4 \\
Q_{run} &= b_1 + \frac{b_2}{V - b_0} + b_3(V - b_0) + b_4(V - b_0)^4 \\
a_i(T) &= c_0 + c_1 T + c_2 T^2, \ \forall i = 1, 2, 3, 4 \\
b_i(T) &= d_0 + d_1 T + d_2 T^2, \ \forall i = 1, 2, 3, 4
\end{aligned} \tag{2.5}
$$

$$
\begin{aligned}
P_{stall} &= K_{p1} V^3 + K_{p2} V^2. \\
Q_{stall} &= K_{q1} V^3 + K_{q2} V^2.
\end{aligned} \tag{2.6}
$$

The *thermal protection relay* in single phase AC motors prevents the motor from overheating. Figure 2.5 shows the characteristics of the thermal relay model, defined by the tripping temperatures, Th_{1t} and Th_{2t}. Th_{1t} is the temperature at which compressor motor begins tripping and Th_{2t} is the temperature at which all compressor motors are tripped. Equation (2.7) is used to compute the winding temperature (T_w). I_c represents the compressor motor current, T_{th} represents the compressor motor heating time constant and R_{stall} denotes the stall resistance of the motor. Based on the computed winding temperature and thermal relay tripping characteristics, the fraction of motors that are not tripped by thermal protection, K_{th}, is calculated.

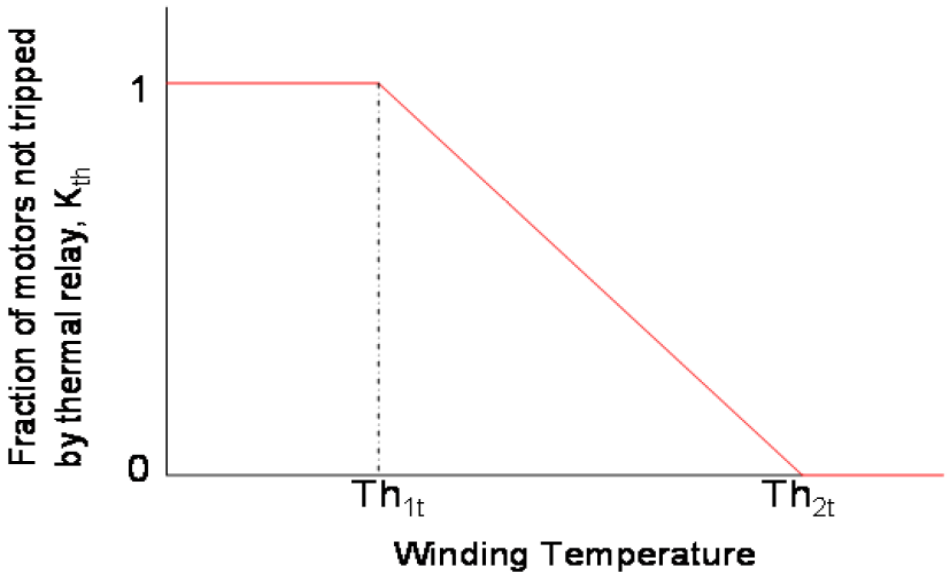

Figure 2.5: Thermal relay model of compressor motors

$$T_w = \frac{1}{1 + sT_{th}}(I_c^2 * R_{\text{stall}}) \tag{2.7}$$

The compressor motor has a definite-time *under-voltage relay* with two thresholds. If the input voltage stays below the threshold value for the specified time period then the fraction of motors, which has under-voltage relay, will be tripped and are not re-connected during the simulation.

The power contactors energizes the compressor motors. The fluctuations in the input voltage affects the ON-OFF status of the contactors. The contactors open when the control voltage drops to 40-45%, and re-close when the control voltage restores above 50-55% range. The contactor model determines the fraction of motors that do not drop (K_{con}) out because of dip in the input voltage. .

2.3.2.3 Dynamic VAR model

SVC is a regulated source of leading or lagging reactive power, whose output varies in response to the demands of automatic voltage regulator. It can maintain virtually constant voltage for dynamic events at the point in the network to which it is connected. It is comprised of inductive and capacitive branches that are controlled by thyristor valves and connected in shunt to the transmission network via a step-up transformer.The thyristor control gives the SVC the characteristics of a variable shunt susceptance. SVC responds very rapidly to the changing network conditions such as contingencies. Unlike mechanically switched compensation, SVCs can operate repeatedly and is not encumbered by the delays associated with mechanical switching. SVC can respond dynamically in 20 to 60 milliseconds.

The static VAr devices are represented as generators in the power flow simulation. In the dynamic simulation, they are represented using CSVGN5, which corresponds to a static var system model in the PSSE program [4]. This model has fast override capability which is activated when the voltage error exceeds a threshold value. It does not separate the equipment to identify capacitor banks and reactors.If the output of the SVC, $B_{\text{svc}}^{\text{max}}$ is positive then the capacitor banks in the SVC equals to $B_{\text{svc}}^{\text{max}}$ times the MVA rating of the generator. If the value

of $B_{\text{svc}}^{\max}$ is negative then it consists of only reactors. The objective of the dynamic optimization is to find the optimal values of $B_{\text{svc}}^{\max}$ at the chosen locations.

2.3.2.4 Voltage Performance Constraints

Historic voltage assessment practice mainly relied on two factors - (a) magnitude of voltage dip and (b) duration of voltage dip. A comprehensive survey of transient voltage dip criteria from utilities, reliability councils, relevant standards, and industry-related papers is presented in [5]. A literature review of industry standards and other technical publications on the influence of voltage on typical protection and controls is provided in [31]. There is a wide variation in the tolerance level of voltages for contactors, relays, large air conditioners and motor protection. They drop out when the voltage magnitude drops to 60%-75%of its nominal value. There are no common practices for motor under-voltage control and protection, especially for smaller equipment. For power electronic loads, Information Technology Industry Council (ITIC) has provided the voltage tolerance curve as shown in fig.2.6. To avoid undervoltage conditions, ITIC curve states that the voltage dip should not exceed 30% from 1.2 cycles to 30 cycles. Further, the voltage dip should not exceed the 20% limit from 30 cycles to 600 cycles and after 10 seconds it should not exceed the 10% limit. WECC transient voltage dip criterion states that for a Category B disturbance (single element outage), should not cause a transient voltage dip that is greater than 20% for more than 20 cycles at load buses, or exceed 25% at load buses or 30% at non-load buses at any time other than during the fault [5]. Also, the steady state voltage limit prescribes at steady state voltage values should be between the bound of 95% to 105%. Figure 2.7 summarizes the WECC voltage performance criteria.

It has to be noted that the WECC transient voltage performance criteria was originally formed based on rotor angle stability requirements. However, this criteria has been applied by many utilities for general transient voltage performance studies. The use of this criteria may be over-conservative, since the criteria were not developed with the specific consideration of FIDVR phenomenon. The WECC modeling and validation group is working on voltage ride-through envelope for power plants during FIDVR events. [6]. Figure 2.8 shows the proposed

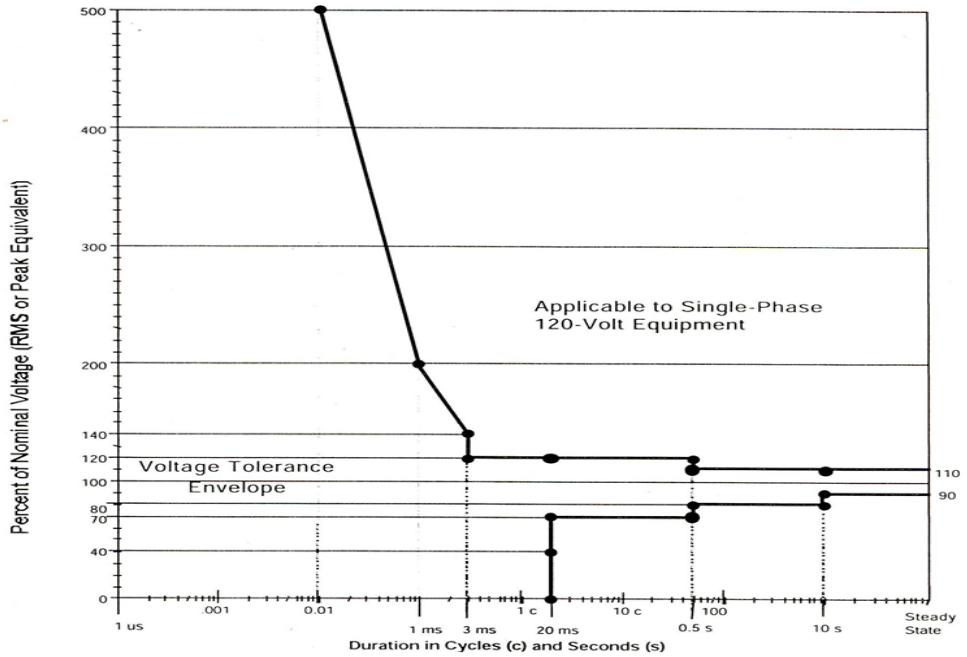

Figure 2.6: Information Technology Industry Council voltage tolerance curve [5]

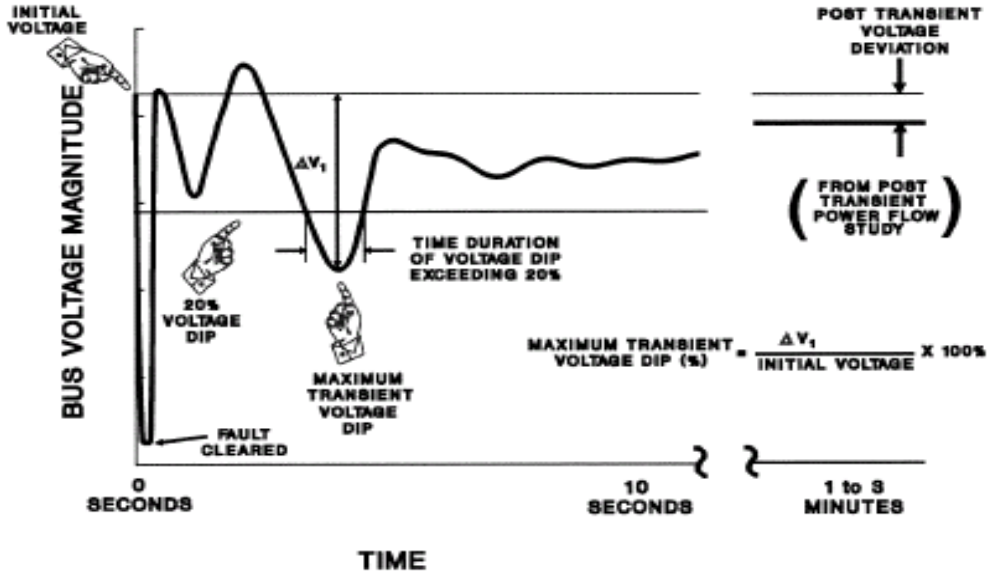

Figure 2.7: WECC Voltage Performance Criteria [5]

voltage ride-through envelope for power plants.

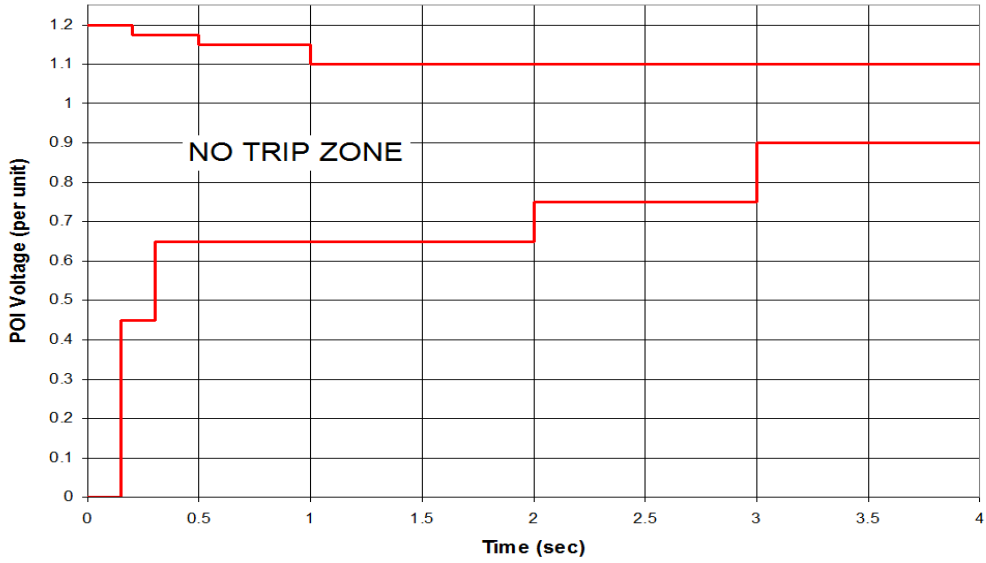

Figure 2.8: Proposed WECC voltage ride-through envelope for power plants [6].

$$
\begin{aligned}
&0.70V_i^0 \leq V_i(t) \leq 1.30V_i^0, \ \forall t \in [t_c + 0.5s, t_c + 2s] \\
&0.80V_i^0 \leq V_i(t) \leq 1.10V_i^0, \ \forall t \in [t_c + 2s, t_c + 5s] \\
&0.95V_i^0 \leq V_i(t) \leq 1.05V_i^0, \ \forall t \in [t_c + 5s, t_{\text{final}}] \\
&\forall i \in \text{Monitored buses}
\end{aligned}
\tag{2.8}
$$

$$
\begin{aligned}
&\mathbb{I}_c := \left\{ t_{cs} \quad | \quad V(t_{cs}) = 0.7V^0, \quad \forall t \in [t_c, t_{final}] \right\} \\
&t_f = \begin{cases} inf\left\{\mathbb{I}_c\right\}, & \text{if } \mathbb{I}_c \neq \emptyset \\ t_{final}, & \text{if } \mathbb{I}_c = \emptyset \quad \& \quad v(t_c) < 0.7V^0 \end{cases} \\
&\mathbb{I}_1 := \begin{cases} [t_c, t_f], & \text{if } (t_f - t_c) * 60 \geq 20\text{cycles} \\ \emptyset, & \text{otherwise} \end{cases}
\end{aligned}
\tag{2.9}
$$

The constraints are formulated based on WECC voltage performance criteria and also the proposed voltage ride through requirements for power plants by the WECC modeling and validation group. An envelope of voltage performance criteria as given in (2.8) for the set of monitored buses is used as constraints in the optimization problem. The set $\mathbb{I}_1$ defined in (2.9) is used to capture the delayed recovery phenomenon, as given by WECC voltage performance

criteria. Equation (2.10) is used as a constraint in the optimization problem to avoid the transient voltage dip. If the voltage profile at all buses adheres to the above described voltage performance criteria, then the occurrence of delayed voltage recovery events can be avoided to a significant extent.

$$\begin{aligned} &\tau := \{t_{\text{end}} - t_{\text{start}} | [t_{\text{start}}, t_{\text{end}}] \in \mathbb{I}_1 \cup \mathbb{I}_2\} \\ &\tau_{ij} \leq 0.33 (= 20 cycles) \\ &\forall i \in LB, j \in \mathbb{R} \end{aligned} \tag{2.10}$$

2.4 Implementation of CVP Approach

The overview of implementation of the dynamic reactive resource planning as a control vector parameterization problem is shown in Fig. 2.9. The following description provides the steps involved in implementing the dynamic optimization based reactive resource allocation.

Step 1: Setup appropriate power flow and dynamic database suitable for studying FIDVR phenomenon (e.g. a summer scenario). The dynamic database should include detailed load model, especially induction motor models.

Step 2: Perform time domain simulations to calculate sensitivities of bus voltages with respect to reactive power injections at various locations.

Step 3: Identify the potential candidate locations for dynamic VAR allocation using TSI and the relative weights of chosen locations are obtained using SVD analysis. The information obtained from TSI and SVD analysis are used in the formation of NLP objective function.

Step 4: Perform LP analysis to initialize the control variables of the NLP optimization problem. The control variables are the maximum value of SVC susceptance needed at chosen candidate locations.

Step 5: Set up the interface between optimization routine and power system dynamics solver. Initialize the parameters for the optimization routine.

Step 6: The dynamics of the power system are solved separately using any standard power system dynamics program with the current value of control variables provided by the optimization routine.

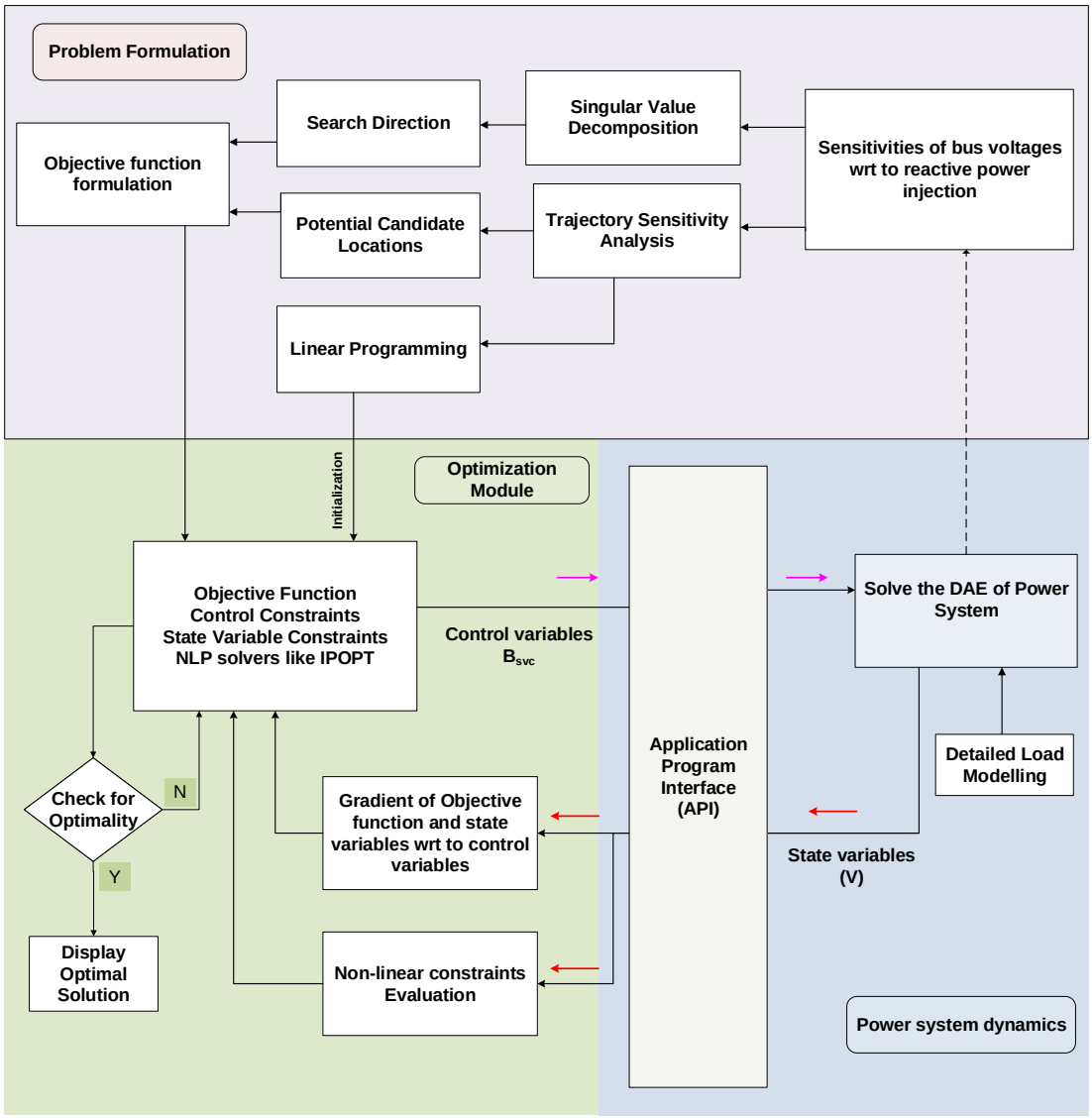

Figure 2.9: Implementation of CVP approach

Step 7: The results from the power system dynamics solver are fed back to optimization routine and are used to evaluate the constraints and gradients of the optimization program.

Step 8: Check whether optimality conditions for local optimal solution given in (2.11) are met. If yes, the optimization routine proceeds to step 9. If not the optimization routine updates the control variables and repeats from step 6. The control variables are updated using the gradient information provided by the optimization routine. Equation (2.11a) gives the first

order necessary conditions for finding a local optimal solution and (2.11b) and (2.11c) provides the complementarity condition.

$$\nabla f(y) + \sum_{i=1}^{m} \lambda_i^c \nabla c_i(x,y) + \sum_{j=1}^{n} \lambda_j^b = 0 \tag{2.11a}$$

$$\lambda_i^c.\min\big[(c_i(x,y) - c_i^L), (c_i^U - c_i(x,y))\big] = 0, i = 1 \cdots m_c \tag{2.11b}$$

$$\lambda_j^b.\min\big[(y_j - b_j^L), (b_j^U - y_j)\big] = 0, j = 1 \cdots n_x \tag{2.11c}$$

Step 9: If all the optimality conditions and stopping criteria specified by (2.13) are met, then an optimal solution is found.

The feasibility error at a given point y, is the maximum violation on the constraints *c(x,y)* and bounds on the decision variable *y*. Optimality error is the maximum violation of the optimality conditions given in (2.11).

$$\text{FeasErr} = \max_{i,j}\big(0, (c_i(x,y) - c_i^U), (c_i^L - c_i(x,y), (y_j - b_j^U), (b_j^L - y_j)\big) \tag{2.12}$$

The optimization criteria used for terminating the optimization program when it reaches a local optimum solution is given by (2.13). Details of the optimization criteria are provided in [32] and its implementation is given in [33].

$$\text{FeasErr} \leq \max(\tau_1 * \text{feastol}, \text{feastol\_abs}) \tag{2.13a}$$

$$\text{OptErr} \leq \max(\tau_2 * \text{opttol}, \text{opttol\_abs}) \tag{2.13b}$$

$$\tau_1 = \max\big(0, (c_i(y^0) - c_i^U), (c_i^L - c_i(y^0), (y_j^0 - b_j^U), (b_j^L - y_j^0)\big) \tag{2.13c}$$

$$\tau_2 = \max(1, \Big\|\nabla f(y))\Big\|) \tag{2.13d}$$

2.5 Improving Solution Efficiency

2.5.1 Trajectory sensitivity analysis

In order to reduce the computational burden, first the optimal locations for SVC placement are identified through the trajectory sensitivity analysis method [25]. The trajectory sensitivity

analysis method finds the influence of a particular location for the placement of dynamic VAR resource. The trajectory sensitivity index, TSI_j is used to identify buses that have the most influence on the voltage magnitude of other system buses, for an injection of reactive power at a particular bus *'j'* as shown in (2.14). $\frac{\partial V_i}{\partial Q_j}$ provides the change in voltage at bus i for a reactive power injection at bus j. W_k and W_{bi} denotes the weighting factor to designate the importance of time instant k and bus i respectively. If the value of TSI at a particular bus is large then the corresponding bus has more influence for placing dynamic VAR source. The variable z in (2.2) is assigned a value of 1 for the influential buses which form the initial set of candidate locations.

$$TSI_j = \sum_{k=1}^{T_k} W_k \left[\sum_{i=1}^{N} W_{bi} \left[\frac{\partial V_i}{\partial Q_j} \right]_{t=t_k} \right] \qquad (2.14)$$
$$W_k \in [0,1],\ W_{bi} \in [0,1]$$

2.5.2 Singular value decomposition

For finding the relative importance between the initial set of candidate locations singular value decomposition (SVD) method is utilized. Singular value decomposition is a method for identifying the direction along which the inputs exhibit the most variation. This method transforms correlated variables into a set of uncorrelated ones that better expose the various relationships among the original data items in the sensitivity matrix. By performing singular value decomposition on the sensitivity matrix ($\frac{\Delta V}{\Delta Q}$), the high dimensional, highly variable set of data points can be reduced to lower dimensional space that clearly exposes the substructure of the original data and orders it from most variation to the least. SVD analysis provides the direction information of the inputs and how it affects the outputs.

The sensitivities computed at specified time instants in the trajectory sensitivity analysis considers reactive power injection at a specified location and does not account for the cross coupling effect from other buses. In order to account for reactive power injections at different locations, sensitivity matrices are formed with the use of trajectory sensitivities at specified time instants as shown in (2.15). SVD analysis will provide the weights W_i in (2.2).

$$\begin{bmatrix} \Delta V_1 \\ \vdots \\ \Delta V_i \\ \vdots \\ \Delta V_n \end{bmatrix} = \begin{bmatrix} \frac{\partial V_1}{\partial Q_1} & \cdots & \frac{\partial V_1}{\partial Q_j} & \cdots & \frac{\partial V_1}{\partial Q_m} \\ \vdots & \cdots & \vdots & \cdots & \vdots \\ \frac{\partial V_i}{\partial Q_1} & \cdots & \frac{\partial V_i}{\partial Q_j} & \cdots & \frac{\partial V_i}{\partial Q_m} \\ \vdots & \cdots & \vdots & \cdots & \vdots \\ \frac{\partial V_n}{\partial Q_1} & \cdots & \frac{\partial V_n}{\partial Q_j} & \cdots & \frac{\partial V_n}{\partial Q_m} \end{bmatrix}_{(t=t_k)} \begin{bmatrix} \Delta Q_1 \\ \vdots \\ \Delta Q_j \\ \vdots \\ \Delta Q_m \end{bmatrix} \tag{2.15}$$

Singular Value Decomposition performed on the sensitivity matrix, $\mathcal{S}$ decomposes it to scaling matrix (Σ) and output ($\mathcal{U}$) and input ($\mathcal{V}$) direction matrices. The most efficient input direction, D, is found using (2.16), which is then used to define the weights of each candidate location. Since the optimization is formulated as a minimization problem, least cost (weight, W) is assigned to the most influential location.

$$\begin{aligned} &\mathcal{S} = \mathcal{U}\Sigma\mathcal{V}^*, \mathcal{U} \in \mathbb{R}^{m\times m}, \Sigma \in \mathbb{R}^{m\times n}, \mathcal{V} \in \mathbb{R}^{n\times n} \\ &D = \mathcal{V}_{i,t} \mid i \in \max(\sigma_{i,t} \left\|\mathcal{U}_{i,t}\right\|_1), \forall t \in [t_c, t_{\text{final}}], \\ &\text{Candidate locations weight}, W \propto \frac{1}{D}, W \in \mathbb{R}^n \end{aligned} \tag{2.16}$$

2.5.3 Linear programming for initialization

$$\begin{aligned} \underset{Q_j}{\text{minimize}} \quad & f_{\text{LP}} = \sum_{j=1}^{N_j} s_j(t) Q_j \\ \text{Subject to:} \quad & V_i^{min} \leq |V_i^0(t)| + \sum_{j=1}^{N_j} \frac{\partial |V_i(t)|}{\partial Q_j} Q_j \leq V_i^{max} \\ & Q_j^{min} \leq Q_j \leq Q_j^{max} \\ & |V_i^{min}(t)| = 1.15 |V_i^0(t)| \\ & V_i^{max} = 1.05 p.u \end{aligned}$$

Instead of arbitrarily guessing a starting point, using the results from a LP approach as a starting point for the NLP program, results in a more reliable and efficient convergence to the final optimal solution. In the LP problem, as shown in (2.5.3), the objective function to be minimized is the total injected reactive power with constraints on the voltage level and SVC

size. The trajectory sensitivities, $s_j(t)$, are used as weights in the objective function of the LP problem.

At each time step the optimization function will calculate the least required amount of VAr injection needed to increase the voltage level by 15% above its uncompensated value ($V_i^0(t)$) for each load bus. The value of 15% increase was chosen to minimize the number of unsolved (infeasible) cases in the optimization procedure and it also provides a reasonable recovery rate for voltage levels at load buses.

$$Q_T = \frac{\sum_{k=1}^{N_k} [\frac{Q_j}{f_{\mathrm{LP}}(Q_j)}]_{t=t_k}}{N_k} \tag{2.17}$$

In order to achieve one set of optimal VAr locations a weighted averaging procedure, given in (2.17), is used with higher weights associated with critical time instants. Critical time instants refer to the time instants following the fault clearing time when the voltage levels are at their lowest point. The averaged reactive power injection values Q_T is used as an input for the CVP approach.

2.6 Simulation Results

The study results based on IEEE 162 bus system and a large scale realistic system in the U.S. are provided in this section. The power system dynamics are solved using PSS/E and the optimization is performed using KNITRO, a third party library available in MATLAB [33]. The interior point algorithm with the finite difference gradient method is used in the NLP optimization algorithm. The application programming interface between the power system DAE solver and the optimization solver is made using PYTHON.

2.6.1 IEEE 162 bus system

The 162 bus system has 17 generators, 111 loads, 34 shunts, and 238 transmission lines [34]. The total generation is 15,546 MW, while the total load is 15,387 MW. This test case consists of one area and twelve zones.

In order to select the most severe credible contingency, several three-phase faults were applied at several 345 kV buses located near major load centers, and the voltage dips at the 69 kV load buses were monitored. These faults were cleared after 6 cycles by opening a 345 kV line. Any bus whose voltage level dips below 50% of its initial level for 0.1 seconds or more is referred as affected bus. The reason for selecting this criteria is that the voltage dip of 50% or more at a load bus for at least 0.1 seconds will likely stall the running motors. The criteria for selecting the most severe contingency are the magnitude of voltage dips at load buses, and the number of affected buses by that contingency. After the performance of contingency analysis, a three phase fault on bus 120 which is cleared by opening the line bus 120-5 after 6 cycles is found to be one of the severe contingency. This contingency has resulted in violations at 12 load buses as shown in table 2.1. For a more accurate load representation, the 12 load buses that are severely affected by the severe contingency were stepped down through distribution transformers to the 12.47 kV level, and the new low voltage buses were assigned the numbers 163 through 174.

Table 2.1: Voltage violation buses along with added new low voltage buses.

Bus number	Load MW	Low-Voltage Bus
111	66.41	163
133	30.1	164
134	17.46	165
135	20.06	166
136	20.06	167
137	20.06	168
139	10.1	169
140	13.58	170
143	21.07	171
144	12.37	172
145	10.83	173
146	21.33	174

Time domain simulation with proper load modeling considerations is required to capture the FIDVR problem. For the severe contingency case in IEEE 162 test system (Bus fault 120), without the representation of air conditioner motor loads the problem of delayed voltage recov-

ery is not even observed as shown in fig. 2.10. Without the representation of induction motor loads, the voltage magnitude at the representative load buses recovered almost instantaneously despite the large disturbance which caused a significant voltage dip.

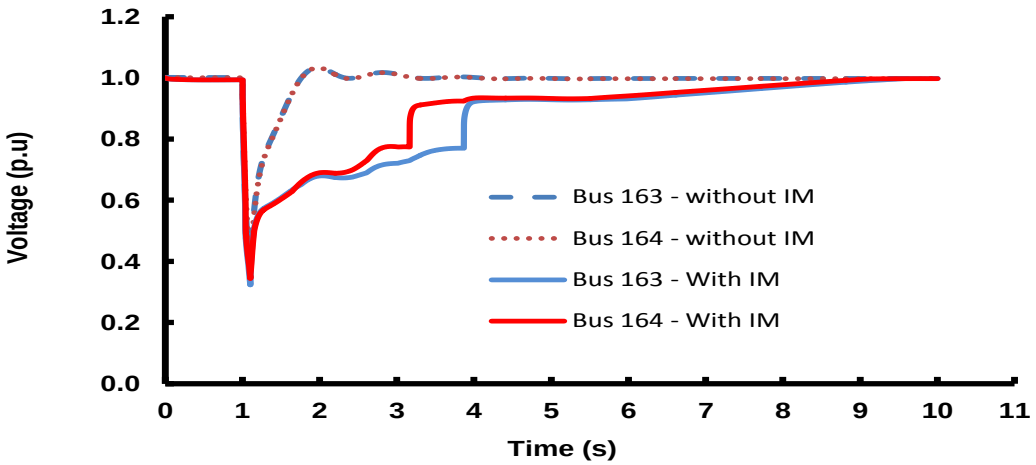

Figure 2.10: Voltage responses with and without induction motor representation

To capture the dynamic behavior of motor loads, a composite load model represented by CMDL was used at the new representative load buses in the dynamic simulation studies. The percentage of three-phase motors driving constant torque loads is 7.2%, three-phase motors driving torque speed-squared loads with high inertia is 7.2% and single phase air conditioner load is 45%. Table 2.2 provides the parameters for single phase induction motor models used. The parameters of three phase large and small motors are taken from Table II in [25].

Table 2.2: Single phase induction motor parameters

Description	Variable	Parameter Value
Compressor motor stall resistance	Rstall	0.124
Compressor motor stall reactance	Xstall	0.114
Compressor stall voltage	Vstall	0.7
Stall Delay (sec)	Tstall	0.33
Fraction of restartable motor	Frst	0.8
Restart Voltage	Vrst	0.7
Restart Delay (sec)	Trst	0.6

With the representation of dynamic behavior of induction motor loads such as decelerating and stalling, the phenomena of delayed voltage recovery is observed at those load buses and is shown in Fig.2.11. The right axis of Fig.2.11 corresponds to the reactive demand of aggregated AC units at the representative load buses. Since the voltages did not recover above 0.70 p.u within 20 cycles the single phase induction motors at the representative load buses stalls, which increases their reactive power demand. If the reactive power demanded from the system is high for a longer period of time, then the recovery of bus voltages becomes slower.

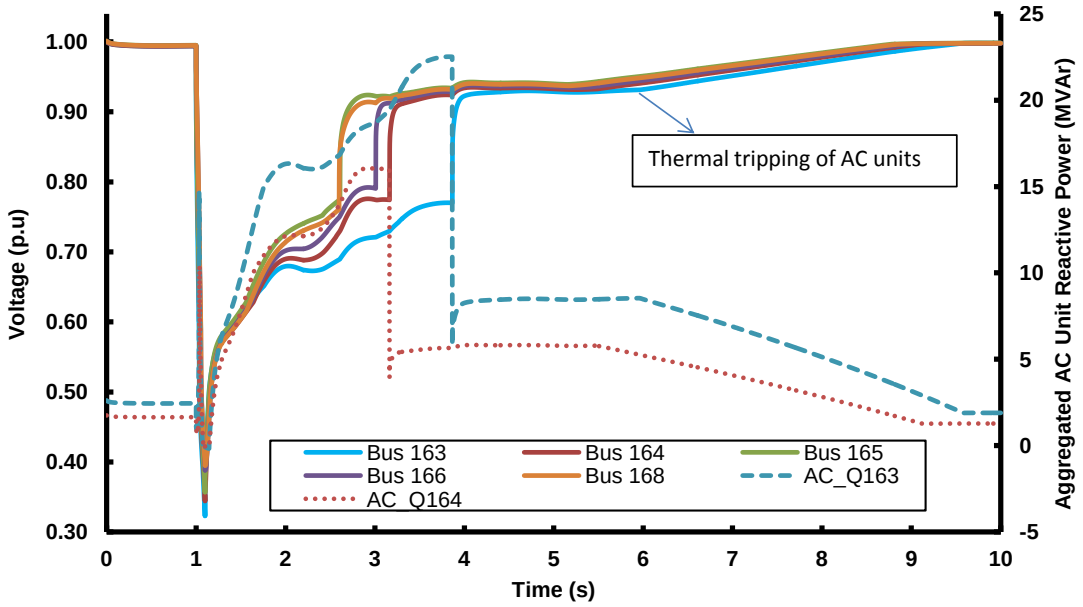

Figure 2.11: Representative load buses voltage responses without SVC and aggregated AC units reactive demands for a three phase fault at Bus 120

From Fig.2.11 it can be observed that the recovery of voltage at bus 163 is slower than that of at bus 164 because the reactive demand of AC units at bus 163 is higher than that of bus 164. The reactive demand of aggregated AC unit at bus 163 increases from 2.5 MVAR to a maximum of 22.5 MVAR, whereas at bus 164 it is increased from 1.7 MVAR to 17.5 MVAR because of stalling of induction motors. Once the voltage recovers above the restart voltage of 0.7 p.u and after a restart delay of 0.6 seconds, the stalled motors capable of restarting returns to normal run state. This reduces the reactive demand of the aggregated AC units. The portion of the motors which are not capable of restarting are eventually tripped by thermal protection.In order to obtain a comprehensive solution and to test the optimization process over

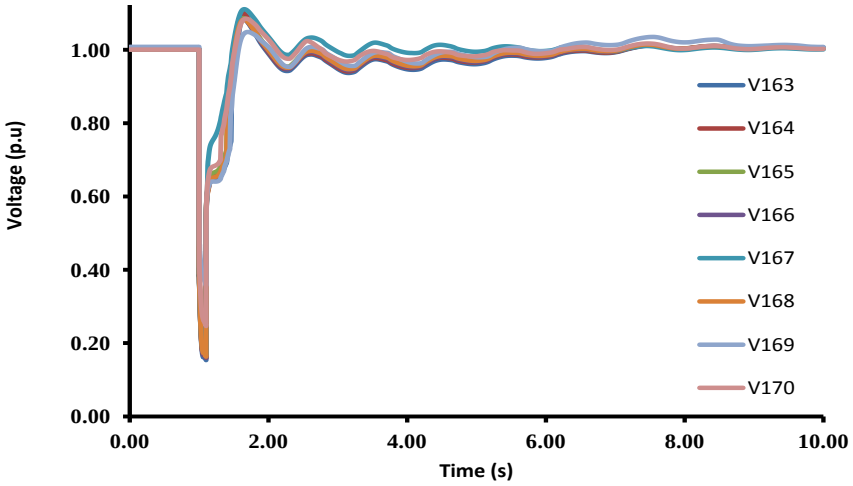

Figure 2.12: Voltages at representative load buses with SVC for three phase fault at Bus 120

several buses with different sensitivities, all the high voltage buses which are directly connected to the representative low voltage load buses are considered as initial candidate buses for VAr injection in the optimization process. Trajectory sensitivities are calculated numerically using finite differences and are used in the formation of sensitivity matrices and also in the calculation of TSI. Trajectory sensitivity index, as reported in column 2 of Table 2.3, identifies the locations sensitivity to reactive power injections. The best combination of locations for the injection of reactive power is identified by the singular value decomposition method. The SVD direction in column 3 of Table 2.3 is used to weight the objective function of dynamic optimization problem.

Table 2.3 summarizes the sensitivity analysis results and the final optimized VAr injection values from LP and two NLP cases. The column 'Bus' represents the candidate locations chosen for SVC installations. The locations are chosen based on the trajectory sensitivity analysis and the trajectory sensitivity index for the candidate locations are provided in the column TSI index. In order to find the relative importance of the chosen candidate locations, SVD analysis is used. The information provided in SVD direction column is used to define the weights W_i of the non linear programming objective function (2.2).

The column 'Max Bsvc' shows the maximum amount of SVC required at the candidate locations obtained using different approaches (a) Linear programming (b) NLP with random initialization (c) NLP using LP results for initialization. Case A corresponds to random ini-

Table 2.3: Results Summary - IEEE 162 bus system

Bus	TSI Index	SVD Direction	Max Bsvc (p.u)		
			LP	Dynamic Optimization	
				Case: A	Case:B
111	39.23	0.1775	0.591	0.7696	0.2252
133	79.80	0.3516	1.486	0.8015	1.2125
134	41.37	0.1852	1.506	0.796	1.0006
135	90.43	0.3587	0.821	0.8034	0.5758
136	92.73	0.3500	0.034	0.701	0.0000
137	94.53	0.3658	0.114	0.8052	0.0253
139	87.54	0.3562	0.06	0.8087	0.7336
140	94.70	0.3646	0.054	0.8057	0.7390
143	136.73	0.2297	0.059	0.7913	0.6112
144	105.43	0.3118	0.194	0.7932	0.0559
145	114.09	0.2967	0.03	0.806	0.6874
146	140.84	0.2243	0.061	0.78	0.6034
Total			**5.011**	**9.4616**	**6.4699**

tialization where reactive power injections at all locations are initialized with a value of 1 p.u. so that the NLP optimization is started within a feasible region. For case B, the initial amount of VAr injections at each locations are identified using the linear programming approach.

The optimal SVC values obtained from dynamic optimization make sure that all the load bus voltages recover above 0.7 p.u within 20 cycles, which is the criterion used in the optimization procedure. The voltage response at the representative load buses with the use of SVC values obtained from the case B dynamic optimization procedure is shown in Fig.2.12. With the optimal dynamic VAr support induction motors run without stalling and the voltage recover faster once the fault is cleared.

2.6.2 Performance evaluation

2.6.2.1 Comparison of DO with LP based methods

The performance of dynamic optimization results is compared against those that of the LP based results in the IEEE 162 bus system. In [7], evaluation of an under voltage protection scheme to take the stalled air conditioner loads off line to prevent slow voltage recovery is

provided. A similar under voltage scheme based on the WECC performance criterion is used to test the efficiency of LP and dynamic optimization solutions. The test criterion used for the performance evaluation is when the voltage at a particular load bus drops below 70% of its nominal value for more than 0.5 sec then 50% of air conditioning loads at that bus are tripped. Based on this criteria, Table 2.4 shows the amount of load tripped when LP and dynamic optimization solution results are used to set the maximum SVC limits. In the case where weighted LP solutions are used, it was observed that 72.52 MW of load is tripped by the under voltage relay action. In the case where dynamic optimization solutions are used, no load is tripped by the under voltage relay action. This shows that dynamic optimization based approach is effective in mitigating FIDVR problems and able to achieve satisfactory voltage performance criteria.

Table 2.4: Performance of LP and Dynamic optimization results - 162 bus system

Weighted LP		
Bus	Load Shed	
	Real (MW)	Reactive (MVAR)
164	6.64	6.1
165	6.92	6.36
166	6.61	6.08
167	3.7	3.4
168	4.72	4.34
169	6.85	6.3
171	6.4	5.89
173	21.75	20
Total	**72.52**	**66.68**
Dynamic Optimization No Load Trip		

2.6.2.2 Comparison of DO with steady state based methods

Several tests were performed on IEEE 162 bus system in order to show the need for dynamic analysis methods and show comparison with steady state based approach used in [20]. Preventive Security Constrained Optimal Power Flow (PSCOPF), available in PSS/E, is used to perform the detailed OPF analysis for the purpose of identifying reactive deficient locations. All the contingencies in zone 3, where majority of loads are present, is considered for the analy-

sis. The contingency B120-5, belong to this particular zone. Though only one contingency was considered for providing the proof of concept for CVP approach, a total of 37 contingencies in zone 3 are considered for the PSCOPF analysis. From the base case simulations, it was found that even considering all 37 contingencies there were no steady state voltage violations and no shunt compensation was needed. However with the base case setup when time domain analysis with detailed load modeling is performed for the contingency B120-5 the problem of FIDVR has been observed. Further simulations were carried out for making a comparison between the locations identified by steady state based approach and our proposed method based on dynamic optimization. In order to identify the reactive deficient locations using OPF methods, the system was stressed and the PSOPF analysis was repeated again. The locations identified by this analysis as opposed to those found using our approach are provided in the table 2.5.

Table 2.5: Locations identified using steady state and dynamic methods

OPF	Trajectory Sensitivity
105,111	111, 133, 134, 135,
122, 143	136, 137, 139, 140
173	143, 144, 145, 146

For the contingency B120-5, even after placing large SVC, as high as 5 p.u, at all the locations identified using OPF analysis, still the problem of FIDVR persisted which can be noticed in fig.2.13. Figure 2.14 (same as Fig.2.12) shows the voltage responses at the representative load buses with the use of dynamic VAr obtained from the dynamic optimization procedure. The locations identified by steady state methods are not enough and ideal for mitigating the FIDVR problem. This example shows the insufficiency of steady state based methods to identify the locations for placing dynamic VARs.

2.6.3 Large scale realistic system

In this section, the curse of dimensionality posed by direct simultaneous method and the scalability of proposed CVP approach to a large scale realistic system are presented. The large power system that has been considered for analysis has 14043 buses excluding the low voltage feeders, with a total generation of 135.5 GW coming from 2950 generators. The overall

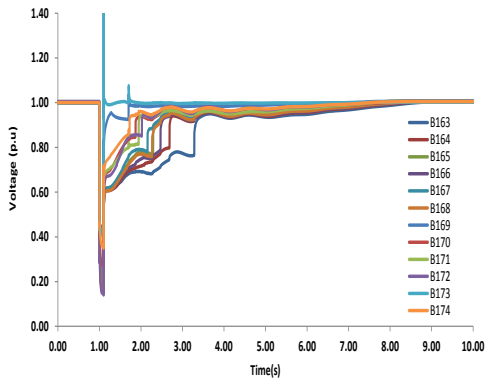

Figure 2.13: Voltages at representative load buses with SVCs at locations provided by OPF

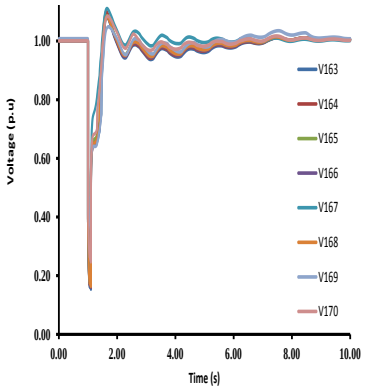

Figure 2.14: Voltages at representative load buses with SVCs at locations provided by dynamic optimization

system components and the components of subsystem under study are shown in Table 2.6. The subsystem or study area refers to the region where the voltage stability study is focused.

Table 2.6: Components of overall system and study area

Overall System		Study Area	
Component	Number	Component	Number
Buses	14043	Buses	948
Plants	2310	Plants	409
Generators	2950	Generators	1140
Shunts	1366	Shunts	361
Lines	11655	Lines	613
Transformers	5023	Transformers	461
Phase Shifters	41	Phase Shifters	0
HVDC Converters	8	HVDC Converters	0

For the considered system, with direct simultaneous method, the number of non-linear equations after the discretization process will be very large. For example, if we consider only the dynamics of generator with 4^{th} order model, there will be 11800 (=2950 X 4) equations. For a 5 second simulation period, even a very coarse step of 0.1 is used for discretization, the resulting number of non-linear equations will be 590 thousand equations. The typical time step used for power system dynamic simulation is 1/2 of a cycle (0.0083s) or even smaller than this when induction motor loads are considered. With the addition of dynamic equations of load models, SVC's and other system equations will lead to millions of discretized non-linear equations. Solving these huge set of non-linear equations along with the optimization constraints will quite

often lead to infeasibility using the direct simultaneous approach. However, our proposed CVP approach overcomes this curse of dimensionality by separating the solution of power system dynamics and utilize the results of dynamics in optimization formulation. The scalability of the CVP approach to large scale system is shown by applying this method to the most critical contingency.

The contingencies are screened for bus violations of 1.05 p.u for upper limit and 0.95 p.u for lower limit. From the full set of contingencies considered, the contingencies that created the largest number of voltage violations are considered to be critical, and if the power flow does not converge, then it is considered to be a case of voltage collapse. For the considered N-1 contingencies, there are no cases of voltage limit violations. Therefore N-2 contingencies are considered and the most critical contingency is a double line contingency at the 500 kV level. This outage is considered to be feasible since the two lines share a common right of way at a certain location. This contingency is simulated by creating a three phase fault at around 40% of one of the 500 kV lines where the probability of fault occurring is high. The fault is applied at 0.1 second and cleared after four cycles by removing two 500 kV lines.

A significant portion of the total load in the system under study during summer peak is air conditioning load. These loads should be properly modeled in order to reflect the transient behavior of the motors during the disturbance. This has been done by including a detailed load modeling consisting of induction motor loads and static loads in the dynamic data. Within the study area 372 loads are represented on the 12.5 kV end of the 69/12.5 kV substation transformer. Each of these load representation includes static loads (28%) and three types of induction motors (72%) namely large motors, small motors and trip motors. The induction motors classification is based on the inertia and ability to trip under low voltage conditions. The approximate constitution of large motors, small motors and trip motors are 10%, 60% and 30% of the total motor load at each load bus. The induction motors are represented using 'CIMTR4' model available in PSS/E software.

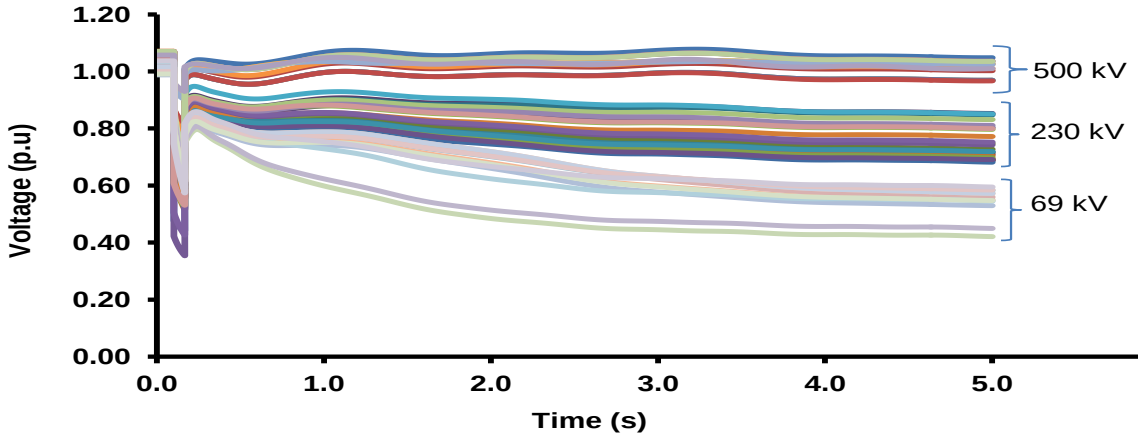

Figure 2.15: Base case bus voltage responses at different kV levels for the realistic power system

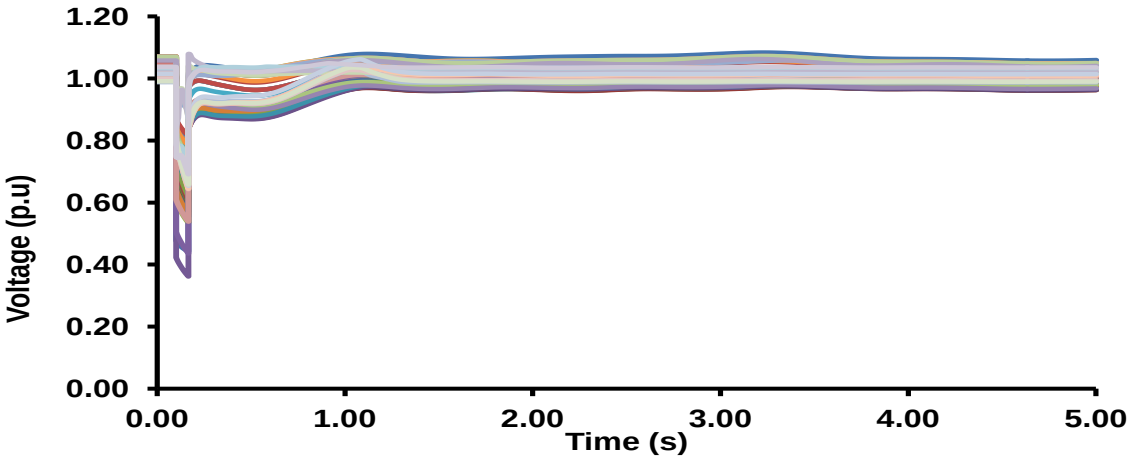

Figure 2.16: Plot of bus voltages at different KV levels with VAR injection from NLP with LP solution initialization.

Figure 2.15 shows the base case voltage responses of buses at different kV levels for the most severe contingency. It can be observed that the fall in voltage level is more pronounced at the 69 kV buses. In order to obtain a comprehensive solution and to test the optimization process over several buses with different sensitivities, the voltage sensitivities of several 230 kV buses that are close to load centers were evaluated. However, since reactive power compensation is more economically feasible on sub-transmission voltage levels, twelve 69 kV buses that are connected to the most sensitive 230 kV buses were selected for dynamic VAR injection.

Trajectory sensitivities are calculated using finite differences and are used in the formation of sensitivity matrices and also in the calculation of TSI. Trajectory sensitivity indices as reported in Table 2.7, identify the 69 kV bus location sensitivities to reactive power injections. The best combination of locations for the injection of reactive power is identified by the singular value decomposition method. The SVD direction in Table 2.7 is used to weight the objective function of the dynamic optimization problem.

Table 2.7: Results Summary - Large power system

Bus Key	**TSI Index**	**SVD Direction**	**Max Bsvc (p.u)**		
			LP	**Dynamic Optimization**	
				Case: A	**Case:B**
100	29.56	0.3345	1.100	0.7447	0.8264
101	32.90	0.4292	0.000	1.3480	0.7776
102	30.05	0.3480	1.074	0.8113	0.1216
103	26.65	0.2178	0.353	0.1193	0.7024
104	29.03	0.2391	0.711	0.3874	0.6269
105	26.69	0.2181	0.672	0.3340	0.6850
106	27.86	0.2268	0.699	0.3646	0.2681
107	31.32	0.2598	0.742	0.4342	0.6527
108	25.27	0.2116	0.674	0.3282	0.6917
109	30.72	0.2595	0.720	0.4152	0.0294
110	26.17	0.2188	0.683	0.3436	0.4208
111	26.74	0.3415	1.475	1.1950	0.2478
Total			**6.58**	**6.8254**	**6.0504**

The weighted averaged values of the optimal VAr injection evaluated by the LP optimization process reported in column IV of Table 2.7 is used as a starting condition for case B of the NLP part of the dynamic optimization problem. Case A corresponds to a randomly initialized starting solution. Column V and VI of Table 2.7 shows the final optimized VAr injection values from the dynamic optimization procedure.

Figure 2.16 shows the voltage response of buses at different kV levels (500, 230 and 69) with the final VAr injection obtained from dynamic optimization procedure with LP solution initialization. The voltage magnitude at all the buses satisfy the WECC voltage performance criteria with the use of the final solution from the NLP optimization program.

The results show that using LP results as an initial guess helps to achieve better results in terms of finding reduced amount of dynamic VAr required compared to random initialization of dynamic optimization procedure. With the use of dynamic optimization, the optimal amount of SVC required to satisfy more stringent conditions on voltage recovery such as WECC voltage performance criteria can be found.

2.7 Conclusions

Short-term voltage instability issue is exacerbated by single-phase low inertia motor loads that represent residential A/C systems, since they tend to decelerate and stall when their voltage magnitude drops below a certain level. Motors have an adverse impact on voltage stability because they consume very large amounts of reactive power within a very short time during a large disturbance. Therefore, using fast dynamic VAR injection devices was found to be useful in alleviating reactive power deficiency near load centers throughout this work. With the use of dynamic optimization, the optimal amount of SVC required to satisfy more stringent conditions on voltage recovery such as WECC voltage performance criteria is found. The results shows that using linear programming results as an initial guess to dynamic optimization program helps to achieve better results in terms of finding reduced amount of dynamic VAR required compared to random initialization of dynamic optimization procedure.

CHAPTER 3. CONTINGENCY CLUSTERING BASED ON FIDVR CHARACTERIZATION

3.1 Introduction

During planning studies due to large number of possible system variations, covering all combinations is very challenging due to its intense computational effort. Direct extension of the CVP approach (2) to handle multiple contingencies will lead to a very large scale problem. To reduce the complexity of this problem, a systematic framework using clustering methods to identify the most important contingencies that act as a representative of group of similarly behaving contingencies. The clustering approach is further extended to group representative contingencies under multiple operating conditions and scenarios. Since the focus of this work is short-term voltage problems, in particular fault-induced delayed voltage recovery (FIDVR), voltage response patterns at different buses is used to define the similarity between contingencies. For comparison of voltage waveforms and its quantification, Kullback Liebler (KL) measure, a novel entropy-based metric is formulated to characterize voltage recoveries. First, the clustering-based approach to identify severe contingencies for a given operating condition is presented. Then the framework is extended to select the representative contingencies from a wide range of operating conditions and scenarios. Simulations have been performed on the modified IEEE 162 bus system to demonstrate and validate the clustering procedure based on FIDVR characterization.

3.2 Motivation and Proposal

Contingency analysis is an important tool used to assess the security of the system under topological changes and component failures. It has been an integral part of power system

planning and operations [35],[36]. The power system undergoes variations in terms of loads, generation and system configurations. Among large number of possible system load variations and contingencies, only a limited number is chosen for analysis using time domain simulations mainly due to intense computational effort. In the planning studies, analyzing all possible contingencies is a computationally challenging problem because of large number of possible system variations. Contingencies must be carefully chosen to cover a wide range of possibilities, while ensuring system security. For reducing the number of contingencies if the most severe contingencies are considered, then there is a possibility of relatively less severe contingencies creating problems in different regions of the system. In order to select a comprehensive list of contingencies that affects different regions of the system, a clustering based approach is proposed in this work. The motivation behind the clustering based contingency analysis is the nature of the FIDVR problem. While the disturbance leading to FIDVR problems may be initiated by different kinds of contingencies, the underlining problem is an inherent weakness in the power system (lack of dynamic VAR support). If the contingencies that exposes same weakness in the system, over certain operating conditions and scenarios, are grouped together then instead of considering all contingencies only severe contingencies in each group acts a representative for all other contingencies in their respective groups. If contingencies can be grouped together based on their similarity in behavioral patterns, then the number of contingencies that has to be considered for analysis can be significantly reduced. A two level clustering process is developed to reduce the number of scenarios, operating conditions and contingencies to be analyzed in the power system planning process. Level 1 clustering groups contingencies at a given operating condition based on their similarity in voltage responses at different buses and level 2 clustering identifies the representative contingencies under various operating conditions and scenarios based on the similarity between level 1 clusters. In order to compare the responses of different contingencies, a quantitative measure that characterize the voltage response is needed.

There are two important factors in the voltage recovery process: (1) rate of recovery (how fast the waveform converges) and (2) level of recovery (the voltage level it converges). The WECC voltage performance criteria is a point-wise condition on the voltage waveform. It can only be inferred whether or not the waveform satisfies the WECC criterion. It cannot be used

to compare quantitatively the recovery nature of several waveforms. The slope or integral-based methods have limitations to quantify the voltage recovery as an index for comparison. Currently there are no quantitative measures, which can take both rate of recovery and steady state settling value of voltage time series into account, while characterizing the voltage for FIDVR phenomenon. Therefore, to encompass both the rate and the level of recovery, the KL divergence, an entropy-based measure of the distance between distributions is derived. KL measure collapses the temporal and magnitude information in voltage time series into a scalar quantity, which forms the basis for comparing different voltage recoveries.

3.3 Characterization of FIDVR

In this work, the entropy, a popular measure of complexity and uncertainty in the signal processing and information theory [37], and time-series analysis [38], is used to characterize the voltage response. The notion of entropy used in this work is from a signal processing perspective as opposed to system perspective. This notion of entropy is not same as the one used in statistical mechanics or dynamical systems literature, where the entropy is defined with respect to probability distribution left invariant under the system dynamics [39, 40].

A method for constructing a probability density function from given voltage time-series data over a finite time interval is used in this work. The entropy is computed for this probability density function, which is then used to characterize the recovery rate of the voltage waveform. The basic idea is the following. If the voltage recovers very quickly to its steady state value, then the corresponding probability density has a high peak near the steady state value, due to the high concentration of the voltage samples at this value. This makes the behavior of the voltage waveform less uncertain. As a result, the entropy of the density function corresponding to fast recovery is low. The opposite holds true when the voltage recovers slowly. Therefore, the entropy for the density function corresponding to slower recovery is high. This observation makes it possible to use entropy as a quantitative measure of the rate of recovery.

3.3.1 Computation of density function from time-series data

It is important to emphasize the criteria as specified by the WECC voltage performance criterion, involve both temporal and magnitude information of the voltage time-series data. WECC voltage performance criteria involve information where it is required for the voltage magnitude to have reached certain values within a particular time interval. These two (temporal and magnitude) pieces of information can be combined with the help of density function. Mathematically speaking, the density function, $p : X \to \mathbb{R}$, is any nonnegative scalar value function with a finite integral. Furthermore, the density function is said to be a probability density, if the integral of the function over X is equal to one, i.e.,

$$p(x) \geq 0, \quad \text{and} \quad \int_X p(x)dx = 1. \tag{3.1}$$

Next, the procedure for the construction of the approximation density function, p, from the voltage time-series data is discussed. Consider voltage time-series data where a fault occurs at $t = T_0$ and is cleared at $t = T_{cl}$. The bus voltage, $v_{\min} < v(t) < v_{\max}$, is observed from the time instant, $t = T_{cl}$ to $t = T_f$. $v_{\min}$ is the voltage level at the time instant when the fault is cleared and $v_{\max}$ is the nominal value before the fault (e.g., 1 pu). The interval $(v_{\min}, v_{\max})$ is divided into N intervals, such that

$$[v_{\min}, v_{\max}) = \bigcup_{i=1}^{N} [v_i, v_{i+1}) = \bigcup_i D_i. \tag{3.2}$$

The time spent by the trajectory in the interval $[v_i, v_{i+1})$ is denoted as Δt_i and defined as,

$$\Delta t_i := \int_{T_{cl}}^{T_f} \chi_{[v_i, v_{i+1})} \left(v(t)\right) dt, \tag{3.3}$$

where $\chi_A(x)$ is the characteristic function of set A,

$$\chi_A(x) = \begin{cases} 1 & \text{for} \quad x \in A \\ 0 & \text{otherwise.} \end{cases} \tag{3.4}$$

$$p_i := \frac{\Delta t_i}{T} = \frac{1}{T} \int_{T_{cl}}^{T_f} \chi_{[v_i, v_{i+1})} \left(v(t)\right) dt. \tag{3.5}$$

It can be verified the sum of p_i over index i adds to one, i.e.,

$$\sum_{i=1}^{N} p_i = \frac{1}{T}\int_{T_{cl}}^{T_f} \sum_{i=1}^{N} \chi_{[v_i, v_{i+1})}\left(v(t)\right) dt = \frac{1}{T}\int_{T_{cl}}^{T_f} 1 dt = 1.$$

The p_i for $i = 1, \ldots, N$ can now be used to approximate the probability density function, $p(x)$, from Eq. (3.1).

In particular,

$$\tilde{p} := (p_1, \ldots, p_N), \tag{3.6}$$

is an approximation to $p(x)$, where the approximation essentially involves discretization of the space X into intervals D_i (3.2). Furthermore, in the limit as $N \to \infty$, the $\tilde{p}$ will converge to p in a weak sense.

3.3.2 Relationship between entropy and rate of recovery

This section discusses the relationship between entropy and the rate of recovery of the voltage waveform.

Definition 1 (Entropy) *The entropy corresponding to a probability distribution function $p(x)$ is defined as follows:*

$$H(p, T) := -\int_X p(x) \ln p(x) dx. \tag{3.7}$$

The entropy corresponding to the approximation, $\tilde{p}$, is defined as

$$H(\tilde{p}, T) := -\sum_{i=1}^{N} p_i \ln p_i. \tag{3.8}$$

Remark 1 *It is to be noted that $p_i \ln p_i$ is taken as 0 for $p_i = 0$, using limit argument.*

Entropy is a measure of uncertainty where larger entropy values imply more uncertainty and vice versa. For example, the entropy corresponding to uniform probability distribution will be maximum and one corresponding to a Dirac delta distribution (where the probability mass is concentrated at a single point and, hence, certain) will be 0, the minimum. For a given voltage waveform, if the voltage magnitude recovers fast, then, it converges to the nominal value quickly. The probability density function computed using the procedure outlined in Section 3.3.1 will

be concentrated closer to the nominal value and, hence, will correspond to a smaller value of entropy. On the other hand, if the voltage magnitude recovers slowing to its nominal value, then, the density function corresponding to such a recovery will be more dispersed and, hence, will lead to a larger value of entropy. So, the entropy can be used as a measure of voltage recovery, where larger values of entropy correspond to a slower recovery and vice versa.

Although entropy serves as a good measure for the rate of recovery, it is insensitive to the final steady-state value of bus voltage. In particular, if the two voltage waveforms recover at the same rate, but converge to two different steady state values then the entropy values will be the same for both cases. However, given the fact these waveforms converge to two different steady-state values, it is desirable that the metric used to characterize the voltage response has the ability to differentiate such cases.

3.3.3 Kullback-Leibler divergence for joint characterization of rate and level of recovery

KL divergence, also known as relative entropy, is a popular measure of distance used in statistics and information theory. It is used to capture the difference between information contained in two different probability density functions and is defined as follows:

Definition 2 *The Kullback-Liebler divergence or relative entropy between two probability density functions, $p(x)$ and $q(x)$, is denoted by $D(p \parallel q)$ and is given by the following formula*

$$D(p \parallel q) = \int_X p(x) \ln \frac{p(x)}{q(x)} dx. \tag{3.9}$$

KL divergence is always non-negative and, zero if and only if, $p = q$. However, it is not a true distance between two density functions, because it is not symmetric and does not satisfy triangular inequality. However, it is convenient to think of KL divergence as a distance between two density functions.

The KL divergence will be used for the purpose of characterizing the rate as well as the level of recovery of the voltage signal. Towards this goal, first a probability density function, $p^{ref}(x)$, corresponding to reference voltage recovery is defined. The reference density function

will correspond to a voltage waveform, which will recover instantaneously to a nominal voltage value, say v_{nom}, following a fault. Hence, p^{ref}, will be a Dirac-delta function with all its mass concentrated at $x = v_{nom} = 1$ p.u. However, strictly speaking, the Dirac-delta function does not qualify the definition of probability density function and, hence, the following approximation for the ideal probability density function is used.

$$p^{ref}(x) = \hat{Z}^{-1} e^{-\Lambda(x-v_{nom})^2}, \quad \hat{Z} = \int_X e^{-\Lambda(x-v_{nom})^2} dx, \tag{3.10}$$

where, $\hat{Z}$ is the normalization constant, introduce to ensure that $\int_X p_{ideal}(x)dx = 1$. The positive parameter, $\Lambda > 0$, controls the concentration of the density near $x = v_{max}$. For a large value of λ, more mass is concentrated near $x = v_{nom}$. Now let $p(x)$ be the probability density function corresponding to a particular voltage waveform with a given recovery. The objective is to compare the "distance" between $p(x)$ and $p^{ref}(x)$ using KL divergence i.e., $D(p \parallel p_{ref})$ to determine the recovery. The KL divergence will capture not only the rate but also the level of recovery. The finite dimensional approximation of the KL divergence formula is given in 3.9. Let $\tilde{p}$ and $\tilde{p}_{ref}$ be the finite dimensional approximations of the density, $p(x)$, and $p^{ref}(x)$, respectively and of the form

$$\tilde{p} = (p_1, \ldots, p_N), \quad \tilde{p}^{ref} = (p_1^{ref}, \ldots, p_N^{ref}). \tag{3.11}$$

where, $\tilde{p}$ is constructed using the procedure outlined in Section 3.3.1, and,

$$\begin{aligned} p_{\text{ref},i} &:= \frac{e^{-\lambda(y_i - v_{\text{nom}})^2}}{Z}, \ i = 1, 2...N \\ Z &= \sum_{i=1}^{N} e^{-\lambda(y_i - v_{\text{nom}})^2} \end{aligned} \tag{3.12}$$

y_i refers to the i^{th} partition of the voltage axis and it corresponds to the voltage level v_i. The parameter λ controls the width of the reference probability distribution, which is concentrated around the nominal voltage level, v_{nom}. The normalizing factor Z, makes the summation of the reference distribution equals 1. The finite dimensional approximation of KL divergence is defined as follows.

Definition 3 *The KL divergence between $\tilde{p}$ and $\tilde{p}^{ideal}$ is denoted by $\mathcal{K}$ and defined as follows :*

$$\mathcal{K}(p||p_{ref}) = \sum_{i=1}^{N} p_i \ln \frac{p_i}{p_{ref,i}} \tag{3.13}$$

The KL divergence could be further simplified to,

$$\mathcal{K} = \ln Z + \sum_{i=1}^{N} p_i \ln p_i + \lambda \sum_{i=1}^{N} p_i (y_i - v_{\text{nom}})^2 \tag{3.14}$$

Now, inspecting (3.14), it can be observed if the recovery is poor, the KL divergence would be higher. If the voltage signal does not recover fast, p_i will be higher for smaller i. The weighting factor $(y_i - v_{\text{nom}})^2$ would be more for smaller i in comparison to larger ones. This would ensure the KL divergence would be more, if the p_i is more for lower voltage levels.

3.3.3.1 Example : Characterization of Voltage waveform using KL measure

The major steps involved in calculating the KL divergence for a sample voltage waveform shown in fig.3.1 (a) are summarized below.

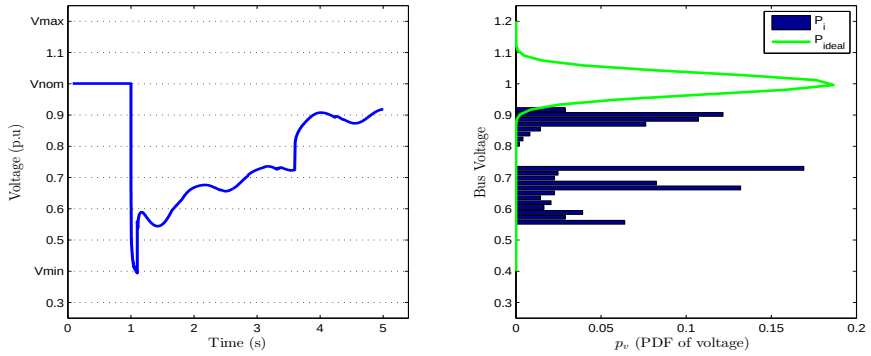

Figure 3.1: (a) Voltage time series (b) Probability density function for the voltage series in part (a) and ideal voltage recovery

Step 1) The voltage axis is partitioned into N subintervals. The voltage samples are observed from fault clearing instant ($t = 1.1s$) to the final observation time ($t = 5s$). The number of voltage samples in each subinterval is counted. This number provides information about the time the voltage waveform is present in a subinterval.

Step 2) The number of samples in a particular subinterval is divided by the total number of samples to obtain the normalized subinterval frequency. This generates the probability density

function of the given voltage waveform. The blue colored bars in Fig. 3.1(b) is the probability density function corresponding to the voltage waveform in 3.1 (a).

Step 3) Construct the probability density function for the reference voltage recovery using (3.12). The P_{ref} in Fig.3.1(b) corresponds to the reference distribution.

Step 4) Calculate the KL divergence measure using (3.13). For the example shown in fig.3.1, the KL value is calculated to be 16.7, which indicates a delayed recovery of voltage.

3.3.4 Critical value of KL divergence

For a general specification of voltage performance as given in (3.15), the KL measure that corresponds to a voltage waveform that traces the voltage envelope is called critical KL value.

$$\begin{aligned} v(t) &\geq V_1,\ T_{cl} \leq t < T_1, \\ v(t) &\geq V_2,\ T_1 \leq t < T_2, V_2 > V_1, \\ v(t) &\geq V_3,\ T_2 \leq t \leq T_f, V_3 > V_2. \end{aligned} \tag{3.15}$$

where, $\Delta T_1 := T_1 - T_{cl}$, $\Delta T_2 := T_2 - T_1$, $\Delta T_3 := T_f - T_2$ and $\Delta T_f := T_f - T_{cl}$. T_{cl} denotes the fault clearing time and T_f denotes the final time period.

If the voltage time series satisfies the performance conditions mentioned in (3.15), then, the corresponding KL divergence satisfies the following upper bound,

$$\begin{aligned} \mathcal{K}^* := &\frac{1}{\Delta T_f}\left(\Delta T_1 \log \Delta T_1 + \Delta T_2 \log \Delta T_2 + \Delta T_3 \log \Delta T_3\right) \\ &+ \frac{\lambda}{\Delta T_f}(\Delta T_1 (V_1 - V^*)^2 + \Delta T_2 (V_2 - V^*)^2 \\ &+ \Delta T_3 (V_3 - V^*)^2) + \log Z - \log \Delta T_f \end{aligned} \tag{3.16}$$

For the voltage bounds specified by the Western Electricity Coordinating council (WECC) voltage performance criteria, the value of KL measure is calculated to be 4.9 considering the parameters $\lambda = 450$ and $N = 50$. A value of KL measure above this critical value signifies violations in the performance criteria. Higher the value of KL measure, more severe the violation of WECC performance criteria at the corresponding bus. When the value of KL measure is below 4.9, it signifies that the voltage signal recovers fast and also settles within the bounds specified by WECC performance criteria.

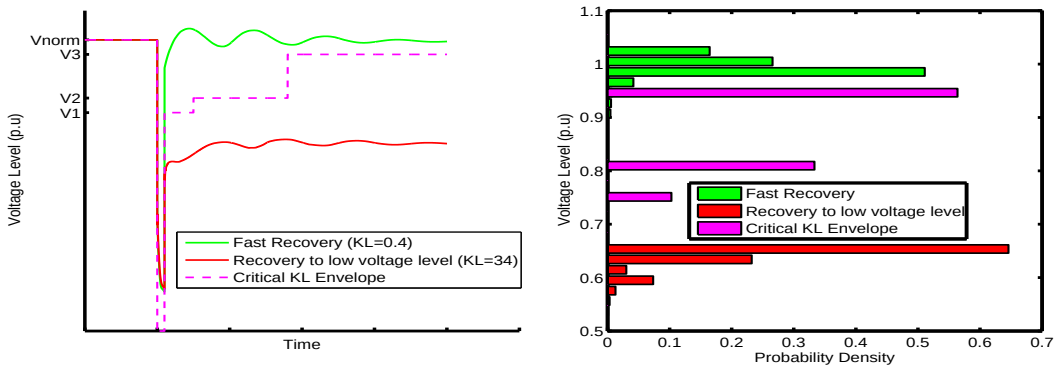

Figure 3.2: (a) Critical voltage performance envelope (b) PDF of voltage responses

A pictorial representation of the voltage performance constraints is shown as dotted lines in fig.3.2.a. Figure 3.2.a also provides a slow and fast recovering voltage waveforms. The PDF corresponding to the voltage responses in Figure 3.2.a are provided in Figure 3.2.b. For the fast recovering voltage waveform the corresponding KL value is 0.4 and for a delayed recovery voltage waveform the KL value is 34, which implies a significant violation in the voltage performance criteria.

In order to validate the characterization of FIDVR by KL measure, the percentage of induction motors in the IEEE 162 bus system is increased from 0 - 45%. As the percentage of induction motor load is increased, the delayed voltage recovery is more pronounced as shown in fig.3.3. Figure 3.4 shows the KL measure for the different percentage of induction motor loads in the IEEE 162 bus system. Higher KL values corresponds to delayed voltage recovery waveforms. The red line in fig.3.4 corresponds to a critical KL value, which is derived based on the WECC performance criteria. If the value of KL is greater than this critical value, then it implies voltage performance violations. On the other hand if the value is less than the critical KL, then there are no violations or in case if there are violations the violations are very small and not severe.

3.4 Clustering of Contingencies

In this section, a framework to classify contingencies into different clusters, according to their behavioral patterns for a given operating condition, in particular, with respect to voltage

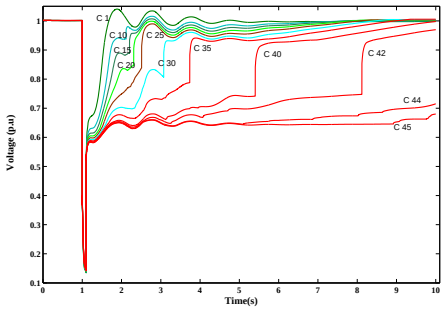

Figure 3.3: Voltage recoveries corresponding to different percentage of induction motor loads. Different labels (starting with letter 'c') corresponds to % of induction motors in the system

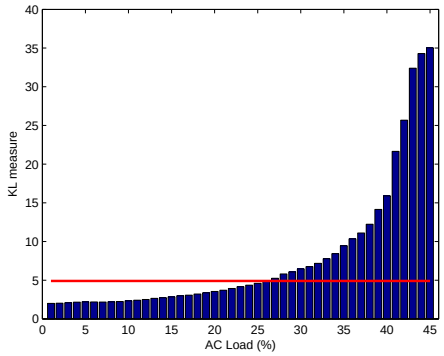

Figure 3.4: KL divergence measure for different percentage of induction motor loads

recovery patterns is presented. The most severe contingency from each cluster becomes the representative of other contingencies in the corresponding cluster. The input set of contingencies, N_C, can be selected based on the operators knowledge about the system, past experiences, most probable contingencies, contingencies of severe type etc. The input set of contingencies are grouped into different clusters for a given operating condition using spectral clustering algorithm. Given a power system with N_B buses and a set of N_C possible N-1 contingencies, the goal is to identify sets of contingencies such that contingencies in the same set would produce similar patterns of response in the system. By utilizing the bus KL numbers, corresponding to different contingencies, the relationship between contingencies is identified using Spearman rank (SR) correlation. The SR correlation values are used to construct the contingency similarity matrix and is provided as an input to the K-means clustering algorithm, which is the clustering engine of spectral clustering algorithm.

3.4.1 Similarity of contingencies

Using the time domain simulation results, KL divergence at each bus is computed for all contingencies and the results are stored in a matrix $\bar{K} \in \mathbb{R}^{N_B \times N_C}$. The element $\mathcal{K}_{ij}$ of the $\bar{K}$ matrix has the summarized information of the voltage time series corresponding to the i^{th} bus and j^{th} contingency in a scalar form. Let U_i and V_j denote the i^{th} row and j^{th} column of $\bar{K}$.

$U_i \in \mathbb{R}^{N_C}$ contains the KL divergence for the i^{th} bus for all contingencies and V_j contains the KL divergence for all buses for the j^{th} contingency.

Numerous measures, such as Euclidean distance, cosine similarity, Pearson and Spearman rank correlation (SC), are available to describe the similarity between two vectors. Euclidean distance yields inconsistent results when the KL vectors corresponding to two contingencies are related by scalar transformations or constant offset. This will provide greater distance between these two contingencies and place them in two different clusters when they are supposed to be in one cluster. Cosine similarity measures the angle between two vectors and is unaffected by scalar transformations of the data. However cosine similarity suffers when there is constant offset between two vectors. Pearson correlation (PC) measures the strength of linear relationship two KL vectors V_{j_1} and V_{j_2} using the formula as shown in (3.17). PC between contingencies j_1 and j_2 is denoted as $\rho^u_{j_1 j_2}$ and is defined using (3.17),

$$\rho^v_{j_1 j_2} := \frac{\sum_{k=1}^{N_B} \left(V_{j_1}(k) - \bar{v}_{j_1}\right)\left(V_{j_2}(k) - \bar{v}_{j_2}\right)}{\sigma_{v_{j_1}} \sigma_{v_{j_2}}},\ j_1 \neq j_2$$

where,

$$\begin{aligned} \bar{v}_{j_1} &:= \frac{1}{N_B}\sum_{k=1}^{N_B} V_{j_1}(k), \quad \sigma_{v_{j_1}} := \frac{1}{N_B}\sum_{k=1}^{N_B}\left(V_{j_1}(k) - \bar{v}_{j_1}\right)^2, \\ \bar{v}_{j_2} &:= \frac{1}{N_B}\sum_{k=1}^{N_B} V_{j_2}(k), \quad \sigma_{v_{j_2}} := \frac{1}{N_C}\sum_{k=1}^{N_C}\left(V_{j_2}(k) - \bar{v}_{j_2}\right)^2. \end{aligned} \tag{3.17}$$

$\bar{v}_{j_1}$ and $\bar{v}_{j_2}$ denotes the mean value of KL vectors corresponding to contingencies j_1 and j_2 respectively. $\sigma_{v_{j_1}}$ and $\sigma_{v_{j_2}}$ represents the standard deviation of KL vectors corresponding to contingencies j_1 and j_2 respectively.

Pearson correlation overcomes the problem of scalar transformations and constant offset but it suffers when there is no linear relationship exists between the two vectors. Spearman rank correlation is a measure of monotone relationship between two vectors. When the KL vectors corresponding to two contingencies are monotonically related Spearman rank correlation will yield a perfect correlation of 1, even if their relationship is not linear. In contrast, Pearson correlation will not yield a perfect correlation when the relationship is not linear. For defining the similarity between the two contingencies it has been found that the SC yields better results

compared to other measures because it measures the monotone relationship between the KL vectors corresponding to different contingencies.

For computing the SC value, first the KL measure of the two contingencies provided in V_{j_1} and V_{j_2} are converted to rank vectors, R_{j_1} and R_{j_2}, respectively. The bus corresponding to the lowest KL value is assigned the least rank (rank 1) and the bus corresponding to highest KL value is assigned the highest rank (rank N). When there are identical KL values in a contingency vector, then a rank equal to the average of their positions in the ascending order of values is assigned to the buses corresponding to rank ties. The rank vectors are used to compute the Spearman correlation using (3.18).

$$\begin{aligned} r_s &:= \frac{\sum_{k=1}^{N_B} \left(R_{j_1}(k) - \bar{r}_{j_1}\right)\left(R_{j_2}(k) - \bar{r}_{j_2}\right)}{\sqrt{\sum_{k=1}^{N_B} \left(R_{j_1}(k) - \bar{r}_{j_1}\right)^2 \sum_{k=1}^{N_B} \left(R_{j_2}(k) - \bar{r}_{j_2}\right)^2}}, \\ \text{where} \bar{r}_{j_1} &:= \frac{1}{N_B}\sum_{k=1}^{N_B} R_{j_1}(k),\ \bar{r}_{j_2} := \frac{1}{N_B}\sum_{k=1}^{N_B} R_{j_2}(k), \end{aligned} \tag{3.18}$$

r_{j_1} and r_{j_2} denotes the mean values of rank vectors corresponding to contingencies j_1 and j_2, respectively.

The Spearman rank correlation, r_s, works on the ranks of two vectors, instead of the actual data provided in the vectors. It takes values between +1 and -1. When r_s takes the value of 1, it indicates a perfect association of ranks between the two contingencies and a value of -1 indicates a perfect negative association of ranks (highest ranked bus in contingency 1 becoming lowest rank in contingency 2 and vice versa). A value of r_s close to zero signifies a weak association between ranks of the two contingencies.

Figure 3.5 shows the scatter plot of KL values for positively correlated contingencies. The Spearman rank correlation value of 0.9986 indicates that contingencies 2 and 64 affect the same set of buses in a similar rank order. A scatter plot of KL values for negatively correlated contingencies is shown in figure 3.6. The buses that are severely affected by contingency 46 are not affected when contingency 55 happens. Similarly, those buses that are severely affected by contingency 55 are not affected when contingency 46 occurs. This negative correlation between contingencies 55 and 46 is captured by the Spearman rank correlation value of -0.376.

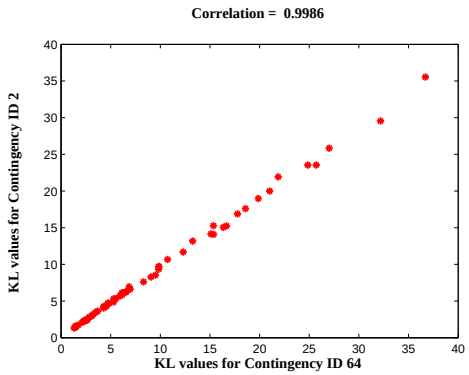

Figure 3.5: Positive correlation between contingencies

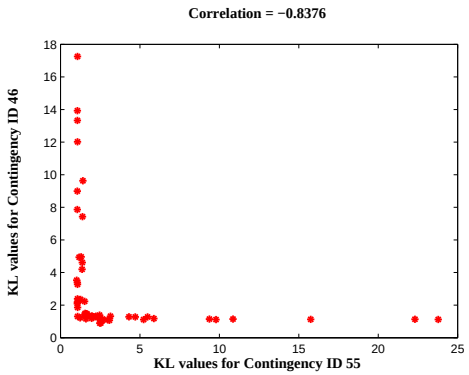

Figure 3.6: Negative correlation between contingencies

3.4.2 Spectral clustering algorithm

A spectral clustering technique [41] is utilized to group the contingencies into different clusters based on the similarity information. The Spearman rank correlation is used to define the similarity between contingencies. The following steps describe the algorithmic procedure involved in grouping contingencies using spectral clustering technique.

Step 1) Pre-processing: This step chooses the set of contingencies and buses that must be considered for further analysis. When the affected region is very small compared to the total number of buses, the computed correlation will lead to misleading similarity information between the two contingencies. Therefore, neglecting non-severe contingencies and buses will improve the accuracy of the results. The threshold values to determine severe contingencies and buses from non-severe cases are system and user dependent. The threshold values for the selection of contingencies and buses are provided as an input to the cluster analysis.

Step 2) Similarity matrix (S): The similarity matrix defines the distance between each contingency with respect to all other contingencies. First, compute the SC between two contingencies, j_1 and j_2, using (3.18). Then, the SC values are converted into the distance measure by using the transformation $d_{j_1 j_2} = 1 - r_s^{j_1 j_2}$. The value of $d_{j_1 j_2}$ provides the distance measure between the two contingencies, j_1 and j_2. If the two contingencies affect similar buses in the same rank order, then the corresponding correlation value will be close to 1 and the distance between them is close to zero. If the SC value is -1, then the distance will have a value of 2,

indicating dissimilarity between the two contingencies. Since the SC value lies in the range of -1 and 1, the distance measure will lie in the range of 0 to 2.

Step 3) Adjacency matrix (A): Calculate the adjacency matrix (A) using a Gaussian similarity function as shown in (3.19a). The parameter, k_p, scales the similarity function value and σ is the connectivity parameter, which defines the extent of similarity between two contingencies. The degree matrix, D, is a diagonal matrix with entries $s_1, .., s_j, .., s_{RC}$, as defined in (3.19b), along its diagonal.

$$A_{j_1 j_2} = k_p e^{-\frac{d_{j_1 j_2}}{\sigma}},\ A_{j_2 j_1} = A_{j_1 j_2},\ j_1 \neq j_2, \text{and} \tag{3.19a}$$

$$s_j = \sum_{k,\ k \neq j}^{N_{RC}} A(j,k),\ A \in \mathbb{R}^{N_{RC} \times N_{RC}}. \tag{3.19b}$$

N_{RC} denotes the reduced number of contingencies that have been obtained after the preprocessing step.

Step 4) Calculate the graph Laplacian matrices using (3.20). Matrix L and L_{norm} represent the unnormalized and normalized graph Laplacian matrix, respectively. L_{norm} is a positive semi-definite matrix and have N_{RC} non-negative real valued eigenvalues, $0 = \lambda_1 \leq \cdots \leq \lambda_{N_{RC}}$.

$$\begin{aligned} L &= D - A. \\ L_{\text{norm}} &= D^{-\frac{1}{2}} L D^{\frac{1}{2}}. \end{aligned} \tag{3.20}$$

Step 5) Identify the preliminary number of clusters using eigenvalue analysis on the Laplacian matrix. If the eigenvalue, 0, has a multiplicity of k, this implies there are k fully disconnected clusters. However, this is an ideal scenario and does not happen in power systems. There are a number of methods available in the literature for choosing the initial number of clusters, k, for the clustering algorithm. Of the available methods, the eigengap heuristic is used to identify the initial number of clusters, where the goal is to identify the number, k, such that all eigenvalues, $\lambda_1, \cdots, \lambda_k$, are small, but λ_{k+1} is relatively large.

Step 6) Compute the first k eigenvectors, $e_1, \cdots, e_k$, of normalized graph Laplacian matrix, L_{norm}.

Step 7) Form the matrix $E \in \mathbb{R}^{N_{RC} \times k}$ using the first k eigenvectors, $e_1, \cdots, e_k$, as columns. Let $y_j \in \mathbb{R}^k,\ j = 1, \cdots, N_{RC}$ be the vector corresponding to the j-th row of E. y_j denotes

the j^{th} contingency from the reduced contingency list in the lower dimensional space. The key aspect of the spectral clustering algorithm is to change the representation from abstract data points V_j in higher dimensional space to y_j in lower dimensional space. The change of representation enhances the cluster properties in the data so the clusters can be identified easily in the new representation, using K-means clustering.

Step 8) Cluster the points, y_j, using K-means algorithm into different clusters, $C_1, \cdots, C_k$. The K-means algorithm partitions the data points, y_j, in the matrix, E, into k clusters. The K-means algorithm identifies the clusters, such that it minimizes the sum of the distance for each data point in the cluster to the centroid of the corresponding cluster.

Step 9) For each identified cluster, recompute the Laplacian matrix with contingencies belonging to the corresponding cluster. Checking further clustering is possible by investigating the dominant eigenvalues of the new Laplacian matrix. If further clustering is possible, repeat the clustering algorithm from Step 5. If further clustering is not possible, stop the clustering algorithm and provide the final results.

A result of contingency clustering is contingencies that produce similar behavioral patterns in system voltage response are grouped together in different clusters, for the given operating condition. The most severe contingency in each cluster will act as a representative for all other contingencies in the corresponding cluster. Only these representative contingencies, which represent all other contingencies, are considered for further analysis. Also, the cluster analysis provides the most severely affected buses corresponding to each cluster.

3.5 Application of Clustering Methods for Multiple Operating Conditions

The power system undergoes continuous variation in loads, generation and system configuration. This presents a large number of scenarios that have to be taken care of during planning stage. The scenarios (operating conditions, load levels, contingencies) have to be chosen carefully such that it covers a wider group of possible cases. The clustering procedure described in section 3.4.2 can be extended to reduce the number of scenarios to be analyzed.

Figure 3.7 provides the framework for grouping contingencies into different clusters under multiple scenarios and operating conditions.

(I) In the first level clustering, the contingencies are grouped into different clusters for each of the chosen $'m'$ different conditions using spectral clustering algorithm. For each of the chosen operating condition, a clustering is obtained. A clustering is a partition of input contingency set into different clusters at a given operating condition.

(II) Level 2 clustering identifies the representative contingencies under various operating conditions and scenarios based on the similarity between level 1 clusters. A hierarchical clustering procedure is utilized to explore the similarity between level 1 clusterings and place them into different cluster groups.

(III) The result of this two level clustering procedure is a master set of contingency clusters. This master set contains similar cluster groups obtained from multiple operating conditions and scenarios.

(IV) The representative contingencies from each of the clusters in the master contingency cluster set are further utilized in the identification of dynamic voltage control area (Refer: 4).

3.5.1 Similarity measure

The first step in the level 2 clustering is to identify the relationship between level 1 clusterings. Numerous measures such as Rand index, adjusted rand index (ARI), Mirkin distance, Jaccard index, variation of information (VOI) are available to compare the similarity between clusterings [42]. Based on the definition of similarity measure, the resulting clustering pattern may be different. In order to explore the pattern of clustering under multiple operating conditions and scenarios, two types of similarity measures (ARI and VOI) are used to create the hierarchical tree structure. The idea of using two types of similarity measures for identifying the patterns is to find the natural divisions of clusters, rather than artificially imposing a group in the given data set. Consider an example of partitioning the input set of N_c contingencies

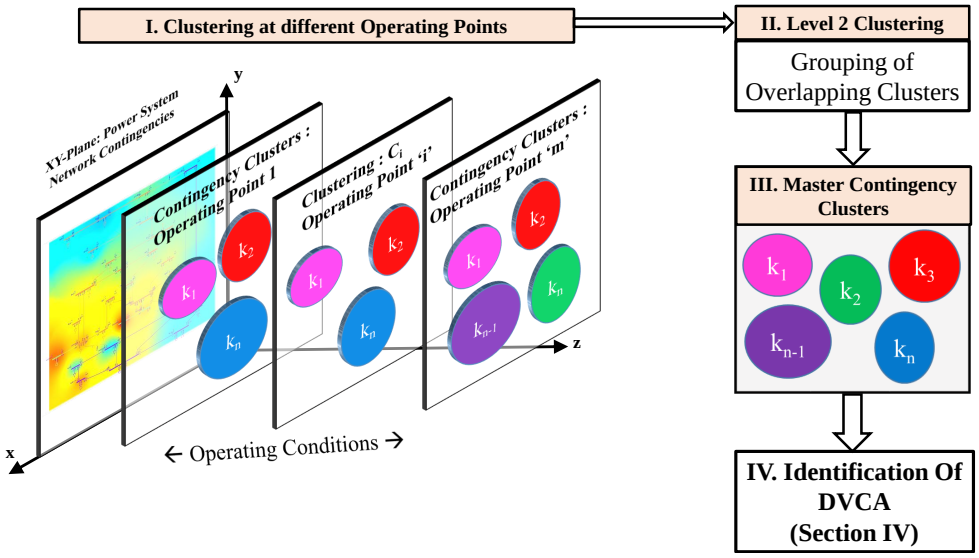

Figure 3.7: Contingency clustering framework for multiple operating conditions

into clusterings, C_i and C_j, corresponding to operating conditions i and j respectively. Let $C_i = k_1, k_2, ...k_{K_i}$ and $C_j = k_1, k_2, ...k_{K_j}$ have K_i and K_j number of clusters respectively.

3.5.1.1 Adjusted Rand index

The ARI compares clusterings by counting the pairs of contingencies on which two clusterings agree or disagree. Fig. 3.8 shows two clusterings, C_1 and C_2, where each clustering has two groups of contingency clusters, k_1 and k_2. Since there is no overlap between contingency clusters within a clustering, any pair of contingencies from the input contingency set will fall into one of the four categories (a,b,c,d) described below.

(a) : Number of contingencies that are placed in same cluster in clustering C_1 and C_2 (e.g contingencies c_1&c_3).

(b) : Number of contingencies that are placed in same cluster in clustering C_1 but not in C_2 (e.g contingencies c_9&c_{11}).

(c) : Number of contingencies that are placed in same cluster in clustering C_2 but not in C_1 (e.g contingencies c_4&c_{10}).

(d) : Number of contingencies that are placed in different cluster in clustering C_1 and C_2 (e.g contingencies c_{13}&c_2).

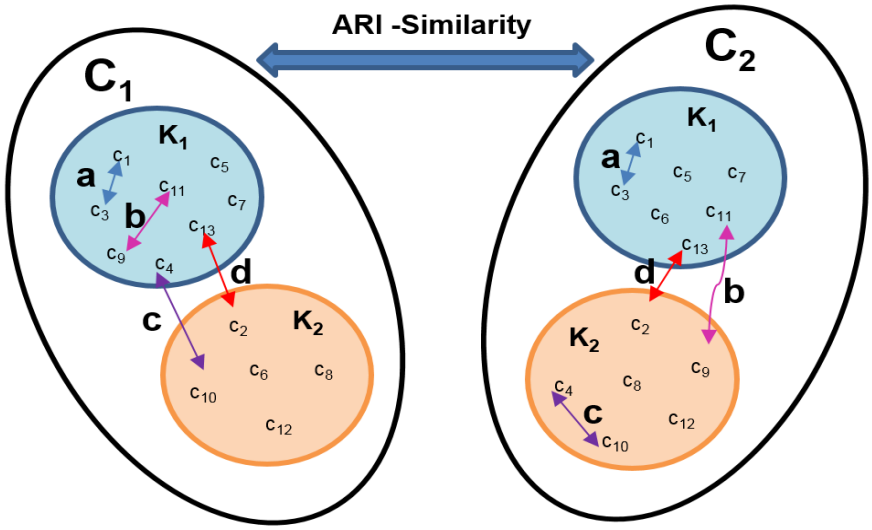

Figure 3.8: Comparing clusterings using adjusted Rand index

$$ARI(C_1, C_2) = \frac{\binom{n}{2}(a+d) - [(a+b)(a+c)+(c+d)(b+d)]}{\binom{n}{2}^2 - [(a+b)(a+c)+(c+d)(b+d)]} \tag{3.21}$$

The items (a, d) and (b, c) are interpreted as agreements and disagreements respectively, between the two clusterings. Equation (3.21) is used to compute ARI and the computed value lies between -1 and 1. The higher the value of ARI, the more similar are the corresponding clusterings. When the two clusterings match perfectly, then the value of ARI is 1. Since the hierarchical clustering requires a similarity measure, where similar clustering have small distance between them, the ARI is transformed to a new distance metric using (3.22). The distance metric, d_{ARI}, will have a value of 0 when the clusterings match and the value increases as the dissimilarity between clusterings increase.

$$d_{ARI}(C_1, C_2) = 1 - ARI(C_1, C_2) \tag{3.22}$$

3.5.1.2 Variation of information

The VOI metric compares the clusterings based on the information provided by one cluster about the another, utilizing information theoretic concepts. Equation (3.23) is used to calculate the VOI metric, where $H(C_i)$ represents the entropy associated with clustering C_i and $I(C_i, C_j)$ represents the mutual information between the clusterings C_i and C_j

$$VOI(C_i, C_j) = H(C_i) + H(C_j) - 2I(C_i, C_j) \tag{3.23}$$

The notion of entropy used is based on Shannon's definition [37] and it measures the information contained in a set as opposed to the use of entropy as a measure of disorder in thermodynamics and statistical mechanics. Suppose for clustering, C_i, if there are n_{k_i} contingencies in cluster k_i, then using (3.24a) the probability of a contingency from the input set being placed in cluster k_i is calculated. Equation (3.24b) is used to compute the entropy associated with a clustering.

$$P(k_i) = \frac{n_{k_i}}{N_c} \tag{3.24a}$$

$$H(C_i) = -\sum_{k_i=1}^{K_i} P(k_i) log P(k_i) \tag{3.24b}$$

If a contingency belongs to cluster k_i in clustering C_i and to cluster k_j in clustering C_j, then the joint distribution of the random variables associated with the two clusterings is given by $P(k_i, k_j)$. The value of $P(k_i, k_j)$ is computed using (3.25a), where $|k_i \cap k_j|$ represents the number of contingencies that are common to both clusters k_i and k_j. The mutual information calculated using (3.25b) provides the information that clustering C_i has about clustering C_j.

$$P(k_i, k_j) = \frac{|k_i \cap k_j|}{N_c} \tag{3.25a}$$

$$I(C_i, C_j) = \sum_{k_i=1}^{K_i} \sum_{k_j=1}^{K_j} P(k_i, k_j) log \frac{P(k_i, k_j)}{P(k_i)P(k_j)} \tag{3.25b}$$

The mutual information between two clusterings is always non-negative and symmetric. When two clusterings are exactly the same, then the mutual information between the clusterings is same as the uncertainty in either of the clustering.

$$I(C_i, C_j) = H(C_i) = H(C_j) \tag{3.26}$$

The VOI metric measures the amount of information lost and gained in forming clustering C_j from C_i. Consequently, lower values of VOI implies better similarity between the clusterings. The VOI metric is always non-negative and lies in the range of 0 and $logN_c$. The metric takes a value of 0 when all the contingencies are placed in one cluster signifying no uncertainty in identifying the clustering. The VOI is directly used as a distance metric in hierarchical clustering without any transformations.

3.5.2 Hierarchical clustering

Hierarchical clustering is a process of identifying groups in the given data set using a nested sequence of partitions [43]. The nested sequence of partitioning allows one to explore the patterns in the given data set, rather than grouping them into pre-determined number of clusters. In this work, agglomerative process of hierarchical clustering is utilized to analyze the patterns among contingency clusterings obtained from different operating conditions and scenarios. The patterns are visually represented using dendrogram, a tree-structured graphical representation of hierarchical clusters.

The tree is a multilevel hierarchical structure that shows the link between the contingency clusters obtained for each of the specified operating conditions and scenarios. Every node in the tree correspond to a clustering object and the length of edge between nodes is a measure of dissimilarity between clustering objects. The nodes at the bottom layer of the tree are called terminal nodes and they correspond to clustering performed at different operating conditions and scenarios. Internal nodes correspond to the clustering object obtained by linking similar clusterings. The three main steps in the process of hierarchical clustering are provided below. In the first step, the distance between every pair of terminal nodes is computed to form the similarity matrix. If the number of terminal nodes (or cases) is N, then the distance between $N * \frac{N-1}{2}$ distinct pairs of nodes have to be calculated to form the $N \times N$, symmetrical similarity matrix. For the purpose of comparative studies, the similarity matrix is computed using Rand index and VOI metric.

In the second step, the clustering objects are grouped into a hierarchical cluster tree using a linkage function. The linkage function determines the order of grouping different clustering objects using the distance information. Single linkage, complete linkage, average linkage, centroid linkage, Ward's method are some of the commonly used linkage functions linkref. In this work, average linkage method is used to combine clustering objects because of its relative robustness. This method takes the cluster structure into account and create clusters with approximately equal variance. The average linkage method defines the distance between clustering objects, $d(C_1, C_2)$, as the average distance from all clustering objects in C_1 to all clustering objects in C_2. Equation (3.27) is used to calculate the distance between clustering objects, where $C_{1,i}$ denotes the i^{th} clustering object in C_1, n_1 and n_2 corresponds to the number of clusterings in C_1 and C_2 respectively.

$$d(C_1, C_2) = \frac{1}{n_1 n_2} \sum_{i=1}^{n_1} \sum_{j=1}^{n_2} d(C_{1,i}, C_{2,j}) \tag{3.27}$$

In the third step, the hierarchical cluster tree is cut into different groups based on the natural divisions in the input data set. The level at which the cluster tree is divided is based on the inconsistency coefficient of the links. The inconsistency coefficient compares the height of a link in a cluster tree with the average height of links below it. If the link join distinct groups, then the value of inconsistency coefficient will be high. A value of low inconsistency coefficient indicate the link that joined the clustering objects are similar. The clustering objects at the bottom of the hierarchical tree have no further objects below them. Therefore, if a link joins two clustering objects at the bottom level then it will have a zero inconsistency coefficient.

3.6 Simulation Results

Simulations have been performed in IEEE 162 bus system. The test system has 17 generators, 111 loads, 34 shunts, and 238 branches. The power flow and dynamics data for the 162 bus system are available in [34]. The total generation capacity and load of the system are 20.60 GW and 17.27 GW respectively. For a more accurate load representation, 22 load

buses were stepped down through distribution transformers to the 12.47 kV level, and the new low voltage buses were assigned the numbers 163 through 184. Dynamic simulation studies are performed using PSSE software [4]. To capture the dynamic behavior of motor loads, a composite load model represented by CMDL was used at the new representative load buses. Additionally, composite load models were also used to represent motor loads at the major load centers (zones 3 and 6). Of the total load for each bus, 30% is specified as three-phase induction motor loads and 35% as single-phase air conditioner loads.

3.6.1 Clustering contingencies - single operating conditions

The modified IEEE 162 bus system has N_B buses (184) and a total of N_C contingencies (316) of the type, a three-phase fault at a bus cleared after 6 cycles by opening one of the transmission lines connected to the faulted bus is considered for simulation studies. The voltage time series corresponding to bus i and contingency j are stored in the vector, $v_{ij}(t),\ 0 \leq t \leq T_f,\ i \in N_B,\ j \in N_C$. T_f represents the final simulation time instant chosen as 5 seconds for all the simulations.

3.6.1.1 Pre-processing

Using the time domain simulation results (v_{ij}), KL divergence at each bus is computed for all contingencies and the results are stored in a matrix $\bar{K} \in \mathbb{R}^{N_B \times N_C}$. Figure 3.9 shows the pictorial representation of the $\bar{K}$ matrix, where each row has KL measures corresponding to a particular bus for all the contingencies. Each column has KL measures for all buses corresponding to a particular contingency. The element, $\mathcal{K}_{ij}$, corresponds to the KL divergence measure for the i^{th} bus and the j^{th} contingency. The recovery information from the voltage time-series has been captured in a scalar form using the KL divergence measure.

The average value of the KL divergence for individual buses for all contingencies could be used to determine the relative severity of an individual bus. Equation (3.28) is used to compute the average KL divergence value for all buses, where $\vec{1} \in \mathbb{R}^{N_C}$ is a row vector for all entries equal to 1. The i^{th} entry of the vector, R_B, contains the average value of the KL divergence for the i^{th} bus, when averaged over all contingencies.

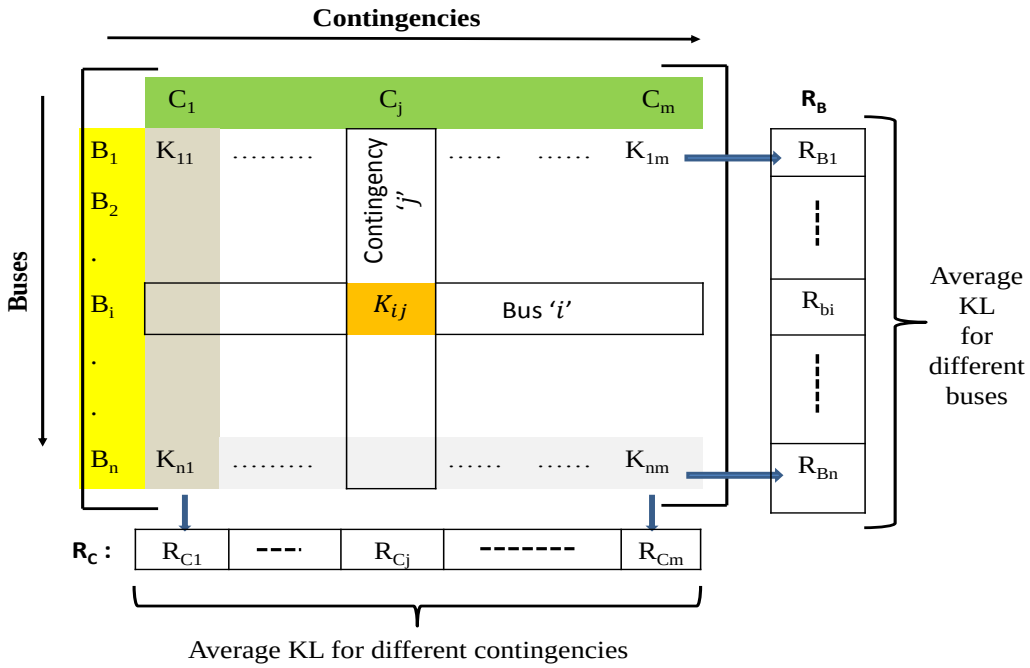

Figure 3.9: Representation of the $\bar{K}$ matrix, where each row has KL numbers of a particular bus for all contingencies and each column has KL numbers of all buses corresponding to a particular contingency

$$R_B := \frac{1}{N_C}\vec{1} * \bar{K}, \;\; R_B \in \mathbb{R}^{N_C}, \vec{1} \in \mathbb{R}^{N_C} \tag{3.28}$$

Figure 3.10 (a) shows the R_B vector plotted against the different buses. The red horizontal line corresponds to the critical value of the KL divergence derived as 4.9 . The buses, whose average KL values are greater than the critical KL value, can be termed as severe buses. However, it is not sufficient to conclude the severity of buses only based on the average KL values because of the masking effect. The number of contingencies that results in performance violations at a particular bus is also important to decide the severity level of a particular bus. Figure 3.10 (b) shows the number of performance violations for all the buses. For example, from Fig.3.10 (a), it is determined bus 148 has the highest average KL value and bus 106 has a relatively less average KL value. However, from Fig.3.10 (b), it is observed that more contingencies create a violation at bus 106 than at bus 148. This example shows that decisions solely based on the average KL value or number of performance violations is insufficient to arrive at critical buses.

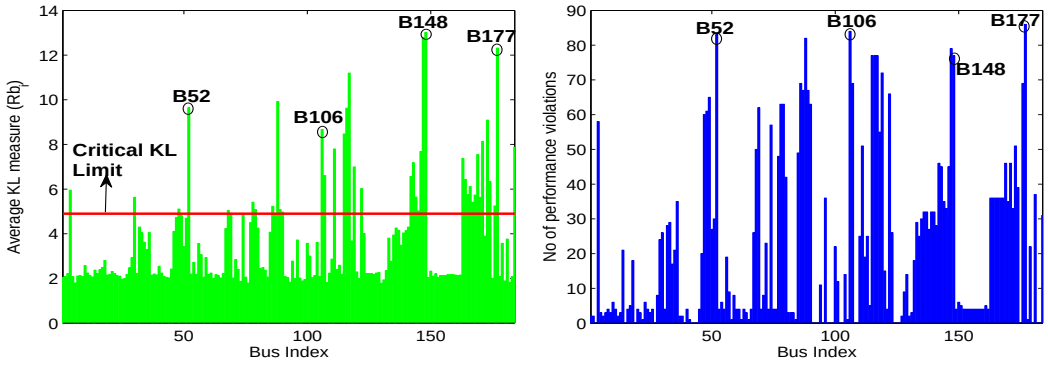

Figure 3.10: (a) Average value of KL divergence for different buses (b) Number of performance violations for different buses

Table 3.1: Top 8 Severe Bus Ids (Sorted in descending severity)

sorted by avg. KL	148	147	177	117	88	52	116	173
sorted by violations	177	106	52	88	147	115	116	117

Table 3.1 shows the top 8 sorted severe bus numbers, based on average KL values (row 1) and number of performance violations (row 2). Although, there are common elements between the lists, the ranking of buses is different for both lists. There are multiple options to combine these two data sets (severity and number of violations) to arrive at the list of critical buses. When the average KL value is below critical and the number of violations is very small, then such buses are termed as non-severe. They can be disregarded for further analysis. Buses with a high average KL values and more performance violations (e.g., Bus 177) can be grouped as the most critical buses. Such information is very valuable when selecting the locations to monitor for voltage performance violations. Similarly, to decide the critical contingencies, both severity of contingency and number of performance violations must be considered. The severity of a contingency is defined as the average KL values for all buses corresponding to that contingency. Equation (3.29) is used to calculate the average KL value for different contingencies. The j^{th} entry in the R_C vector captures the severity level for the j^{th} contingency. The severity of different contingencies and the number of buses that violate the WECC performance criterion are shown in Figs. 3.11 (a) and (b), respectively.

$$R_C := \frac{1}{N_B}\bar{K} * \vec{1},\ R_C \in \mathbb{R}^{N_C}, \vec{1} \in \mathbb{R}^{N_B}. \tag{3.29}$$

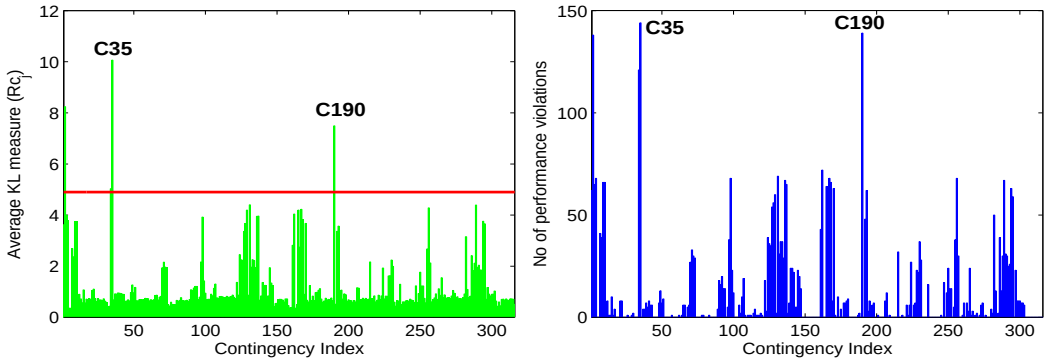

Figure 3.11: (a) Average value of KL divergence for different contingencies (b) Number of performance violations for different contingencies

If the number of violations for a particular contingency is small, the recovery is tolerable for that specific contingency, provided the severity level is small. Contingencies that have a lower severity value and a small number of violations are termed as non-severe. A higher severity value and fewer number of violations signifies these contingencies are severe for only certain buses. Contingencies that have lower severity value and a larger number of violations, affect a wider region of the network (e.g., C190 - Refer to Figs.3.11 (a) & (b)). The most critical contingencies are those with a higher severity value and a large number of performance violations (e.g., C35).

Table 3.2: Top 8 Severe Contingency Ids (Sorted in descending severity)

sorted by avg. KL	35	2	190	34	131	289	256	167
sorted by violations	35	190	2	34	162	131	4	98

Table 3.2 provides the indices for the top 8 sorted severe contingencies, based on the average KL value for contingencies and number of performance violations. The actual contingencies corresponding to the IDs shown in 3.2 are provided in Appendix A. The number of performance violations and severity level can be used to identify critical contingencies. Non-severe contingencies can be eliminated for further system level analysis.

For further analysis, only those contingencies affecting more than 5% of the total number of buses are considered. This reduces the number of contingencies from 316 to 71. Also, the KL values for buses that do not have violations for more than 10 contingencies are discarded for further analysis. After the pre-processing step, the $\bar{K} \in \mathbb{R}^{184\times316}$ has been reduced to $\bar{K} \in \mathbb{R}^{70\times71}$.

3.6.1.2 Spectral clustering

The correlation matrix, as plotted in Fig 3.12, shows the correlation values between different contingencies, where the rows and columns represent the contingency identification numbers (cIDs) in the reduced contingency list. The different colors in the matrix plot corresponds to SC values as indicated along the sidebar in fig 3.12. When the correlation value is close to 1, the matrix block has shades of red signifying the strong similar behavior between the cIDs given by the row and column number (e.g. cIDs 1 and 2). Similarity signifies both the contingencies affect the same set of buses in the same rank order based on the KL values. When the correlation value decreases below 0.6, then the contingencies exhibit weak correlations. When the correlation value become negative, the matrix block has shades of blue, signifying dissimilarity between these corresponding contingencies (e.g. cIDs 1 and 22). Dissimilarity signifies buses severely affected by one contingency are not affected by another contingency.

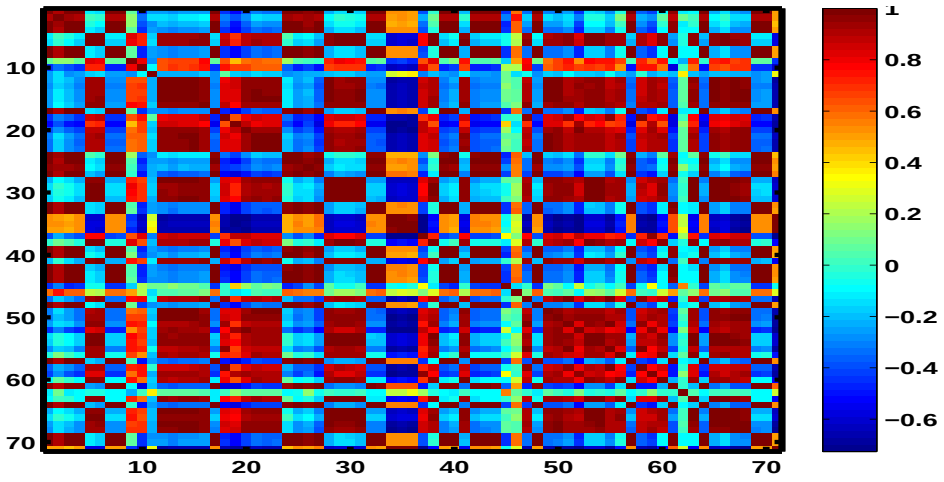

Figure 3.12: Plot of Spearman correlation between all contingencies. Rows and columns represents indicies of different contingencies

The SC values between contingencies are converted into distance between contingencies using the transformation provided in Step 2 of section III.B. Strongly correlated contingencies will have a distance close to 0 and weakly correlated contingencies will have a distance close to 2. Since the correlation between contingencies changes from strong to weak, the corresponding distance between them increases from 0 to 2. The distance between contingencies is used to compute the adjacency matrix utilizing a Gaussian similarity function. The computed adjacency matrix using (3.19a) will have values in the range of 0 to 1. A value of 1 in the adjacency matrix implies contingencies belonging to corresponding row and column are adjacent and belong to the same group of contingency cluster. If the adjacency value between two contingencies is close to 0, then it implies they are dissimilar and belong to a different contingency cluster. The goal of the clustering algorithm is to group contingencies with adjacency values close to 1 with respect to each other. Such groupings will result in contingencies that create a similar voltage response in the system placed in the same cluster.

Figure 3.13.(a) shows the eigenvalue plots for the analysis of 71 contingencies. From the eigenvalue analysis of the normalized Laplacian matrix, the preliminary number of clusters is 2. The first two eigenvectors of the matrix L_{norm} are used to represent the similarity data in a reduced dimensional space. K-means clustering algorithm is performed using the number of clusters and corresponding eigenvector data. The distance measure used by the K-means algorithm is city block distance. Figure 3.13.(b) shows the plot of the second eigenvector after rearranging the rows based on K-means cluster results. If the eigenvector 2 is thresholded at -0.05, then the part below -0.05 corresponds to cluster 1 and the part above -0.05 corresponds to cluster 2. Each data point in Fig. 3.13.(b) corresponds to a contingency ID.

When the correlation information between the contingencies is placed in random order as shown in Fig. 3.12, the presence of clusters is difficult to discern. However, after clustering analysis, the two clusters, shown by red colored regions along the diagonal of the adjacency matrix, are clearly separated in Fig. 3.14. The shades of red imply contingencies have strong similar behavior with respect to the other contingencies in the same cluster and shades of blue imply their separation from contingencies in other clusters. There are 28 contingencies in cluster 1 and 43 contingencies in cluster 2, as indicated in Fig. 3.14. The contingencies are ordered

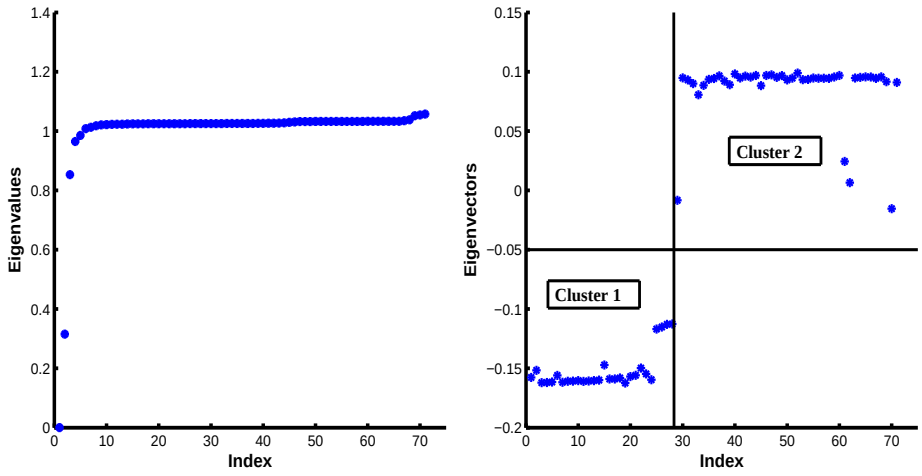

Figure 3.13: (a) Plot of eigenvalues (b) Plot of eigenvectors

such that the most severe contingency in a cluster is placed first and the least severe contingency is placed last. For example, cIDs 1 and 30 are the most severe contingencies in clusters 1 and 2, respectively. Similarly, cIDs 28 and 71 are the least severe contingencies in clusters 1 and 2, respectively. The first 23 contingencies in cluster 1 exhibit strong similar behavior with respect to each other, where as cIDs 24-28 exhibit a strong similarity among themselves, but relatively weak similarity with respect to the other contingencies in the cluster. This is due to the fact these five contingencies are less severe and affect only a subset of buses affected by the most severe contingency in cluster 1. It can be also noted these contingencies exhibit a strong dissimilarity with contingencies in cluster 2. Similarly, a few contingencies in cluster 2 exhibit a weak correlation with other contingencies in cluster 2, but they have a strong dissimilarity with cluster 1 contingencies.

3.6.1.3 Validation of clustering results

Cluster validity refers to the procedure of evaluating the results of the clustering technique. In this paper, validation is accomplished using internal criteria of validating clustering procedure. With respect to the internal criteria, the two commonly used measures for validating clustering results are compactness and separation. Compactness measures the closeness of contingencies within a cluster and separation measures how distinct or well separated a cluster is from other clusters. A silhouette coefficient combines the idea of both cohesion and separation

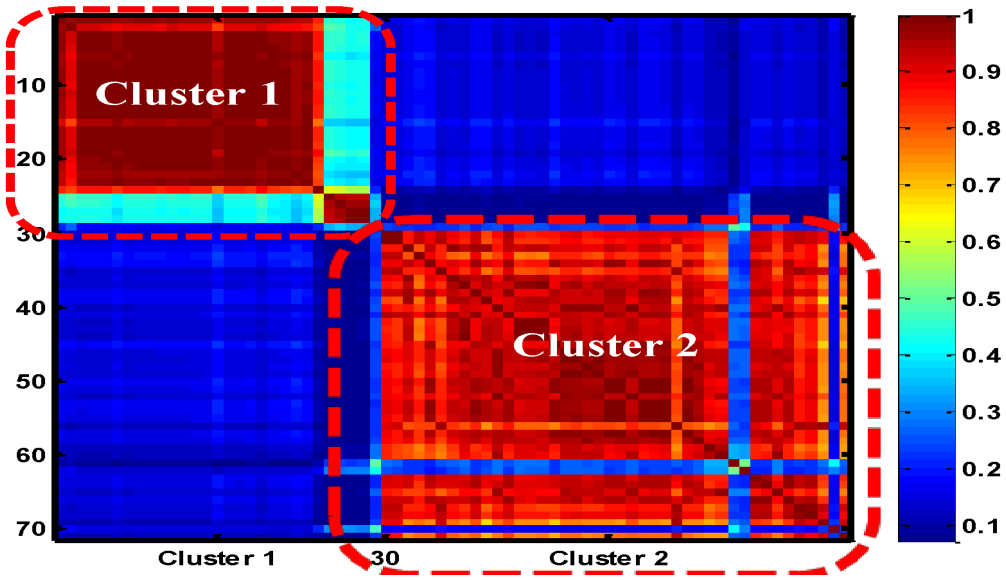

Figure 3.14: Plot of Adjacency Matrix - After clustering. Rows and columns represent rearranged indices of different contingencies.

for clusters and clusterings [44]. Silhouette values help interpret cluster results and provide a graphical representation of how well each object lies within its cluster. The silhouette value for the i^{th} data point, $s(i)$, is calculated by using the formula, $s(i) = \frac{b(i)-a(i)}{max\{a(i),b(i)\}}$. The average dissimilarity of i^{th} contingency with all other contingencies within the same cluster is denoted by $a(i)$. The average dissimilarity of the i with contingencies of other clusters where contingency i is not a member is calculated and the lowest dissimilarity is denoted as $b(i)$. The city block distance measure, as used in k-means clustering, is used to define the dissimilarity. The value of $a(i)$ defines how well the contingency, i, is related to the cluster it belongs. When the value of $a(i)$ is smaller, the matching of contingency i to its assigned cluster is better. The value of $b(i)$ defines how well contingency i is separated from other clusters. The larger the value of $b(i)$, the poorer is the matching of contingency i to the other clusters. The value for $s(i)$ lies between -1 and 1. When the value of $a(i) << b(i)$, then the value for $s(i)$ will be close to 1. A value of $s(i)$ close to 1 signifies the corresponding contingency is properly clustered. When the value of $s(i)$ is close to 0, then the contingency is on the border line between two clusters. When the value of $s(i)$ is close to -1 signifies a misclassification of the contingency.

For illustration of clustering validation, sample plots of silhouette values for two different

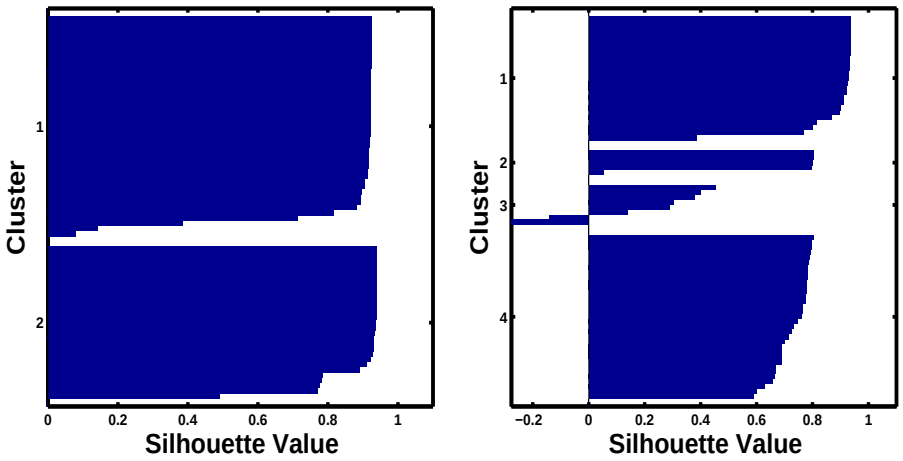

Figure 3.15: Silhouette plots for clustering with (a) k=2 (b) k=6

numbers of clusters (k=2 and 4) are shown in Figs. 3.15.(a) and 3.15.(b). The average silhouette value for clustering with k as 2 and 4 are determined 0.8739 and 0.6409, respectively. The higher the value of the average silhouette value, the better the clustering result. When the value of k is specified as 4, some of the silhouette values become negative, indicating the contingencies are improperly clustered.

The silhouette value can be used to provide the natural number of clusters within a data set and compare the two different clusterings. The average silhouette value over the entire data set provides a measure of how appropriately the contingencies have been clustered. An average silhouette greater than 0.5 indicates reasonable partitioning of data into appropriate clusters and a value less than 0.2 indicates the data do not exhibit cluster structure [44].

The number of clusters, k, an input to the k-means algorithm, is decided by the number of dominant eigenvalues of the Laplacian matrix. The silhouette plot is used to confirm the claim that the number of clusters identified using dominant eigenvalues, indeed, provide the best clustering results. Figure 3.13 shows the eigenvalues plot for the Laplacian matrix used to obtain the preliminary number of clusters as 2. To verify this claim, the clustering procedure is repeated with different number of clusters and the average silhouette value is computed for each case. Table 3.3 shows the average silhouette values for clusterings with different number of clusters. The average silhouette value is maximum when the number of clusters is 2, which indicates the natural number of clusters available in the provided data set is 2.

Table 3.3: Average silhouette values for different clustering

No.of clusters	2	3	4	5	6	7
Average silhouette value	0.8739	0.8627	0.6409	0.6039	0.6119	0.537

3.6.2 Multiple operating conditions

The idea of contingency clustering is extended to account for multiple operating conditions. The total load of the system at the base case operating condition is 17.27 GW and the total available generation capacity in the system is 20.724 GW. From the PV analysis, it is found that a maximum of 11.76% of the base load can be increased uniformly at all load buses. For illustration of clustering contingencies under multiple operating conditions, 15 different load levels were considered. Case S1 corresponds to the base load level, cases S2 - S5 and cases S6 - S9 corresponds to increase and decrease of 1%, 3%, 5%, 7% load from the base case respectively. Since the base case is already in stressed condition, light loading conditions are considered to provide variations in the operating conditions. Cases S10-S15 correspond to decrease in load level of 15%, 17%, 19%, 21%, 23% and 25% from the base case load level.

For each of the considered operating conditions, 316 contingencies of the type, a three-phase fault at a bus cleared after 6 cycles by opening one of the transmission lines connected to the faulted bus are considered for analysis. After performing time domain simulation of contingencies for all the considered cases, it was found that 236 (out of 316) contingencies does not create short-term voltage problems. Therefore in the pre-processing 3540 out of 4740 cases are discarded for further analysis. The remaining 80 severe contingencies are analyzed under 15 different operating conditions for their behavioral similarity.

Utilizing the KL measure and spectral clustering method, the contingency clusters for each of the considered cases have been found. The base case scenario (S1) has resulted in two clusters, where cluster 1 and 2 have 28 and 43 contingencies respectively. The remaining nine of the 80 contingencies are non-severe and are not considered in the level 1 clustering procedure for the base case condition. The most severe contingency from each cluster acts as a representative of other contingencies in the corresponding cluster. Instead of considering all

71 severe contingencies, only the two representative severe contingency can be considered for further analysis and planning studies.

Each of the cases, S1 to S15 has resulted in two groups of contingency clusters. The two groups of contingency clusters indicates that there are two weaker (VAR deficient) regions in the system. Contingencies that exposes the same weakness in the system are placed in the same cluster. As the load level increases, the number of contingencies in each cluster increases and also the contingencies have become more severe. Case S5 (load level: 107%) has 80 severe contingencies, where as case S15 (load level: 75%) has only 29 severe contingencies. It has been observed that at light load levels (cases S10 - S15), the number of severe contingencies are much less compared to that of base case.

The level 2 clustering procedure identifies and groups the level 1 clusters based on their similarity. To explore the patterns between the 15 level 1 clusterings, a hierarchical clustering strategy is used. The similarity matrix between clusterings to generate the hierarchical cluster tree are obtained using ARI and VOI metric. The use of two types of metric is to verify the consistency in the identified patterns rather than imposing a pattern obtained due to a clustering method.

3.6.2.1 Hierarchical clustering using ARI metric

Table 3.4 shows the dissimilarity distance metric between clusterings obtained using ARI for seven of the selected cases. For the selected cases, the percentage increase or decrease in load level from base case is shown in parenthesis in table 3.4. The ARI value close to 1 indicates a high degree of similarity between the clusters formed at operating conditions (E.g. case S1 and S3). The ARI between the clusterings in case S1 and S3 is 0.9049, which is converted into dissimilarity distance of 0.0951 using (3.22). On the other hand, the similarity between clusterings at case S1 and S15 is low (ARI=0.0890) and is reflected as increased distance between them (d_{ARI}=0.9110).

Figs. 3.16 correspond to the cluster tree obtained using average linkage method utilizing the distance metric from ARI metric. The indices along the x-axis correspond to the number

Table 3.4: Distance between clusterings at different operating conditions using ARI

Case Load (%)	S1 (Base)	S3 (+3)	S5 (+5)	S7 (-3)	S9 (-5)	S10 (-15)	S15 (-25)
S1	0.0000	0.0951	0.1504	0.0812	0.1730	0.5413	0.9110
S3	0.0951	0.0000	0.0643	0.1713	0.2489	0.5474	0.8922
S5	0.1504	0.0643	0.0000	0.2229	0.2906	0.5431	0.8723
S7	0.0812	0.1713	0.2229	0.0000	0.1387	0.5461	0.9192
S9	0.1730	0.2489	0.2906	0.1387	0.0000	0.5160	0.9180
S10	0.5413	0.5474	0.5431	0.5461	0.5160	0.0000	0.6619
S15	0.9110	0.8922	0.8723	0.9192	0.9180	0.6619	0.0000

of clusterings in the given data set and they form the terminal nodes of the tree. The total number of terminal nodes in a tree equals the chosen number of operating conditions for study. The terminal nodes are linked based on the distance metric to form new clustering object or an internal node. The links between nodes are shown using an upside-down U-shaped lines. The internal node numbers are marked in circles in Fig. 3.16. For example, nodes 1 and 2 are linked to form node 16, which in turn is linked with node 6 with a height of 0.0334. In order to determine the natural cluster divisions, the height of each link in the cluster tree is compared with the heights of neighboring links below it in the tree. If the link has approximately same height with respect to the links below it, then there are no distinct divisions between the clustering objects grouped at this level of the hierarchy. These links have high level of consistency because the distance between the clustering objects that are being joined is approximately the same as the distance between the clustering objects they contain. If the link height differs from that of the links below it, then it is inconsistent with the links below it. An inconsistent link indicates that the clustering objects joined by this link below to different clustering groups. The inconsistent links identifies the natural divisions in a cluster tree where the similarity between objects change abruptly. In Fig. 3.16, the height of last link that joins two groups of clustering objects (blue and red) is 0.6804. The inconsistency coefficient for this link is 1.0294 which indicates that it joined relatively distinct clustering objects as opposed to the links below them.

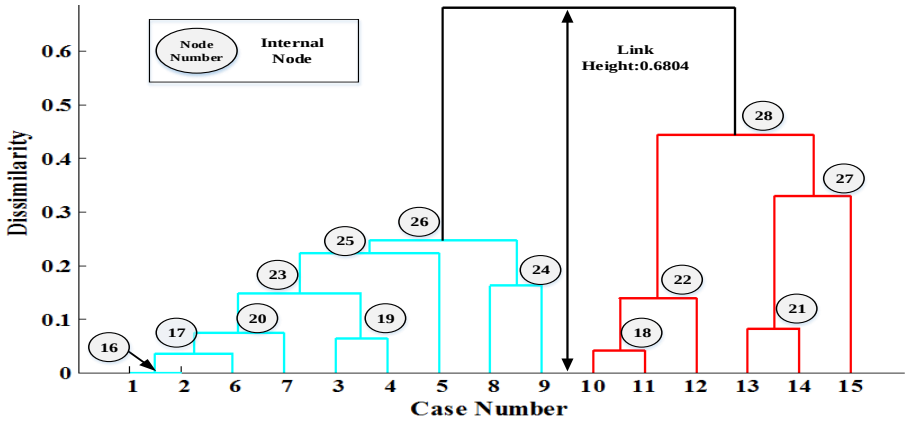

Figure 3.16: Hierarchical cluster tree using ARI and average linkage method

3.6.2.2 Hierarchical clustering using VOI metric

Table 3.5 shows the dissimilarity distance metric between clusterings obtained using VOI for some of the selected cases. Theoretically, for the severe input contingency set, the VOI can have a maximum of 2.3026 for two dissimilar clusterings if the number of possible clusters in each clustering is limited to 10. The small VOI values in table 3.5 indicate that clusterings at different operating conditions being similar. Comparing the distance metric in table 3.4 and 3.5, the distance values obtained using VOI are greater than that of ARI because of the wide range of VOI metric. Both ARI and VOI metric are sensitive to the variations in the contingency clusters performed at different operating conditions. These distance matrices are used to construct the hierarchical cluster trees.

Table 3.5: Distance between clusterings at different operating conditions using VOI metric

Case Load (%)	S1 (Base)	S3 (+3)	S5 (+5)	S7 (-3)	S9 (-5)	S10 (-15)	S15 (-25)
S1	0.0000	0.2052	0.2612	0.2181	0.3817	0.8652	1.3174
S3	0.2052	0.0000	0.1434	0.3649	0.4628	0.8468	1.2721
S5	0.2612	0.1434	0.0000	0.4091	0.4824	0.8137	1.2229
S7	0.2181	0.3649	0.4091	0.0000	0.3847	0.8943	1.3343
S9	0.3817	0.4628	0.4824	0.3847	0.0000	0.8727	1.3471
S10	0.8652	0.8468	0.8137	0.8943	0.8727	0.0000	1.0949
S15	1.3174	1.2721	1.2229	1.3343	1.3471	1.0949	0.0000

Except for few changes in the order of clusterings, both ARI and VOI identified the same pattern in the clustering groups. In figs. 3.16 and 3.17, group 1 (blue) represents similar

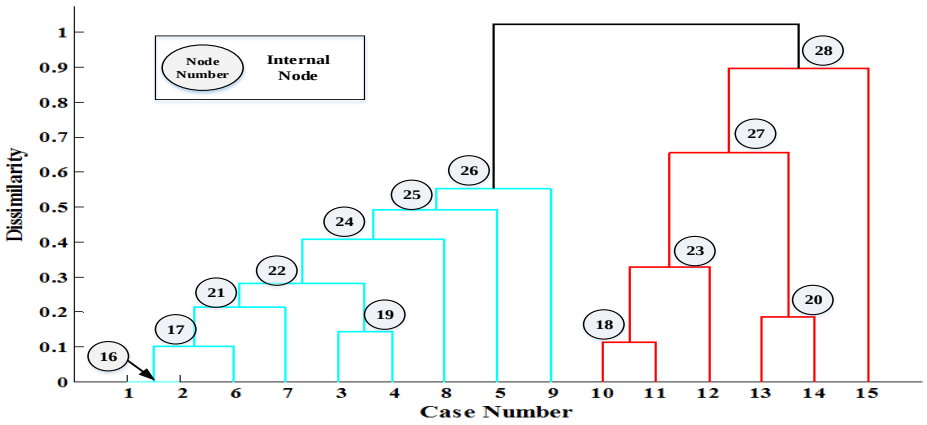

Figure 3.17: Hierarchical cluster tree using VOI metric and average linkage method

contingency clusters obtained at higher load levels, whereas group 2 (red) correspond to clusters obtained at relatively lower load levels.

Fig.3.18 shows the summary of contingency selection process for planning studies using clustering method. A total of 316 contingencies were analyzed under 15 different operating conditions. The pre-processing of 4740 time domain simulation cases has termed 236 contingencies as non-severe, since they did not create any short-term voltage problems. For each of the considered 15 operating conditions, the remaining 80 contingencies were grouped into clusters using spectral clustering method. For example, case S1 has classified the 71 severe contingencies in 2 cluster groups. The resulting cluster groups for all the 15 cases are further grouped into clusters using a hierarchical clustering procedure. The level 2 clustering has grouped 9 cases (S1-S9) in one group and 6 cases (S10 - S15) in another group.

By selecting a representative case from each clustering group (collection of operating conditions), the number of operating conditions needed for further analysis is reduced. For the simulation cases, only two cases are required to equivalently represent the selected 15 different operating conditions. Also, by selecting representative contingencies from each of the representative clustering group, the number of contingencies to be analyzed is reduced. For this simulation study, only four contingencies are required to represent 80 severe contingencies under 15 different operating conditions.

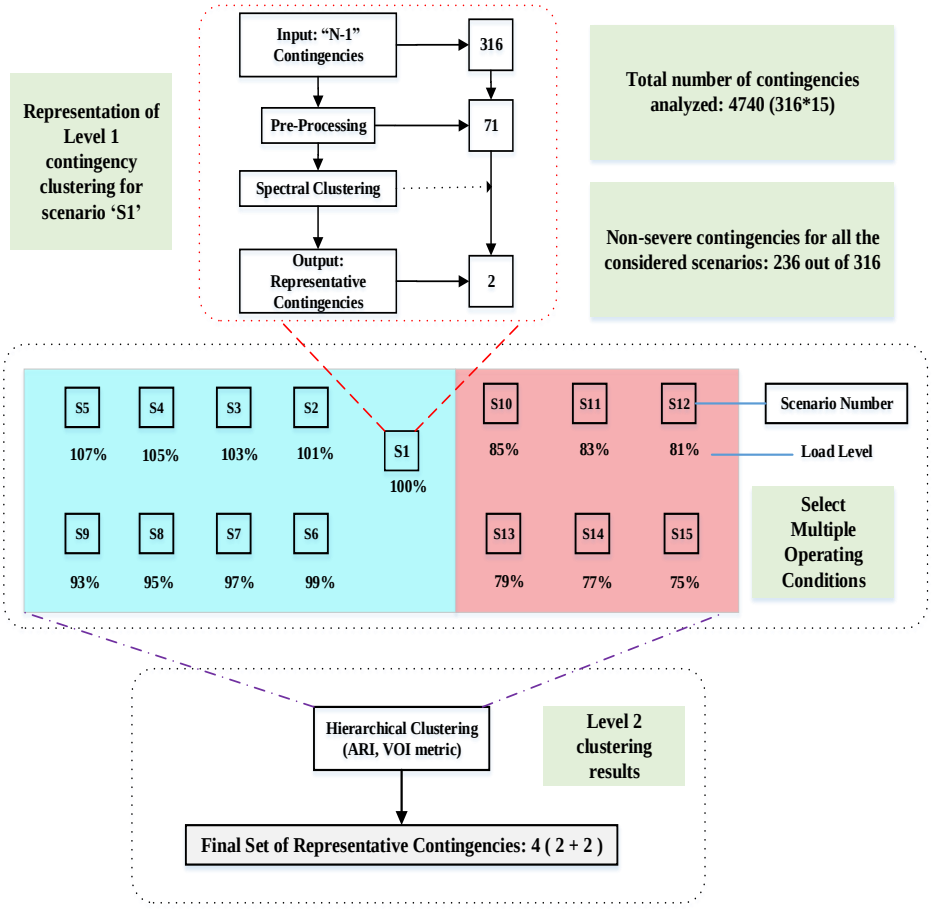

Figure 3.18: Summary of contingency reduction using clustering method

3.7 Conclusions

KL divergence, an entropy-based quantity, has been used to characterize both the rate and level of voltage recovery. It provides a quantitative measure of voltage recovery phenomenon and is very useful for comparing different voltage waveforms. A two level clustering framework utilizing KL measure is developed to identify the representative contingencies under multiple operating conditions and scenarios. The first level clustering uses spectral clustering method to group the contingencies based on their similarity patterns of bus responses. The key aspect of the spectral clustering algorithm is to change the representation from abstract data (voltage time series) in higher dimensional space to a representation in lower dimensional space utilizing eigenvectors. The change of representation enhances the cluster properties in the data so that the clusters can be identified easily in the new representation, using K-means clustering. K-means is a part of spectral clustering algorithm that identifies the contingency clusters. Clustering contingencies based on their similarity reduces the number of contingencies to be considered for further analysis, since the severe contingency for each cluster is representative of all other contingencies in this cluster.

Hierarchical clustering method is used to explore and group clusterings corresponding to multiple operating conditions. In order to show the identified patterns are not an imposition of the clustering method, two different types of similarity measures are used to obtain similar pattern of hierarchical structure. The clustering based contingency analysis will significantly reduce the number of contingencies, scenarios and operating conditions that has to be considered for planning studies. Clustering also provide the set of affected buses by each contingency cluster under different operating conditions and scenarios. The severely affected buses provide indications about the regions that need dynamic VAR support due to their susceptibility to short-term voltage problems. Also, this approach provides a comprehensive list of contingencies that exposes different weaknesses in the system.

CHAPTER 4. DYNAMIC VOLTAGE CONTROL AREAS

4.1 Introduction

The ability of the system to respond to events that lead to short-term voltage problems depends upon the amount of dynamic reactive resources placed at critical locations. These locations should be placed in the areas they most likely are needed. Existing reactive power planning methods identify the locations and amount of VAR resources for a set of most probable contingencies or to eliminate low voltage problems in a region for a particular contingency. The dynamic VAR locations identified based on the selected contingencies may not be able to provide sufficient support, if one of the following conditions occurs (a) if the severity of the planned contingencies increases, (b) if a more severe, unplanned contingency that expose reactive deficiency in the same region that has been planned for, (c) if a new unplanned contingency that expose reactive deficiency in a different region of the system. To overcome these shortcomings, instead of planning based on severe contingency screening method, a novel philosophy based on the identification of system weakness is developed. A novel concept called dynamic voltage areas was developed to address the importance of the location of dynamic reactive reserves. This chapter details the motivation, formulation and identification of DVCA from the supply-side solution perspective (i.e addition of dynamic reactive resource). Simulations have been completed on the modified IEEE 162 bus system to illustrate the concept of DVCA. Finally, the concept of DVCA was extended for demand-side solutions (load shedding) using appropriate modifications in the formulation.

4.2 Motivation and Proposal

Reference [45] describes a method to identify voltage control areas based on steady state analysis. This method uses the PV curve tracing method to push the system to the point of instability for all considered contingencies. For each considered case, modal analysis is performed at the point of instability to identify the critical modes of instability. Based on the participation factors (PFs) of buses corresponding to the critical mode, data mining techniques are employed to identify contingency clusters and the voltage control area (VCA). The measure used for contingency clustering is similarity in PFs. Generators that have high PFs are chosen as the initial set of control candidates to represent each contingency cluster. The PFs corresponding to zero eigenvalue (critical mode) indicate the buses contributing to the instability. Heuristic rules have been applied to group contingencies that are related to the same VCA and also to identify the specific buses and generators that form each VCAs.

As the short-term voltage problems, especially FIDVR, is mainly driven by the stalling behavior of induction motors, it will be of interest to identify the areas that are vulnerable to these problems. Also, it is important to identify the contingencies that are most likely to create these short-term voltage problems. If the areas that are prone to short-term voltage problems are identified, then by placing sufficient dynamic reactive support at strategic locations will ensure safe and secure system operations under all circumstances. To accomplish the above goal, a novel concept called dynamic voltage control areas is proposed. As opposed to the voltage control areas defined in [45], the proposed DVCA defines the voltage control areas from a dynamics perspective. DVCA identification separates the reactive deficient areas into different groups and also provides the most effective control locations in each area.

A DVCA is defined as a section of a power system that responds as a cohesive unit to avoid short-term voltage stability problems within that section. Figure 4.1 shows a conceptual picture of the proposed DVCA concept. There are three DVCA in fig 4.1, where each DVCA has a cluster of contingencies, affected buses and effective control locations for mitigating the short term voltage problems in that area. The red line in each DVCA corresponds to the representative contingency for the corresponding DVCA contingency clusters. The nodes

represented in blue correspond to the affected buses and nodes with D-VAR (dynamic VAR resources) are the most effective control locations. For example, given a voltage deviation within a DVCA, the dynamic reactive resources within that DVCA respond together to prevent short-term voltage stability problems in this area. As long as minimum levels of dynamic reactive reserves are maintained in each area, then the likelihood of occurrence of short-term voltage stability problems will be minimized.

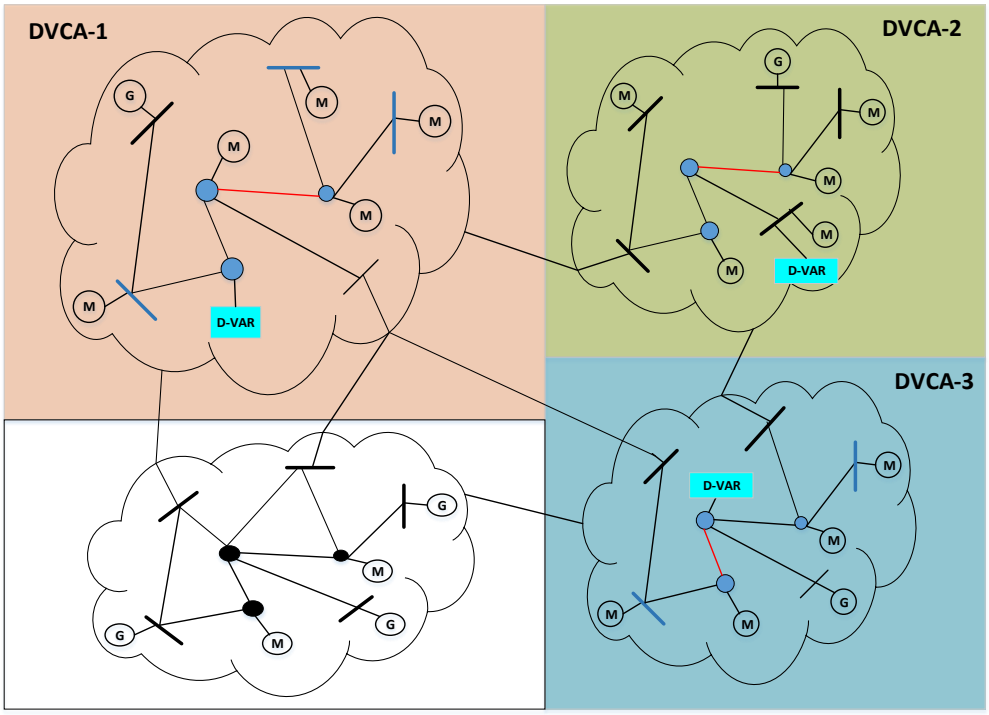

Figure 4.1: Illustration of dynamic voltage control areas - Red lines correspond to the representative contingency, blue nodes represent the affected buses, D-VAR nodes are the most effective control locations

For identifying DVCA, the KL measure is used to define the similarity between contingencies. The KL measure indicates the relative participation of buses contributing to short-term voltage problems.

4.3 DVCA from Supply-Side Solutions Perspective

Figure 4.2 provides the important steps involved in the process of identifying DVCA from the supply-side solutions perspective. The DVCA control locations are the most effective buses

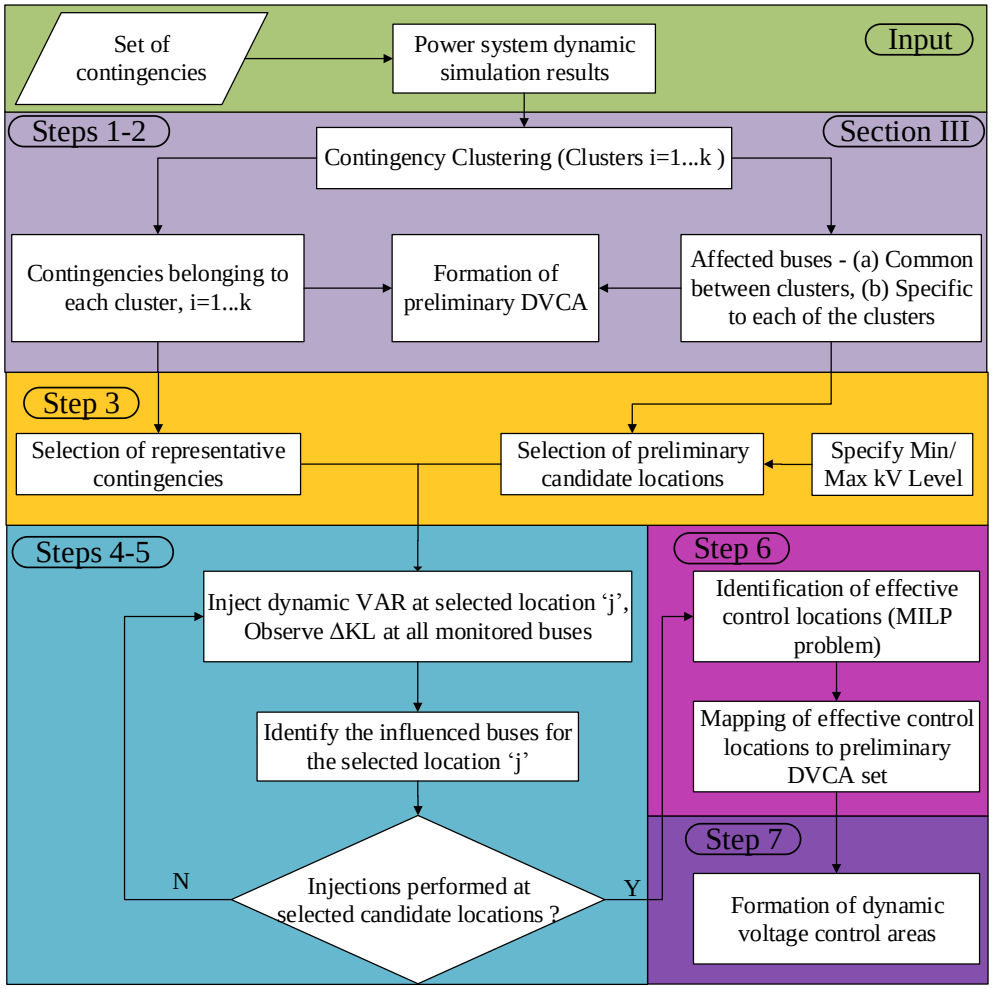

Figure 4.2: Overview of steps involved in the identification of dynamic voltage control areas

for the addition of new dynamic VAR resources.

Step 1) Clustering of contingencies: Groups of contingencies behaving similarly are identified through the clustering procedure (Refer Section 3.4.2). The most severe contingency from each cluster is a representative of all other contingencies in the corresponding cluster. Only the representative contingencies are chosen for further analysis.

Step 2) Identification of affected buses: For each cluster, all buses with violations of performance criteria form the set of violated buses corresponding to the cluster. Among the violated buses, some buses are affected only by contingencies specific to a particular cluster and some buses are affected by contingencies belonging to different clusters. The affected buses are grouped into different sets, such as specific to each clusters and common between clusters

through a hierarchical clustering procedure. The number of common affected buses between clusters is used as the similarity measure for the hierarchical clustering procedure (Refer Section 3.5.2).

Step 3) Identification of preliminary DVCA: Each set of affected buses along with its corresponding contingency clusters form the preliminary DVCA. The contingency clusters provide the group of contingencies that result in the violations in the buses belonging to its DVCA. For example, if the set of affected buses correspond to buses common to two clusters, then contingencies corresponding to these two clusters have influence on this set of buses.

Step 4) Identification of potential control candidate locations: In the DVCA identification procedure, one of the challenges is to identify the initial control candidate locations, which are effective locations for placing dynamic reactive resources. Placement of dynamic VAR devices, such as SVC and STATCOM, at lower kV levels is relatively cheap, but it will not help wider range of buses in the system. On the other hand, placing them at higher kV levels helps a wider range of buses to improve their voltage levels, but is very costly. Therefore, based on economic considerations, the loads buses between the specified minimum and maximum kV levels are chosen as preliminary candidate locations.

Step 5) Sensitivity studies: The influence of potential control candidate locations is identified through sensitivity studies. The trajectory sensitivity index (TSI) is used in [25] to identify the relative effectiveness of locations for placing dynamic VAR sources. Similar to TSI, sensitivities to the KL measure are used to capture the effectiveness of selected candidate locations. For the representative contingencies, the change in KL measures at all monitored buses to injection of dynamic VARs at the chosen candidate locations are calculated.

Step 6) Identification of effective control locations: The effective control locations are identified by a mixed integer linear programming (MILP) problem utilizing the KL sensitivities from Step 5. The constraints of the MILP include the specified performance criterion on KL values at all monitored buses and limitations on the maximum amount of reactive sources that can be placed at each location. Details of the MILP problem are provided in section 4.4. The MILP identifies the effective control locations and amount of dynamic VARs required to meet

the specified KL performance criteria, considering the representative contingencies from cluster analysis.

Step 7) Identification of DVCA: The effective control locations identified by the MILP problem are mapped to its corresponding preliminary DVCA set. The mapping results in effective control locations that influence a set of affected buses for a given set of contingencies. After mapping, if a preliminary DVCA set does not have any control locations, then it is merged with its corresponding common preliminary DVCA sets. The area of influence of control candidate locations are identified from the sensitivity study results. For injection of dynamic VARs at a control location, the buses that produced a change in the KL value above a certain specified threshold value form the area of influence for the corresponding control location. Each resulting group with a set of contingencies, affected buses, and effective control locations forms a DVCA.

4.4 Mixed Integer Linear Programming

Sensitivity studies with different levels of dynamic reactive power injection are performed to identify the influence of VAR injections on the KL measure at different buses. The results of sensitivity studies are utilized to formulate the MILP optimization problem. The general formulation of the MILP optimization problem for handling multiple contingencies is provided in (4.1).

Objective function: The objective of this MILP formulation is to identify effective control candidate locations (integer variables) and the minimum amount of dynamic reactive power needed to meet the required short-term voltage performance constraints. The parameters, C_B^i, $C_{Q_{ml}}^i$, denote the fixed cost and variable cost respectively, based on the size of the dynamic VAR device at location i. The status of the integer variable, B^i, determines the selection of location i for dynamic VAR placement. The variable, Q_{ml}^i, provides the amount of dynamic VAR device required at location i for contingency m and level l. The constants, $N_{\text{cont}}, N_{\text{lev}}, N_{\text{Loc}}$, define the number of contingencies, the number of levels used for dynamic VAR injection in sensitivity studies, and the number of initial candidate locations, respectively.

$$\underset{B,Q}{\text{minimize}}\ F = \sum_{i}^{N_{\text{Loc}}} C_B^i B^i + \sum_{m}^{N_{\text{cont}}} \sum_{l}^{N_{\text{lev}}} \sum_{i}^{N_{\text{Loc}}} C_{Q_{ml}}^i Q_{ml}^i,$$

Subject to

$$\begin{aligned}
(C1):\ & \sum_{j}^{N_{\text{Loc}}} \frac{\partial K^i}{\partial Q_{ml}^j} Q_{ml}^j \leq K^* - K_{m,i}^{(0)}, \\
(C2):\ & \sum_{l}^{N_{\text{lev}}} Q_{ml}^i \leq B^i Q_{\max}^i, \\
(C3):\ & Q_{ml}^{R,i} W_{ml}^i \leq Q_{ml}^i \leq Q_{ml}^{R,i} W_{m(l-1)}^i, \\
& \qquad \forall i \in \text{SMon},\ \forall m \in \text{SCont}, \\
& B \in \{0,1\},\ Q \in \mathbb{R}^{N_{\text{Loc}}},\ W \in \{0,1\}
\end{aligned} \tag{4.1}$$

There are Nc continuous variables that is used to calculate the maximum amount of dynamic VAR support needed at the input candidate locations. The total number of integer variables for N_{Loc} initial candidate locations with N_{lev} levels of sensitivity analysis, for all N_{cont} contingencies, is $N_{\text{Loc}} + N_{\text{cont}} * N_{\text{lev}} * N_{\text{Loc}}$. There are two sets of integer variables,

1. N_{Loc}: Number of location variables to select a candidate bus for the placement of dynamic VAR support.

2. $N_{\text{cont}} * N_{\text{lev}} * N_{\text{Loc}}$: Number of indicator variables to derive a linear formulation of the optimization problem

Constraints C1: The performance constraints include the KL divergence measure at the monitored buses should be less than the critical value of the KL divergence measure for all the contingencies. For contingency m, $K_{m,i}^{(0)}$ is the base case KL measure at location i. K^* denotes the critical value of the KL divergence measure based on WECC performance criteria. $\frac{\partial K^i}{\partial Q_{ml}^j}$ provides the change in KL measure at bus i for a change in the maximum amount of dynamic VAR support at location j. The sensitivity information is calculated around the dynamic VAR support operating level, l, and for contingency, m. The calculation of sensitivity information around multiple operating levels is to approximate the non-linear variations of KL measure to changes in dynamic VAR support limits using piece-wise linear functions.

Constraints C2: The constraints set C2 provide limits to the maximum amount of dynamic VAR placed at a given location. The maximum capacity of the dynamic VAR device at selected location, i, is given by $Q^i_{\max}$. The selection of location i for dynamic VAR placement is decided by the integer variable, B^i. If the i^{th} location selection variable, B^i is zero, then the reactive support from that location, Q^i_{ml}, will be zero.

Constraints C3: The constraints set C3 is included to preserve the linearity of the optimization formulation. The integer, W^i_{ml}, is an indicator variable that indicates whether Q^i_{ml} has reached its corresponding range limit, $Q^{R,i}_{ml}$. If the indicator variables are not used, then the MILP may select a reactive support variable Q_{ml} at higher levels, without reaching the limits of its corresponding lower level variable Q_{ml-1}. Sets SMon and SCont define the sets of monitored buses and contingencies, respectively.

4.4.1 MILP solution process

The process of finding solution to the MILP problem involves exploring a tree of linear programming relaxations. Most of the existing MIP solvers employs the following procedure to identify the optimal solution. The MIP solver selects a node from the tree and solves an LP-relaxation problem at that node. Then it attempts to generate cutting planes to cut-off the current solution and invokes a heuristic to try to find an integer feasible solution that is close to the solution of the current LP relaxation problem. Based on the fractional values for integer variables in the current solution, the solver selects a branching variable and places two nodes that result from branching up or down on the branching variable into the tree. The MIP solver processes active nodes in the tree until either no more active nodes are available or some limit has been reached. Nodes are called *active* if they have not yet been processed. After a node has been processed, it is no longer active. Table 4.1 provides a list of commercial and open source MIP solvers along with their application program interfaces.

In this work, the *branch and cut search* procedure is used to solve the MIP optimization problem. The branch-and-cut procedure manages a search tree consisting of nodes. Every node represents an LP or QP sub-problem that is, to be solved, to be checked for integer constraints,

Table 4.1: List of various MIP solvers along with their API interfaces

MIP Solver	Type	Interfaces
Cplex	Commercial	C, C++, Java,.NET, MATLAB, PYTHON, Excel
Gurobi	Commercial	C, C++, Java,.NET, MATLAB, PYTHON
LINDO	Commercial	C, MATLAB, Visual Basic
Mosek	Commercial	C, C++, Java, .NET, Python
XPRESS-MP	Commercial	C, C++, Java, .NET, VBA
KNITRO	Commercial	C, C++, MATLAB
BLIS	Open	C++
CBC	Open	C++
GLPK	Open	C
lp_solve	Open	C
MINTO	Open	C
SCIP	Open	C
SYMPHONY	Open	C

and if needed, analyzed further. A branch is the creation of two new nodes from a parent node. Typically, a branch occurs when the bounds on a single variable are modified, with the new bounds remaining in effect for that new node and for any of its descendants. For example, if a branch occurs on a binary variable, that is, one with a lower bound of 0 (zero) and an upper bound of 1 (one), then the result will be two new nodes, one node with a modified upper bound of 0, and the other node with a modified lower bound of 1. The two new nodes will thus have completely distinct solution domains.

A cut is a constraint added to the existing MIP problem. The addition of cut will limit the size of the solution domain for the continuous LP or QP problems at every nodes, without eliminating legal integer solutions. This will reduce the number of branches that have to be processed in the MIP solution process.

Each node, after its relaxation is solved, has an optimal objective function value, $Z_{Node,i}$. At any given point in the algorithm, there node whose $Z_{Node,j}$ value is less (in minimization problems) than all the others is chosen as the "'best node"'. This best node value is compared to the objective function value of the incumbent solution.

The resulting MIP Gap, expressed as a percentage of the incumbent solution, serves as a measure of progress toward finding and proving optimality. When active nodes no longer exist,

then these two values will have converged toward each other, and the MIP Gap will thus be zero, signifying that optimality of the incumbent has been proven.

4.5 Simulation Results

Simulations have been performed in the modified IEEE 162 bus system. The modified test system has 184 buses, 17 generators, 111 loads, 34 shunts, and 238 branches. For a more accurate load representation, 22 load buses were stepped down through distribution transformers to the 12.47 kV level, and the new low voltage buses were assigned the numbers 163 through 184. To capture the dynamic behavior of motor loads, a composite load model represented by CMDL was used at the new representative load buses. Additionally, composite load models were also used to represent motor loads at the major load centers (zones 3 and 6). Of the total load for each bus, 30% is specified as three-phase induction motor loads and 35% as single-phase air conditioner loads.

4.5.1 Formation of preliminary DVCA

Results from the contingency clustering analysis (Chapter 3) provide information about the set of contingencies and buses affected by them under various operating conditions. Without loss of generality, the identification of DVCA has been demonstrated using contingencies corresponding to base case operating condition. There are two contingency clusters in the base case operating condition, where cluster 1 has 28 contingencies and cluster 2 has 43 contingencies. Cluster 1 and cluster 2 contingencies results in KL violations at 43 and 40 buses respectively. Table 4.2 shows the top 10 severely affected buses along with the severity of violations for each of the contingency clusters. The number of violations of a bus (# violations) indicates the total number of contingencies that result in KL performance violations at the corresponding bus. For example, all the 28 contingencies in cluster create KL performance violations at bus 171 and the sum of all KL violations is 1022.01. Similarly, 39 out of 43 contingencies have resulted in KL performance violations at bus 147.

Table 4.2: Top 10 affected buses corresponding to each contingency clusters. Affected buses are sorted based on the number of contingencies they have violated

No	Cluster 1			Cluster 2		
	Bus	# violations	Sum of Violations	Bus	# violations	Sum of Violations
1	171	28	1022.01136	147	39	456.1774951
2	163	28	1019.14742	117	39	338.0832361
3	169	28	791.595515	52	39	228.4769517
4	164	28	728.482531	148	36	666.819915
5	166	28	628.468776	106	35	203.6779951
6	168	28	521.691306	116	34	241.3980171
7	165	28	490.637562	119	34	101.5432054
8	174	28	450.428301	177	32	1074.993844
9	167	28	417.555615	88	32	338.4928543
10	170	28	360.55767	115	32	160.0202477

Also, it has been observed that the buses with large KL violations for the representative contingencies result in KL violations for other contingencies in the corresponding cluster. There are 14 buses severely affected by contingencies in both clusters 1 and 2. There are 29 buses severely affected only by cluster 1 contingencies and 26 buses severely affected only by cluster 2 contingencies. Three preliminary DVCA groups are formed by grouping the severely affected buses along with their corresponding contingency clusters as shown in table 4.3.

Table 4.3: Formation of preliminary DVCA

	DVCA1	DVCA2	DVCA3
No of severe contingencies	28	43	71
No of affected buses	29	26	14

Each preliminary DVCA contains information regarding contingency clusters and affected buses. The preliminary DVCA 1 has 28 severe contingencies from cluster 1 and 29 buses affected by these contingencies. Similarly, the preliminary DVCA 2 has 43 severe contingencies from cluster 2 and 26 affected buses. The preliminary DVCA 3 corresponding to the 14 common affected buses includes the contingencies from both clusters. The affected buses corresponding to three preliminary DVCAs are shown in table 4.4.

Table 4.4: Affected buses in the preliminary DVCAs

Preliminary DVCA	# No of affected buses	Affected buses
DVCA1	29	48,50,51,110,112,133,135,136,137,138, 139,140,141,142,143,144,145,146,163, 164,165,166,167,168,169,170
DVCA2	26	34,36,49,56,57,67,68,69,71,77,78, 79,80,85,86,87,89,90,96,104,107, 122,123,176,181,184
DVCA3	14	4,52,74,88,106,111,115, 116,117,119,147,148,173,177

4.5.2 Identification of effective candidate locations

The effective candidate locations for the placement of dynamic VAR resources are identified using a MILP optimization. The sensitivities of the KL measure with respect to VAR injection at different candidate locations are used to formulate the constraints of the MILP problem as described in section 4.4. For the selection of preliminary candidate location using sensitivity studies, 92 load buses in the range of 69-345 kV levels are considered. For each selected potential candidate location, a dynamic VAR source with maximum capacity as 1 p.u, 3 p.u and 5 p.u is placed and the change in the KL measure for each injection level is observed. The different VAR injection levels are considered to account for the non-linearity in change in KL measure with respect to dynamic VAR injections. The sensitivity studies are performed only for the representative contingency from each cluster. Contingency ID 2 and 34 acts as a representative for cluster 1 and cluster 2 respectively. The details of different contingencies are provided in appendix A.

The MILP problem is solved by using a branch and cut search algorithm in CPLEX. This optimization problem identifies the best candidate locations and the amount of dynamic reactive power needed to achieve satisfactory voltage performance, considering all representative contingencies from each cluster.

The results of the MILP optimization are shown in table MILPresults. For the representative contingency from each cluster, the MILP chooses 6 candidate locations as optimal locations from the initial set of 92 candidate locations. The chosen control locations that pri-

Table 4.5: MILP optimization results

Bus No	Max B_{svc}	DVCA
117	1	2
133	3	1
135	3	1
144	2.45	1
147	1	2
148	1	3

marily influence the affected buses in preliminary DVCA 1, 2, and 3 are determined 3, 2, and 1, respectively. The control locations corresponding to each preliminary DVCA set along with its influential buses and set of contingencies define the DVCA.

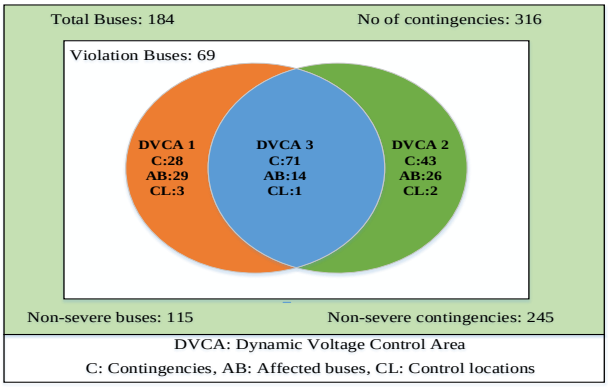

Figure 4.3: Summary of DVCA results

Figure 4.3 shows the summary of the three DVCAs for the modified 162 bus system. Each DVCA has three components: (1) set of similarly behaving contingencies, (2) buses affected by this contingency set, and (3) effective control buses that mitigate the problems in the affected buses. DVCA 1 has 28 contingencies, 29 affected buses, and 3 effective control candidate locations. Similarly, 26 buses are severely affected by 43 contingencies in DVCA2 and 2 candidate locations from the 18 affected buses are most effective in mitigating the short-term voltage stability problems. The 14 buses in DVCA3 are affected by both contingencies in DVCA1 and DVCA2, and, therefore, DVCA3 has 71 contingencies. The one control location in DVCA3 provides dynamic VAR support to the 16 buses in DVCA3 for all the 71 contingencies in DVCA3. As long as the minimum levels of dynamic reactive reserves are maintained in each area, the likelihood of short-term voltage instability is minimized within the corresponding area.

To validate the claim that only representative contingencies are sufficient to perform the MILP optimization, the optimization procedure is repeated with the top 3 contingencies from each cluster set. The MILP optimization yielded the same control candidate locations obtained in the case where only the representative contingencies are used. This approach greatly reduces the number of dynamic simulations that must be performed, while dealing with multiple contingency analyses during the planning stage.

4.6 DVCA from Demand-Side Solutions Perspective

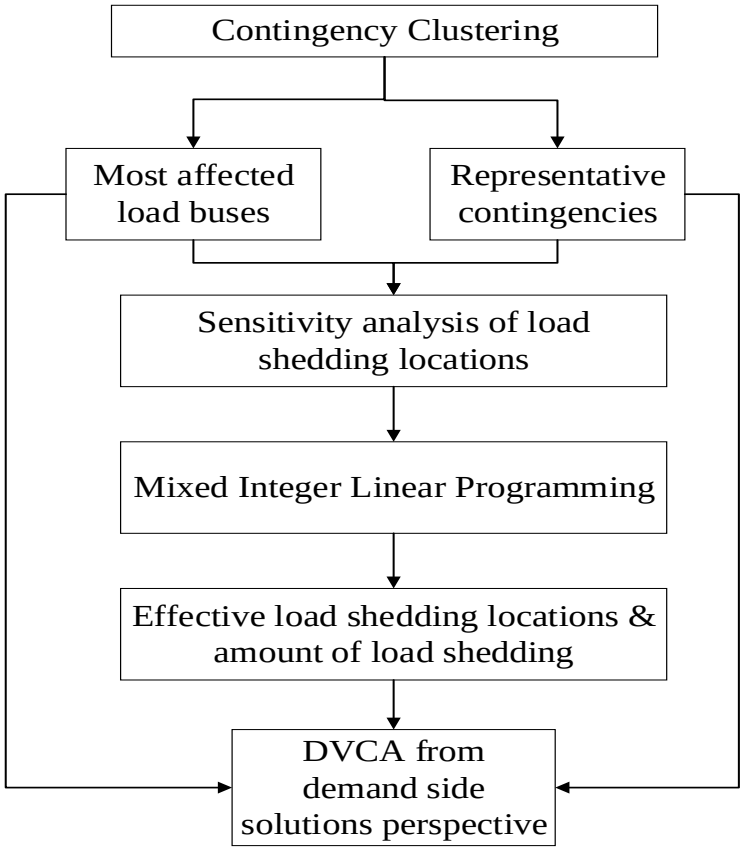

Figure 4.4: Overview of steps to derive DVCA from demand side solutions perspective

Even after placing dynamic reactive resource at strategic locations, if sufficient reactive reserves cannot be made available for a certain disturbance then the primary means to avoid short-term voltage problems is to shed loads. The ideal loads to shed are heavily inductive

loads. When heavily inductive loads are shed, both the system active and reactive power loads are reduced.

For short-term voltage problems, the system operator may not have sufficient time to shed the loads quickly to arrest the impending low voltage issues. Several utilities have installed protective relays that can automatically trip loads to avoid voltage collapse. One such system that automatically trips selected loads when voltage falls below a threshold level, for a specified time, is called under-voltage load shedding scheme (UVLS). The essential components of DVCA are contingency clusters which exposes the dynamic reactive power weakness in that area, the buses that are affected by these contingencies and control locations that are effective in mitigating the problem. When DVCA is defined from demand-side perspective, the chosen control action is load shedding. The overview of steps involved in the process of identifying DVCA from the demand-side solutions perspective is provided in fig.4.4. The controls in the identified DVCA will provide the locations and the amount of loads to be shed.

The effective control locations (load shed locations) have to identified using sensitivity studies through extensive off-line simulations. From the contingency clustering analysis, groups of contingencies that produces similar response in the system and buses that are affected by each contingency clusters are identified. The most severe contingency in each cluster is a representative of all other contingencies present in that cluster. The weak buses corresponding to each cluster are considered as candidate locations for load shedding. For every representative contingency and for every selected candidate locations, induction motor loads are shed to find the effectiveness of load shedding at the particular location. The effectiveness is calculated using the performance improvement in system bus voltages, which is characterized by KL measure. A MILP formulation similar to the one described in section 4.4 can be used to identify the most effective load shedding locations and the amount of loads to be shed for improving voltage performance. These control locations will provide more improvement in KL measure especially at weak buses. Based on the influence of candidate locations and contingency cluster information, buses and contingencies that form the DVCA are identified.

4.7 Conclusions

DVCAs identify the different regions that are prone to short-term voltage problems. The essential components of DVCA are contingency clusters which exposes the dynamic reactive power weakness in that area, the buses that are affected by these contingencies and control locations that are effective in mitigating the problem. The effective control locations are identified using a mixed integer linear programming problem, which utilizes the location sensitivity information from extensive off-line simulations. The most important application of DVCA is identifying the different dynamic VAR deficient regions in the system, along with the contingencies that exposes these weak regions. The severely affected bus locations in each DVCA can be used as locations for placing PMUs to monitor short-term voltage problems. The formulation of DVCA is provided from both supply-side and demand side solution perspective. DVCAs from supply-side perspective identifies the control locations as buses that are effective for placing dynamic VAR support devices, whereas the demand-side DVCAs have load shedding bus locations that are effective in mitigating short-term voltage problems as its control locations. Because of the DVCA identification, the control problem for load shedding can be designed in a distributed fashion restricting the study area to each individual DVCA.

CHAPTER 5. DYNAMIC OPTIMIZATION USING KL MEASURE

5.1 Introduction

In order to respond to unforeseen events, spare MVAR capability has to be held in reserve, just as in the same manner that spare MW capability is held in reserve to respond to unforeseen events. For mitigating short-term voltage problems, fast acting dynamic reactive resources are needed. These dynamic VAR resources respond rapidly, in the order of within few cycles, to system voltage deviations. For avoiding short term voltage problems, maintaining an adequate level of dynamic reactive reserves is the key. The dynamic VAR requirements of the system for normal and disturbance conditions must be carefully examined and should be placed at strategic locations to provide support to the system. In chapter 2, the need for using dynamic optimization methods for placing dynamic VAR resources was established. A control vector parametrization (CVP) approach, a class of dynamic optimization methods, for placing dynamic VAR resources was formulated and results were validated on IEEE 162 bus system and a large utility system for a single contingency case. In this chapter, an improved formulation of CVP method is developed to accommodate multiple contingencies while planning for dynamic VAR resource allocation. The improvements in terms of formulation of the optimization problem, solution procedure, and improving the efficiency of finding the optimal solution are presented in detail in this chapter. Simulations have been performed on the modified IEEE 162 bus system to illustrate the concept of the improved CVP approach. Finally, the results of the improved CVP approach that are used to validate the philosophy of "dynamic VAR planning based on the weakness of the system" are presented.

5.2 Motivation and Proposal

In chapter 2, a direct sequential dynamic optimization approach known as CVP was developed for identifying the optimal locations and amount of dynamic VAR resources to mitigate short-term voltage problems. This CVP approach overcomes the curse of dimensionality posed the direct simultaneous dynamic optimization methods. The scalability of CVP for large utility scale power system models have been demonstrated in chapter 2. However, the demonstrations were shown only for a single contingency case. While planning for the placement of costly dynamic VAR resources, it is very essential to consider a wide range of contingencies, scenarios, and operating conditions. The direct extension of the CVP approach for multiple contingencies and scenarios will again lead to the curse of dimensionality. On the one hand it is essential to consider a wide range of system conditions and on the other hand it is important to limit the size of the problem in order to find an optimal solution using dynamic optimization methods.

To limit the size of the optimization problem, the number of contingencies considered in the optimization has to be reduced. Clustering methods described in chapter 3 identifies the most important contingencies that acts as a representative of other contingencies under various operating conditions. The consideration of only representative contingencies in the optimization significantly reduces the problem size without compromising wide range of system conditions.

Another reason for the increase size of the dynamic optimization problem is the way the constraints are formulated. The constraints of the CVP optimization problem in chapter 2, checks the specified voltage limits at all the monitored buses for every time step. If the temporal and the magnitude information of the voltage time series can be equivalently captured in a scalar quantity, then the number of constraints of the CVP problem can be greatly reduced. To accomplish this, KL measure, introduced in chapter 3, is utilized and a new formulation of CVP is developed in this chapter.

In order to avoid the complexity of solving a mixed integer dynamic optimization problem, the selection of effective control locations is done based on the concept of dynamic voltage control areas. The concept of DVCA ensures that the selected candidate locations are effective for a cluster of contingencies under multiple operating conditions. The relative weights of selected

candidate locations are obtained by utilizing KL measure and singular value decomposition. The relative weights of the candidate locations are used in conjunction with the constraint gradients to update the optimization variables at every solution iteration.

Thus, the improved CVP formulation utilizing KL measure, contingency clustering and DVCA will identify the optimal locations and amount of dynamic VARs required to mitigate short-term voltage problems. Because of the evaluation of dynamic VAR requirements in the transient time frame, the identified dynamic VAR locations and amount will ensure safe operation not only for the planned contingencies but also for the wide range of contingencies and system operating conditions they represent.

5.3 Formulation of Dynamic Optimization for Multiple Contingencies

In this section, the improved formulation of CVP optimization for multiple contingencies is presented. Equation (5.1) provides the multiple contingency dynamic optimization (MCDO) formulation to identify the optimal amount of dynamic VAR resources.

$$
\begin{aligned}
&\underset{BMAX}{\text{minimize}}\ F(U) = \sum_{m}^{N_{\text{cont}}} \sum_{i}^{N_{\text{Loc}}} C^{i}_{B_m} BMAX^{i}_{m}, \\
&\text{Subject to} \\
&\text{Power System Dynamics:} \\
&\dot{x} = f(x,y),\ g(x,y) = 0 \\
&\text{WECC Voltage Performance Constraints} \\
&KL^{i}_{m}(BMAX^{j}_{m}, V^{i}(x,y)) \leq KL^{*}(\lambda, N),\ \forall j \in \text{SLoc} \\
&\text{Limits:} \\
&BMAX^{i}_{\min} \leq BMAX^{i}_{m} \leq BMAX^{i}_{\max}, \\
&\qquad \forall i \in \text{SMon},\ \forall m \in \text{SCont}, \\
&BMAX \in \mathbb{R}^{N_{\text{Loc}}},\ C^{i}_{B_m} \in \mathbb{R}
\end{aligned}
\tag{5.1}
$$

5.3.1 Objective function

The objective of this CVP optimization is to minimize the amount of dynamic VAR requirements at the selected candidate locations. $BMAX_m^i$ refers to the maximum susceptance of the dynamic VAR device at location i, for contingency, m. $C_{B_m}^i$ is the relative weight assigned to location i for contingency m. N_{cont} corresponds to the total number of representative contingencies and N_{Loc} corresponds to the total number of selected candidate locations. The vector $U = [BMAX_1^1, \cdots, BMAX_1^{N_{\text{Loc}}}, \cdots, BMAX_m^i, \cdots, BMAX_{N_{\text{cont}}}^1, \cdots, BMAX_{N_{\text{cont}}}^{N_{\text{Loc}}}]^T$ represents the collection of all optimization variables. The candidate locations are selected using the concept of DVCA (Refer Chapter 4) and their relative weights are identified using singular value decomposition (Refer section 5.5.1).

5.3.2 Constraints

(1) *Power system dynamics :* One of the major aspects of this MCDO problem is having the power system dynamic behavior as constraints of the optimization problem. The power system dynamic behavior is represented using a set of DAE equations, where f and g represent the set of differential and algebraic equations respectively. These DAEs model the behavior of generators, exciters, governors, induction motors, power system network etc and defines the electromechanical state of the power system at any instant of time. The variables x and y represents the state (e.g. generator rotor angle, speed, internal EMF etc) and algebraic variables (e.g. bus voltages) of the power system dynamics model.

For studies involving short-term voltage problems, it is essential to include the dynamics of induction motor loads in the set of DAEs. The induction motor dynamic model should have a reasonable representation of the motor stalling phenomenon, motor current, real and reactive power consumption in the stalled state, and also provide indication of the amount of motor loads tripped by protection schemes. Without the proper representation of dynamic behavior of induction motor loads, it is difficult to represent the actual behavior of the power system for short-term voltage stability studies.(2) *WECC voltage performance :* The total

amount of dynamic VAR compensation required is determined based on the power system time domain response following the representative WECC/NERC B contingencies. The dynamic VAR devices act to maintain the bus voltages so that it satisfies the WECC voltage performance criteria. WECC transient voltage dip criterion states that for a Category B disturbance (single element outage), should not cause a transient voltage dip that is greater than 20% for more than 20 cycles at load buses, or exceed 25% at load buses or 30% at non-load buses at any time other than during the fault. Also, the steady state voltage limit prescribes at steady state voltage values should be between the bound of 95% to 105%. WECC voltage performance criterion involve both temporal and magnitude information of the voltage time-series data. WECC voltage performance criterion is a point-wise criterion and if this criterion has to be evaluated at all the monitored buses, for all the considered contingencies, then it will increase the number of constraints. To limit the number of constraints, KL measure are utilized to transform the temporal and magnitude information of the voltage time series into an equivalent scalar quantity. Now, the WECC voltage performance criterion is evaluated as a constraint in KL measure at all the monitored buses. KL_m^i is the KL measure at the monitored location i, for contingency m and is a function of voltage time series $V^i(x, y)$, which is in turn function of available dynamic VAR support $BMAX_m^j,\ \forall j \in \text{SLoc}$. $KL^*(\lambda, N)$ is the critical KL value, above which the WECC voltage performance criterion will be violated. The larger the values of KL are, the more severe the WECC voltage performance violations. The critical KL value is a function of λ, the parameter that controls the width of the reference distribution and N, the number of partitions made in the voltage axis.

(3) *Limits on the size of VAR device* The final set of constraints provide the limits on the size of the dynamic VAR device that has to be placed at each location. The limits on the size of the VAR device depends upon the physical constraints such as space availability and economics associated with installment. $BMAX^i_{\min}$ and $BMAX^i_{\max}$ are the minimum and maximum possible limits of the maximum susceptance of the dynamic VAR device at location i.

5.4 Solution Methodology

The MCDO identifies the optimal amount of dynamic VAR compensation required at the selected candidate locations to satisfy the WECC voltage performance constraints for all representative contingencies. The MCDO problem is solved using the control vector parameterization (CVP) approach (Refer Chapter 2 for details). The overview of steps involved in the MCDO solution process is provided in fig.5.1. The MCDO solution process has three major divisions (a) Preparation of NLP optimization (b) NLP Optimization routine (c) Interaction with power system dynamics solver.

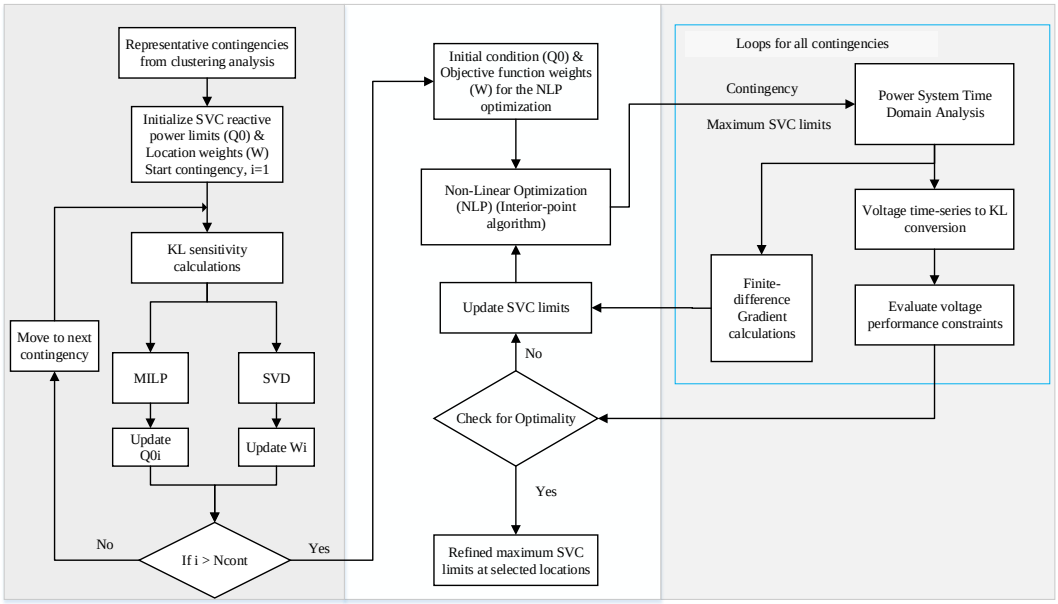

Figure 5.1: Overview of dynamic optimization for multiple contingencies

5.4.1 Prepartion of NLP optimization

In the CVP approach, the dynamic optimization problem is converted into a NLP problem by discretization of control variables. For the MCDO problem, the control variables are $BMAX_m^i$, $\forall i = 1 : N_{\text{Loc}}$, the maximum susceptance of SVC at the selected candidate locations. Since the control variables exhibit constant profile for the entire optimization time window, no discretization of control variables are made at the intermediate time steps. This particular selection of control variable reduces the complexity associated with the selection of approxima-

tion functions for the discretized time-dependent control variables. The solution of the state variables ($x(t)$) are obtained by the forward integration of the DAE system. The solution of NLP problems using numerical methods are in essence, *iterative* in nature. These iterative methods requires a reasonable good starting point for the NLP optimization algorithm so that it can reach the optimal solution in finite number of iterations. Based on the local information obtained from the current iteration, i, the NLP optimization algorithm calculates the next iteration's direction and step length. One of the information that is utilized to calculate the updates on the optimization variables is the gradient of the objective function. By appropriately weighing the candidate locations based on its relative importance, the NLP optimization algorithm can utilize this gradient information to reach the optimal solution in an effective manner. Singular value decomposition (SVD) is used to identify the relative weights of candidate locations. The details of SVD technique for identifying the candidate location weights for different representative contingencies are provided in section 5.5.1. For starting the NLP optimization problem with a good initial guess, the solution from MILP problem is utilized. The MILP problem is also used to fix the candidate locations for dynamic VAR placement. The details of MILP in the preparation of NLP optimization are discussed in section 5.5.2

5.4.2 Optimization routine

The solution procedure of the dynamic optimization has three components - (a) Non-linear programming (NLP) solver, (b) power system DAE solver, and (c) sensitivity calculations to provide gradients for updating optimization variables. Gradient based NLP solvers such as active set algorithms, interior-point methods (IPM) are some of the preferred solvers for solving the non-linear programming problem. IPMs approach the optimal solution from the interior of the feasible region. IPM, also known as barrier methods, replaces the NLP problem by a series of barrier sub-problems controlled by a barrier parameter. The sub-problems in every iteration are solved using sequential quadratic programming (SQP) and trust regions. Detailed description of IPM for NLP problems can be found in [46].

In CVP, the dynamics of the system is solved separately using forward integration methods and the solution is utilized to evaluate the constraints of the NLP problem. This feature of

CVP facilitates the use of commercial grade programs like PSSE, PSLF etc to solve the system of DAEs that represent the dynamic behavior of power system. The advantages of separating the system dynamics from the NLP problem are (a) overcomes the curse of dimensionality, if the system dynamics have to be solved simultaneously with the NLP constraints, (b) the use of commercial grade programs provide the advantage of having advanced component models and solution algorithms. The CVP approach is flexible to adopt the advancements in dynamics system modeling and DAE solution strategies.

The key information the NLP solver requires to update its decision variable for the next iteration is the gradient of the objective function and the Jacobian matrix of the constraints. The accuracy of these first-order derivative information makes the NLP solver more efficient and robust. If the exact first order derivatives to calculate the gradients of objective function and constraints are not possible to obtain, then approximation of these first order derivatives can be made through finite difference methods.

Equation (5.2) provides the forward-finite difference approximation of the constraint C_i variation to change in the variable u_j at the k^{th} iteration. Equation (5.3) provides the Jacobian matrix of the constraints of the NLP problem, where $\nabla C_i(U)$ represents the variation of constraint C_i with respect to the variation of all optimization variables (U). The computational cost of the finite-difference method depends upon the number of optimization variables (Nu). The system dynamics has to be solved $Nu + 1$ times and constraint functions are evaluated for all the simulations. In every computation one of the optimization variables changes by a pre-defined amount (Δu) from the current optimization iteration value and with the base case computation where all optimization variables remains at the current iteration k values. At the end of all simulations for gradient computations, (5.4) is used to calculate the gradients of all constraints.

$$\nabla C_i(u_j) = \frac{C_i(u_j^k + \Delta u_j) - C_i(u_j^k)}{\Delta u} \tag{5.2}$$

$$J_m(U) = \begin{bmatrix} \nabla C_1(U)^T \\ \vdots \\ \nabla C_i(U)^T \\ \vdots \\ \nabla C_{Nc}(U)^T \end{bmatrix}, \quad \nabla C_i(U) = \begin{bmatrix} \frac{\partial C_i}{\partial u_1} \\ \vdots \\ \frac{\partial C_i}{\partial u_j} \\ \vdots \\ \frac{\partial C_i}{\partial u_{Nu}} \end{bmatrix}, \; U = \begin{bmatrix} u_1 \\ \vdots \\ u_j \\ \vdots \\ u_{Nu} \end{bmatrix} \tag{5.3}$$

$$\nabla_{u_j} J^k = \frac{J^k(u_1, \cdots, u_j + \Delta u_j, \cdots, u_{Nu}) - J^k(U)}{\Delta u_j} \tag{5.4}$$

$$\nabla F = [\frac{\partial F}{\partial u_1}, \cdots, \frac{\partial F}{\partial u_j}, \cdots, \frac{\partial F}{\partial u_{Nu}}], \; \frac{\partial F}{\partial u_j} = C^j_{Bm} \tag{5.5}$$

The NLP solver utilizes the gradient of the objective function and constraints Jacobian matrix to compute the optimization variables update vector for the next iteration.

5.4.2.1 Convergence criteria

This subsections describes the convergence criteria and stopping tests used by NLP algorithms to declare local optimal or infeasible solutions. In the theory of numerical optimization, the convergence of an optimization method makes it a theoretically valid optimization routine.

Equation (5.6) provides the first order conditions for identifying a local optimal solution.

$$\nabla f(u) + \sum_{i=1}^{N_c} \lambda_i^c \nabla c_i(x(u), y(u)) + \sum_{j=1}^{N_x} \lambda_j^b = 0 \tag{5.6a}$$

$$\lambda_i^c.(c_i^U - c_i(x(u), y(u))) = 0, i = 1 \cdots N_c \tag{5.6b}$$

$$\lambda_j^b.\min\big[(u_j - b_j^L), (b_j^U - u_j)\big] = 0, j = 1 \cdots N_x \tag{5.6c}$$

$$c_i(x(u), y(u)) \leq c_i^U, \; i = 1 \cdots N_c \tag{5.6d}$$

$$u_j^L \leq u_j \leq u_j^U, \; j = 1 \cdots N_x \tag{5.6e}$$

$$\lambda_i^c \geq 0, \tag{5.6f}$$

$$\lambda_j^b \geq 0, \text{ if } u_j^U \text{ is finite}, \tag{5.6g}$$

$$\lambda_j^b \leq 0, \text{ if } u_j^L \text{ is finite}, \tag{5.6h}$$

λ_i^c is the Lagrange multiplier corresponding to the constraint $c_i(x)$, and λ_j^b is the Lagrange multiplier corresponding to the bounds on variable u_j. The Lagrange multiplier, λ_j^b, can take either positive or negative value depending upon whether the corresponding variable is upper or lower bounded as indicated by (5.6g)-(5.6h).

The NLP optimization algorithm also stops if it encounters one of the following,

1. When the norm of the gradient becomes small, i.e $\left\|\nabla f(u^i)\right\| \leq \epsilon$
2. When the iteration step size becomes small, i.e $\left\|u^{i+1} - u^i\right\| \leq \epsilon$
3. When the relative change in the objective function becomes small, i.e $\frac{f(u^i)-f(u^{i+1})}{f(u^i)} \leq \epsilon$

5.4.3 Interaction with power system DAE solver

The relative weights of different candidate locations obtained from SVD are used as cost coefficients (W) in the objective function. With the initial amount of dynamic VAR compensation from the MILP optimization, the power system time domain analysis is invoked to solve the DAE of the system for all the representative contingencies. The voltage time series of all the monitored buses obtained from the DAE solution is converted into KL measure. KL measure provides a quantitative measure of rate of voltage recovery and also the voltage level to which the time series converges in a scalar quantity. In the NLP problem, the voltage performance constraints are formulated in terms of KL measure. Thus, the results from the power system DAE solution is used to evaluate the NLP constraints at every optimization iteration. The performance of KL measure of all the monitored buses is evaluated based on the critical KL value corresponding to WECC voltage performance criteria. If the KL measure at a particular bus is greater than the critical KL value, then the voltage recovery at the corresponding bus violates the WECC performance criteria.

Also, the optimization routine interacts with the power system DAE solver to calculate the sensitivity of KL constraints to the change in the maximum amount of dynamic VAR device at the selected candidate locations. The finite difference block provides the necessary contingency details, B_{max} values for the VAR devices, and candidate locations as inputs to the power system DAE solver. Utilizing the sensitivity information from all candidate locations,

the finite difference block constructs the constraints Jacobian information, which is provided to the optimization routine.

5.5 Improvements in Solution Efficiency

5.5.1 Singular value decomposition

Singular value decomposition is used to identify and order the dimensions along which the inputs exhibit the most variations. Utilizing SVD, any rectangular matrix, $A \in C^{m \times n}$, can be decomposed into product of three matrices - output direction matrix (U), scaling matrix (Σ), and input direction matrix (V), as shown in (5.7). The output and input direction matrices, U and V, are of the size $(m \times m)$ and $(n \times n)$ respectively. The scaling matrix (Σ) is a diagonal matrix of the size $(m \times n)$ and it contains the singular values of matrix A as its diagonal entries. The singular values in scaling matrix (Σ) indicate the variance of the linearly independent components along each dimension.The columns of the matrix U contains the orthonormal eigenvectors of AA^T and the columns of the matrix V has the orthonormal eigenvectors of $(A^T A)$.

$$A^{(m \times n)} = U^{m \times m} \Sigma^{m \times n} V^{T\ (n \times n)} \tag{5.7}$$

$$\begin{aligned} A^{(m \times n)} V^{(n \times n)} &= U^{m \times m} \Sigma^{m \times n} \\ A v_i &= \sigma_i u_i,\ \forall i = 1 : n \end{aligned} \tag{5.8}$$

Utilizing the orthogonality of the input direction vectors in V matrix (5.7) can be transformed into (5.8). By selecting the input direction vector, v_i, corresponding to the maximum singular value, σ_i, the maximum change can be observed in the output vector, u_i. For enhancing the solution efficiency of the MCDO optimization problem, SVD is used to identify the relative weights of the candidate locations identified by the MILP optimization. For each of the selected MILP candidate locations, the variation of KL measure at the monitored locations for VAR injections at the selected location is calculated. The sensitivity information from all NL

candidate locations is utilized to form the Jacobian matrix, J_m ((5.9)), where 'm' represents a particular contingency ID. The entry $\frac{\partial KL_i^m}{\partial Q_j^m}$ corresponds to the change in the KL measure at the monitored bus, i, for VAR injection at the candidate location, j.

$$J_m = \begin{bmatrix} \frac{\partial KL_1^m}{\partial Q_1^m} & \cdots & \frac{\partial KL_1^m}{\partial Q_j^m} & \cdots & \frac{\partial KL_1^m}{\partial Q_{NL}^m} \\ \vdots & & \vdots & & \vdots \\ \frac{\partial KL_i^m}{\partial Q_1^m} & \cdots & \frac{\partial KL_i^m}{\partial Q_j^m} & \cdots & \frac{\partial KL_i^m}{\partial Q_{NL}^m} \\ \vdots & & \vdots & & \vdots \\ \frac{\partial KL_p^m}{\partial Q_1^m} & \cdots & \frac{\partial KL_p^m}{\partial Q_j^m} & \cdots & \frac{\partial KL_p^m}{\partial Q_{NL}^m} \end{bmatrix} \tag{5.9}$$

Similarly, the sensitivity matrices for the selected candidate locations are calculated for all the representative contingencies chosen for the dynamic optimization study. Equation (5.10) shows the structure of the Jacobian matrix considering all the representation contingencies of the MCDO problem. By performing, SVD analysis on the Jacobian matrix, the relative weights of candidate locations under different conditions can be identified.

$$J_{full} = \begin{bmatrix} J_1 & \cdots & & \cdots & 0 \\ \vdots & \ddots & & & \vdots \\ 0 & \cdots & J_m & \cdots & 0 \\ \vdots & & & \ddots & \vdots \\ 0 & \cdots & 0 & \cdots & J_{NCont} \end{bmatrix} \tag{5.10}$$

5.5.2 MILP

The NLP part of the CVP optimization requires the initial set of candidate locations for dynamic VAR placement as an input. The selection of input set of candidate locations affects the efficiency of the CVP solution process. If this input set of locations is not chosen properly, then it degrades the performance of NLP optimization. In general, as the size of the input candidate locations set increases, the amount of time required to solve the NLP optimization increases. If the input locations set contains non-effective candidate buses, then the NLP optimization may converge to an infeasible solution. In this work, the effective control candidate

locations are identified using the concept of dynamic voltage control areas (DVCA). The DVCA employs a MILP optimization problem to identify the most effective control candidate locations that are effective in mitigating short-term voltage problems. The MILP optimization provides the following results, which are used as inputs to the dynamic optimization problem,

1. Initial set of effective candidate locations for the placement of dynamic VAR resources.
2. Initial amount of dynamic VAR compensation at the selected candidate locations, which is used as a starting solution for the NLP optimization problem.

5.6 Simulation Results

Simulations have been performed in the modified IEEE 162 bus system. The modified test system has 184 buses, 17 generators, 111 loads, 34 shunts, and 238 branches. For a more accurate load representation, 22 load buses were stepped down through distribution transformers to the 12.47 kV level, and the new low voltage buses were assigned the numbers 163 through 184. The system has a total of 15.387 GW real power demand and 1174 MW of reactive power demand. To capture the dynamic behavior of motor loads, a composite load model represented by CMDL was used at the new representative load buses. Additionally, composite load models were also used to represent motor loads at the major load centers (zones 3 and 6). Of the total load for each bus, 30% is specified as three-phase induction motor loads and 35% as single-phase air conditioner loads. The loads in zone 1 and 12 are not represented with composite induction motor loads.

For the base case operating condition, out of 316 N-1 contingencies considered for analysis, 71 are identified as severe contingencies by the initial screening process. These 71 contingencies are classified into two cluster groups. The most severe contingency from each cluster group is treated as a representative contingency for the corresponding cluster group. Contingencies 2 and 34 are selected as the representative contingencies for clusters 1 and 2 respectively. The details of all the contingencies are provided in appendix A.

Base case simulation results: Figures 5.2 and 5.3 shows the voltage response of the 5 severely affected buses for the representative contingencies of clusters 1 and 2 respectively. The KL

values corresponding to the voltage responses of buses shown in figs. 5.2 and 5.3 are provided in table 5.1. The higher the KL values, the greater the violation in voltage performance.

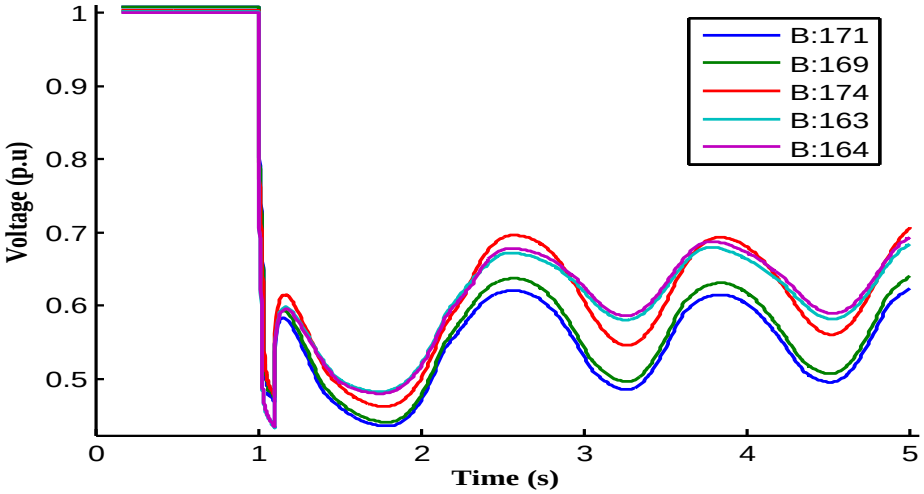

Figure 5.2: Voltage responses of top 5 violating buses for the representative contingency of cluster 1

Table 5.1: KL values of the top 5 violating buses for the representative contingencies

Cluster 1		Cluster 2	
Bus	KL values	Bus	KL values
171	95.92395	177	42.00372
169	91.3023	148	30.22546
174	73.38107	163	27.38258
163	71.13043	173	24.78475
164	69.73211	147	22.8866

MILP optimization results: The KL performance at all the monitored buses are observed after employing the dynamic VAR compensation at the locations identified by the MILP optimization. With the usage of dynamic VAR resources, the KL performance violations have been reduced but not completely eliminated. For cluster 1 representative contingency, 11 buses had KL violations and 14 buses exhibited KL violations for cluster 2 representative contingencies.

Table 5.2 shows the top 5 buses with KL violations after employing the dynamic VAR compensation from the MILP optimization for cluster 1 representative contingency. It also shows the KL values of the top 5 buses that exhibited maximum KL violations in the base case

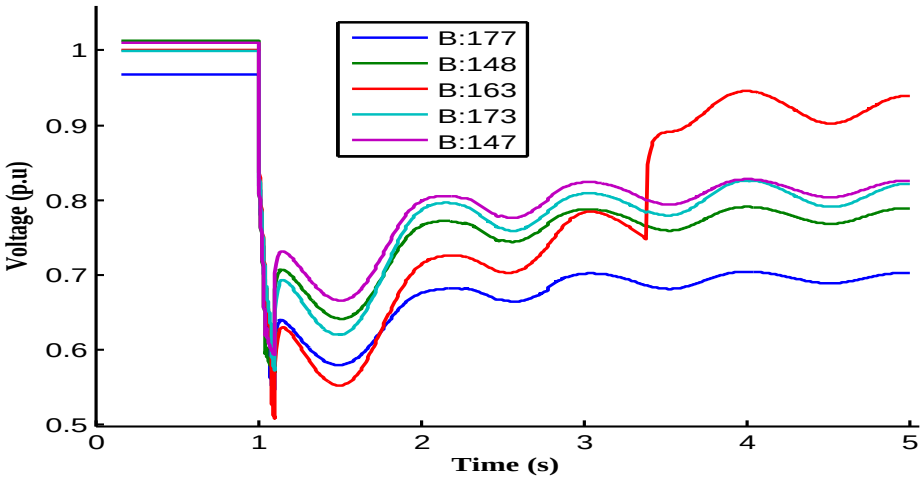

Figure 5.3: Voltage responses of top 5 violating buses for the representative contingency of cluster 2

Table 5.2: KL values for the top 5 violating buses in base case and MILP case, after employing MILP solution for cluster 1 representative contingency

Base Case Violation Buses		MILP Top 5 violations	
Bus No	KL Values	Bus No	KL Values
171	0.752	148	17.32
169	0.745	147	10.84
174	1.146	117	9.39
163	0.644	116	8.482
164	0.587	52	8.338

condition. The voltage responses of the buses in table 5.2 are shown in figs. 5.4 and 5.5.

Similarly, table 5.3 shows the top 5 buses with KL violations after employing the dynamic VAR compensation from the MILP optimization for cluster 2 representative contingency. It also shows the KL values of the top 5 buses that exhibited maximum KL violations in the base case condition. The voltage responses of the buses in table 5.3 are shown in figs. 5.6 and 5.7.

MCDO results: Utilizing the MILP solution as the NLP starting solution, the amount of dynamic VAR compensation at the identified locations are further refined using dynamic optimization. Three different cases are used to construct the relative weights of different locations in the objective function. In case A, the relative weights are identified using the maximum SVD

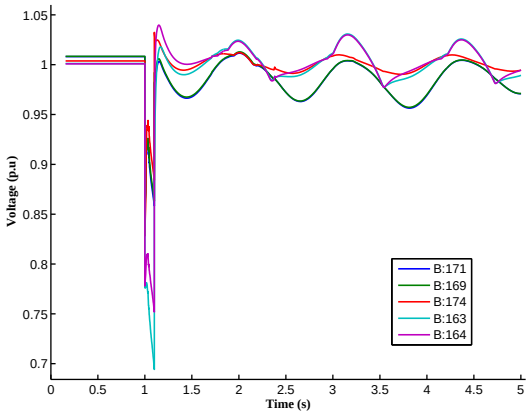

Figure 5.4: Voltage responses at top 5 base case violation buses for the cluster 1 representative contingency with LP solution

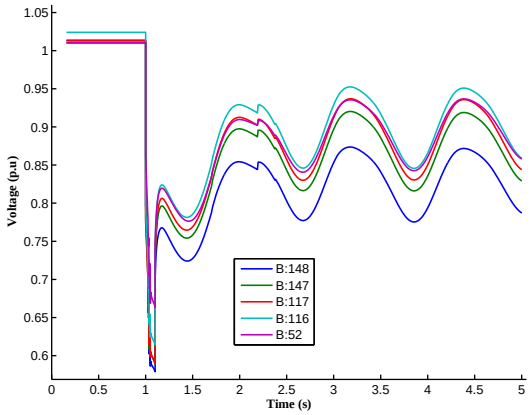

Figure 5.5: Voltage responses of top 5 violating buses for the cluster 1 representative contingency with LP solution

Table 5.3: KL values for the top 5 violating buses in base case and MILP case, after employing MILP solution for cluster 2 representative contingency

Base Case Violation Buses		MILP Top 5 violations	
Bus No	KL Values	Bus No	KL Values
177	3.949	148	14.068
148	14.068	78	9.3029
163	0.911	68	8.3807
173	1.389	69	7.8269
147	7.116	79	7.7294

direction. In case B, the inverse of relative weights used in case A are used to construct the objective function cost coefficients. Case C assumes a uniform weights for all the considered locations. The relative weights of selected candidate locations for the three different cases are provided in table 5.4. The most sensitive location in case A (e.g Bus 144 for cluster 1) is made as the least sensitive location for case B.

The NLP part of the dynamic optimization for multiple contingencies was solved using interior point algorithm in KNITRO solver. PSSE is used to perform time domain simulations of the power system model. The finite difference gradients of constraints are computed in MATLAB using PSSE simulation results. The maximum number of iterations for the NLP solver is limited to 15, to reduce the unnecessary computations for infeasible cases. Table 5.5 provides the results of the dynamic optimization for the considered three different cases.

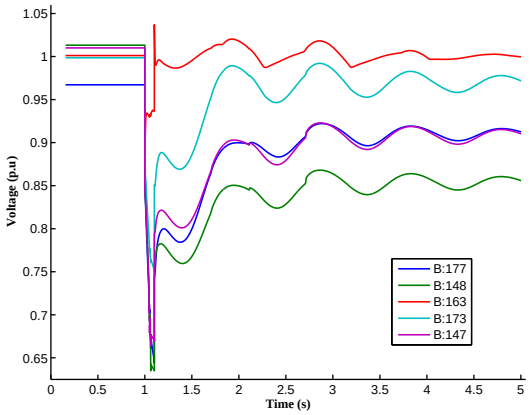

Figure 5.6: Voltage responses at top 5 base case violation buses for the cluster 2 representative contingency with LP solution

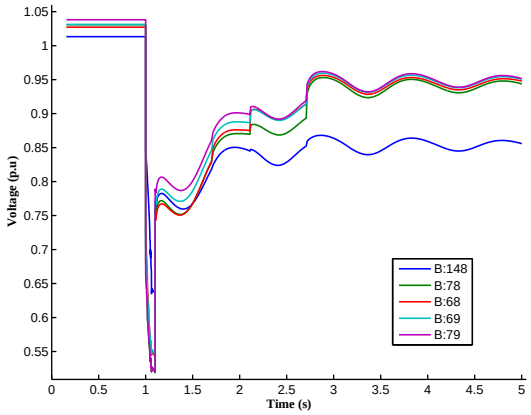

Figure 5.7: Voltage responses of top 5 violating buses for the cluster 2 representative contingency with LP solution

Table 5.4: NLP inputs - Relative weights of selected candidate locations and starting solution

	Case A		Case B		Case C		Initial Max Bsvc	
Bus No	cluster 1	cluster 2	cluster 1	cluster 2	cluster 1	cluster 2	cluster 1	cluster 2
117	0.0592	0.5460	0.6649	0.1276	1	1	0	2
133	0.5111	0.2141	0.0771	0.3254	1	1	1.5	0
135	0.5140	0.1071	0.0766	0.6507	1	1	3	0
144	0.5173	0.1071	0.0761	0.6507	1	1	2.45	0
147	0.0540	0.5888	0.7298	0.1183	1	1	0	3
148	0.4479	0.5353	0.0879	0.1301	1	1	1	1

It also provides the dynamic VAR compensation output of the NLP optimization for each of the representative contingencies. C1 and C2 correspond to the representative contingencies of cluster 1 and 2 respectively. The columns *Max Bsvc* provide the final values of maximum SVC limit at the selected candidate locations.

The following inferences can be made from the results shown in table 5.5.

- Case A and C converges to a local optimal solution, whereas Case B converges to an infeasible solution. The selection of proper weights for the locations in the objective function plays an important role in the convergence of the NLP optimization.
- Case C (uniform relative weights) took more number of iterations to converge to an optimal solution, when compared to case A (SVD based relative weights). The selection

Table 5.5: Multiple contingency dynamic optimization results

	Case A			Case B			Case C		
Bus No	C1	C2	Max Bsvc	C1	C2	Max Bsvc	C1	C2	Max Bsvc
117	0	2.05	2.05	1.02	0.8	1.02	0.88	1.95	1.95
133	1.16	0	1.16	0	0.88	0.88	1.4	0.94	1.4
135	2.73	0	2.73	1.45	1.51	1.51	2.91	0.98	2.91
144	2.22	0	2.22	0.84	1.34	1.34	2.36	0.94	2.36
147	0	3.11	3.11	4.17	1.91	4.17	2.93	2.95	2.95
148	1.53	1.84	1.84	0.26	1.21	1.21	0.95	1.95	1.95
Total			13.11			10.13			13.52
Convergence	Local Optimal			Infeasible			Local Optimal		
No of iterations	3			15			7		
CPU time (s)	900			8200			2300		

of relative weights based on SVD direction increases the computational efficiency of the dynamic optimization algorithm.

- The amount of dynamic VAR compensation obtained from dynamic optimization is more when compared to that of the MILP optimization. The increased amount is to completely eliminate the KL voltage performance violations at all buses.

- The MCDO simulations have been performed with a base value of 100 MVA. Therefore, a total of 1311 MVAR dynamic VAR is required to maintain the KL voltage performance constraints at all buses for the representative contingencies. This large amount of dynamic VARs are required to prevent the stalling of induction motors, which form 65% of the total load in the system.

MCDO solution computational time: All simulations have been performed in a 64-bit desktop PC with i5 processor operating at 3.40 GHz. For IEEE 162 MCDO optimization routine with two representative contingencies, cases A, B and C took 900 seconds (3 iterations), 8200 seconds (15 iterations), and 2300 seconds (7 iterations) respectively. The majority of time is spent in the finite-difference Jacobian calculations. As the size of the system increases, the MCDO solution computational time will increase mainly because of the increased computational time in performing the time domain simulation of large systems. Though the MCDO computational time will increase still it will be able to handle large systems with this improved

formulation as opposed to the direct simultaneous methods which suffers from the curse of dimensionality.

Figures 5.8 and 5.9 provide the voltage responses of all buses, with the use of dynamic VARs from MCDO, for the representative contingencies from cluster 1 and 2 respectively. The KL values of all the monitored buses are below 5, indicating no violations in the WECC voltage performance criteria.

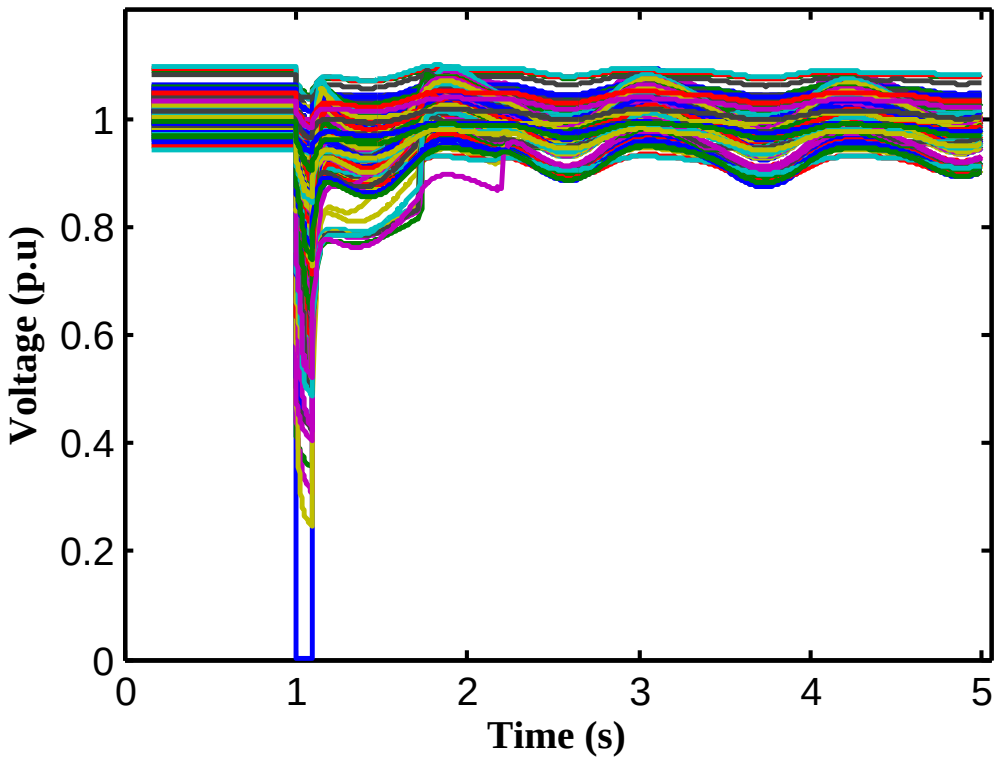

Figure 5.8: Voltage responses of all buses for cluster 1 representative contingency using MCDO results

5.6.1 Validation

The main reason for using selected representative contingencies in the dynamic optimization is to limit the size of the optimization problem while effectively capturing the characteristic features of other contingencies. Each representative contingency acts as a representative of other contingencies in the corresponding cluster because they exhibit a similar behavior in creating

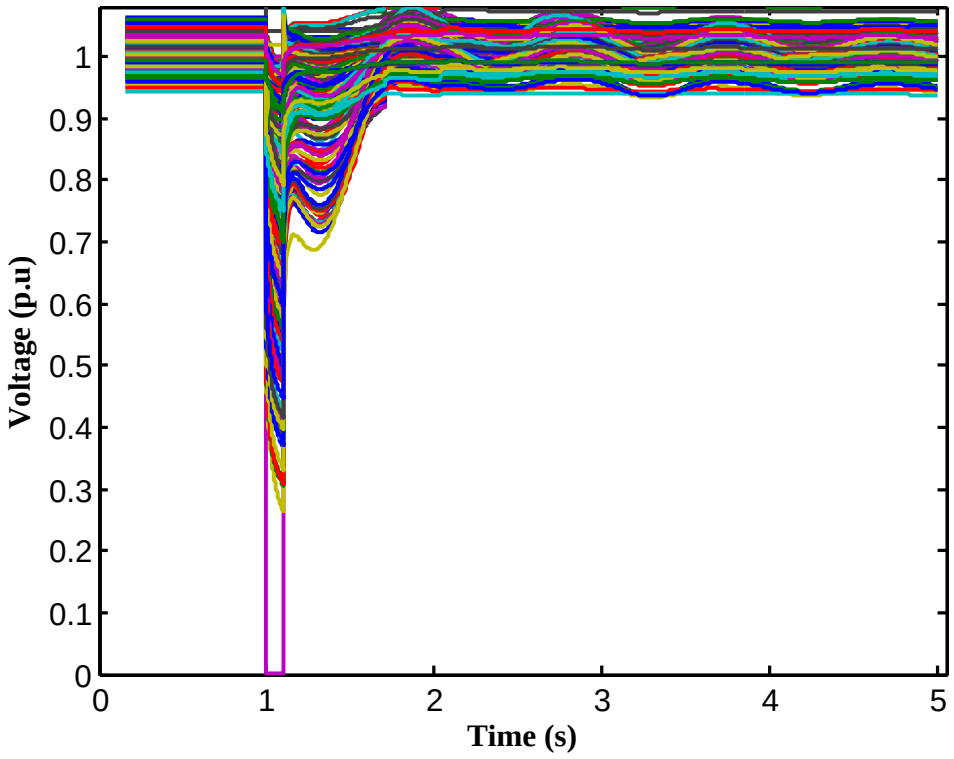

Figure 5.9: Voltage responses of all buses for cluster 2 representative contingency using MCDO results

short-term voltage problems. If the violations for the most severe contingency in every cluster groups are mitigated then the violations created by other similarly behaving contingencies will be taken care of, except for a few special cases. To validate the results of multiple contingency dynamic optimization results, simulations have been performed with and without the use of dynamic VAR support and the comparison results are shown in table A.1 (Appendix: 6.3.2). This table presents the details of the contingencies, number of KL violations in the base case condition (no dynamic VAR support), number of KL violations after installing dynamic VAR solutions obtained from dynamic optimization, and the contingencies that are included in the clusters.

The following are the key inferences from the validation results:

- The dynamic VAR planning using representative contingency screening method was able to mitigate 85% of bus KL violations. There were a total of 2309 KL voltage performance violations in the base case simulation of 316 contingencies. With the use of dynamic VAR resource obtained from MCDO, the number of violations have been reduced to 334. The MCDO was performed with only 2 representative contingencies.

- Most of the KL violations after the use of MCDO solution are relatively small when compared to the base case condition. The majority of these KL violations are created by contingencies that are not included in the clusters. These contingencies have created violations less than the threshold number of buses and hence they are not included for further analysis in the pre-processing stage of the clustering analysis.

- Among the contingencies that are included in the clusters, there are 2000 violations in the base case and 180 violations after the use of MCDO results. This suggests that the representative contingencies were able to mitigate the violations of other contingencies that have been included in their corresponding clusters.

- The maximum number of violations after employing MCDO solution is created by contingency ID 35. This is a special contingency in cluster 2. In the base case condition, the KL violation buses exhibited oscillatory voltage waveforms. Such highly non-linear cases need special treatment because they cannot be considered in the MILP optimization procedure. With the solution from the MCDO process, the number of violations have been reduced from 113 to 28. If the dynamic optimization is repeated for contingency ID 35, starting from the MCDO solution, the remaining violations can be eliminated.

5.6.2 Use of load shedding

In this section, the results of the study that allows certain percentage of induction motors load shedding while evaluating the dynamic VAR requirements of the system. The criteria for shedding loads is derived based on the WECC voltage performance criteria. If the bus voltage

stays below 0.7 p.u for more than 20 cycles then certain percentage of induction motors were allowed to disconnect using an under-voltage protection scheme. Two different percentages of load shedding were considered for comparison, where case A corresponds to 20% load shedding and case B corresponds to 40% load sheding. Table 5.6 provides the optimal amount of VAR requirements obtained from the dynamic optimization for 20% and 40% of induction motor load sheds.

Table 5.6: Comparison of MCDO results with different levels of load shedding

Max allowable load shed	0	20%	40%
Bus No	Max Bsvc		
	Base	Case A	Case B
117	2.05	0.00	0.00
133	1.16	0.00	0.00
135	2.73	1.02	0.68
144	2.22	1.24	1.11
147	3.11	1.12	0.00
148	1.84	2.55	1.28
Total	13.11	5.93	3.06
Percentage reduction in SVC amount		54.75	76.64

The following are the inferences from the results presented in table 5.6.2:

1. With 20% allowance of load shedding, the number of dynamic VAR locations is reduced from 6 to 4 and with 40% load shedding allowance only 3 locations are needed to mitigate all the KL performance violations.

2. In case A, the total amount of dynamic VAR resources is 5.93 p.u., which corresponds to a 54.75% reduction when compared to the base case where no load shedding is allowed.

3. Similarly with case B, where high amount of load shedding allowance is made, the total amount of dynamic VAR resource is reduced to 3.06 p.u from 13.11 p.u. in the base case. This corresponds to a 76.64% reduction in the dynamic VAR requirements.

These study results shows that the use of demand-side controls like load shedding can reduce the amount of investments made in installing new dynamic VAR devices. With the

increasing trend in demand response programs, load control can be a part of solutions that are used to mitigate short-term voltage problems. They offer economic benefits by deferring the installments of costly dynamic VAR resources. The use of supply-side solutions like adding new dynamic VAR devices are also necessary until the threat of short-term voltage problems are reduced to a considerably lower level. Otherwise, the lack of sufficient dynamic VAR support may lead to frequent short-term voltage problems like FIDVR, which in turn require the loads to be shed frequently. Depending upon the severity of the problem and cost of installing new devices, the MCDO formulation has to be extended to accommodate demand-side controls. Such an integrated supply and demand side controls framework will provide the planners with different choices to arrive at both economical and compliant solution for short-term voltage problems.

5.7 Conclusions

In this chapter, an improved CVP formulation to identify the optimal amount of dynamic VARs required to mitigate the short-term voltage problems under multiple contingencies is provided. KL measure is utilized to significantly reduce the size of the dynamic optimization problem. The concept of DVCA is utilized to identify the initial set of effective control candidate locations. The efficiency of the dynamic optimization problem is improved by SVD and MILP formulations. SVD provides the relative weights of candidate locations for multiple operating conditions, which are used to compute the gradient of the objective function. The solution of MILP provides the starting point for the NLP optimization routine, which makes it to converge to the optimal solution in a faster way.

CHAPTER 6. CONCLUSIONS

6.1 Conclusions

A comprehensive, dynamic optimization based VAR planning strategy to mitigate short-term voltage problems was developed in this work. The developed approach evaluates the reactive power needs dynamically using time domain simulations and accounts for a wide range of contingencies, scenarios and operating conditions. Control vector parameterization, a dynamic optimization approach was used to identify the most effective bus locations and the optimal amount of dynamic VAR compensation required to overcome the short-term voltage problems.

Short-term voltage problems are exacerbated by single-phase low inertia induction motor loads that represent residential A/C systems, since they tend to decelerate and stall when their voltage magnitude drops below a certain level. Stalled motors have an adverse impact on voltage stability because they consume very large amounts of reactive power within a very short time during a large disturbance. Appropriate load models that can capture the dynamic behavior of induction motor loads have to be used in the planning studies. The use of inaccurate load models may not adequately identify potential short term voltage problems and give false confidence about system's ability to handle short term voltage problems. The system exposure to short term voltage problems like delayed voltage recovery can be a symptom of a larger issue - inadequate dynamic reactive support. Therefore, the use of dynamic VAR support devices is necessary until the threat of induction motor stalling is significantly reduced.

Control vector parametrization, a dynamic optimization method is used to identify the optimal amount of reactive power needed to mitigate short term voltage problems which occurs in the system with high penetration of induction motor loads. With this approach, the

dynamics of the system especially load dynamics are properly accounted for while performing optimization. The CVP method based on direct sequential approach overcomes the curse of dimensionality posed by direct simultaneous approach, by separating the solution of system dynamics from the optimization routine. This feature of CVP enables to utilize commercial software like PSSE to solve power system dynamics and utilize the results in the optimization routine. The scalability of this CVP approach has been shown by testing this methodology on a large scale realistic power system.

In order to cover a wide range of possibilities in the power system planning process, a two level clustering procedure to reduce the number of scenarios, operating conditions and contingencies was developed. To facilitate the clustering process, KL measure, a quantitative measure that captures the rate of recovery of bus voltages and its level of recovery in a scalar quantity was developed. The clustering procedure identifies the most important contingencies, scenarios and operating conditions that act as representative of other cases that exposes dynamic VAR deficiency in the system. Utilizing the clustering results, a novel concept called dynamic voltage control areas was derived. DVCAs identify the different regions that are prone to short-term voltage problems. Each DVCA has three essential components namely, the buses that are vulnerable to short-term voltage problems, the contingencies that exposes these problems and the most effective control locations to mitigate these problems. A mixed integer linear programming problem was formulated to identify the most effective bus locations for the placement of dynamic VAR compensation. The optimal amount of dynamic VAR as identified by the dynamic optimization is able to provide sufficient reactive support not only for the contingencies considered in the optimization process but also for all other representative cases.

The specific contributions of the research are summarized as follows,

1. Development of control vector parametrization, a dynamic optimization approach to solve the dynamic VAR planning problem. (a) Overcomes the curse of dimensionality posed by previous dynamic optimization formulations. (b) Scalable approach to handle large scale realistic power system models.

2. Classification of contingencies according to their behavioral patterns using clustering

methods. (a) Development of KL measure, a quantitative measure that captures the rate and level of recovery of voltage waveforms in a scalar quantity.(b) Two-level clustering method handles multiple contingencies, scenarios, and operating conditions.

3. Identification of dynamic voltage control areas. (a) DVCA identifies different VAR deficient areas in the system and the contingencies that exposes the weakness. (b) Formulation of MILP to identify the most effective control locations to mitigate short-term voltage problems at the affected buses.

4. Improvement of the CVP solution process using (a) Singular value decomposition (b) Linear programming to provide starting solution for the NLP optimization routine.

6.2 Future Work

The dynamic VAR planning study methodology developed in this thesis work can be further enhanced by: 1) Comparing the effectiveness of different types of dynamic VAR support strategies and their cost/benefit assessment; 2) Utilization of reactive support from geographically distributed, power electronics based distributed generation (DG) resources; and 3) Improvisation in the dynamic optimization procedure through parallelization, multistart algorithms.

6.2.1 Integrated supply side and demand side solutions

If the system does not experience short-term voltage problems frequently, then load shedding can be considered as a viable and cheaper option to mitigate these problems. In planning studies, while evaluating the dynamic VAR requirements of the system, load shedding can also be considered as an option in addition to adding new VAR resources. To accomplish this, an integrated control scheme that effectively combines both supply-side (addition of dynamic VAR resources) and demand-side controls (load shedding) to meet the dynamic VAR requirements of the system. The optimization formulations discussed in this work can be extended to include demand side controls. A preliminary description of identifying DVCA's demand side control locations is provided in Chapter 4.6. Depending upon the severity of the problem and cost of

installing new devices the user can select appropriate choices to arrive at both economical and compliant solution for short-term voltage problems. Some preliminary results on the benefits offered by load shedding strategies are discussed in Chapter 5.6.1.

In this thesis, the majority of work in identifying DVCA was based on supply-side perspective. The DVCA identification can be extended to accommodate both supply-side and demand-side controls in an integrated framework. Then the controls in DVCA will include addition of new dynamic VAR resources in the bulk system and rank ordered load shedding locations and amount of load shedding. Further, the reactive support from DG resources and wind farms can also be used as controls in each DVCA. The extension of the formulation provided in this work for multiple resources require processing of large data, and proper modeling (eg: smart inverters) of reactive support capability from DG resources and wind farms.

6.2.2 Reactive support from DG resources

There has been a significantly increasing trend in the development and usage of distributed energy resources including distributed generation (DG) and demand response (DR) in power system operations. DG in the form of solar PV, small wind, biomass, gas-fired micro-turbines, combined heat and power (CHP) resources, and energy storage have been increasingly deployed in the distribution system and expected to continue its growth in the future. DG with inverter controls can be used to provide reactive power and voltage control. Solar PV or electric vehicles (EV) with an inverter, or wind generators with converters can accomplish the same function as STATCOMs or SVCs but at much less cost. This functionality is most beneficial when active power generation is low e.g. solar outside of peak production periods. Also, the DG resources are distributed geographically, therefore providing greater flexibility in providing reactive support. To utilize DG resources for providing reactive support requires significant modeling efforts. One approach is to develop aggregate DG models for transmission level studies. Recently, the modeling and validation work group (MVWG) of the western electricity coordinating council (WECC) expanded its scope of its Renewable Energy Modeling Task Force (REMTF) to address the modeling and representation of PV systems for transmission level studies. The REMTF recognizes the fact that representing distribution-connected PV

systems in transmission studies is more challenging. Another approach is to represent induction motor loads and DG resources at the distribution feeder level and evaluate the dynamic VAR requirements using an integrated transmission-distribution analysis. Since the geographically distributed DG resources are coordinated properly to provide reactive support, these resources can reduce the installments of new dynamic VAR devices.

Smart inverters in PV systems can manipulate and control real power and reactive power independently. These inverters sense local conditions, such as voltage and frequency, and respond with autonomous actions. Their functionalities include volt-var control, frequency-watt control, and provide dynamic grid support as a part of low voltage ride through.

6.2.3 Dynamic optimization solution enhancements

Parallel computations can be used to speed up some time-consuming procedures in the NLP routine to improve overall computational performance of the CVP algorithm. The NLP routine spends majority of its time in calculating the finite difference gradients. Parallel finite difference gradient computation will greatly reduce the overall solution time of the NLP optimization. Parallelism can be introduced at two levels, (a) Calculating the constraints Jacobian matrices for different contingencies concurrently (b) Calculating the sensitivities of different candidate locations in parallel to construct the constraints Jacobian matrix corresponding to a single contingency. Parallel computing can also be utilized to increase the computational efficiency of performing time domain simulations for different contingencies while evaluating NLP constraints, calculating KL sensitivity matrix for MILP optimization, and contingency clustering.

The convergence of the CVP algorithm can be improved by using multistart algorithms. The multistart procedure uses many initial points for the NLP optimization problem and can be run in parallel on shared memory multi-processor machines. The NLP optimization routine finds a local optimal solution from each of the initial points and returns the solution with the best objective function as the final solution. The use of many initial points will also help to find a pool of local optimal solutions.

Extension of clustering methods to other power system problems: In this work, clustering methods are used to identify similarly behaving contingencies under various operating conditions. The construction of similarity matrix forms the essential part of clustering methods. KL measure of monitored buses for different contingencies is used to construct the similarity matrix. By developing appropriate similarity matrix, the clustering methods described in this work can be utilized to study other power system problems like generator coherency identification, contingency classification for studies using steady-state analysis etc.

6.3 List of Publications

6.3.1 Peer-reviewed journal publications

1. **M. Paramasivam**, A. Salloum, V. Ajjarapu, V. Vittal, N. B. Bhatt, Shanshan Liu, "Dynamic Optimization Based Reactive Power Planning to Mitigate Slow Voltage Recovery and Short Term Voltage Instability," *Power Systems, IEEE Transactions on*, vol. 28, no. 4, pp. 3865–3873, Nov. 2013

2. **M. Paramasivam**, S. Dasgupta, V. Ajjarapu, and U. Vaidya, "Contingency analysis and identification of dynamic voltage control areas," *Power Systems, IEEE Transactions on*, vol. 30, no. 6, pp. 2974–2983, Nov. 2015

3. S. Dasgupta, **M. Paramasivam**, U. Vaidya, and V. Ajjarapu, "Entropy based analysis of delayed voltage recovery," *Power Systems, IEEE Transactions on*, vol. 30, no. 5, pp. 2460–2468, Sept. 2015

4. S. Dasgupta, **M. Paramasivam**, U. Vaidya, and V. Ajjarapu, "Real-Time Monitoring of Short-Term Voltage Stability Using PMU Data," *Power Systems, IEEE Transactions on*, vol. 28, no. 4, pp. 3702–3711, Nov. 2013

5. S. Dasgupta, **M. Paramasivam**, U. Vaidya, and V. Ajjarapu, "PMU-based Model-Free Approach for Real-Time Rotor Angle Monitoring," *Power Systems, IEEE Transactions on*, vol. 30, no. 5, pp. 2818–2819, Sept. 2015

6.3.2 Conference publications

1. S. Dasgupta, **M. Paramasivam**, U. Vaidya, and V. Ajjarapu, "PMU-based model-free approach for short term voltage stability monitoring," *Power and Energy Society General Meeting, 2012 IEEE*, July. 2012

APPENDIX A. LIST OF CONTINGENCIES AND VALIDATION RESULTS

Table A.1: Validation of representative contingencies based dynamic VAR planning

Contingency ID	From Bus	To Bus	No. of violations in base case	No. of violations after MCDO	Is included in cluster
1	1	2	38	0	1
2	1	3	111	0	1
3	1	4	41	0	1
4	1	5	39	0	1
5	2	7	0	0	0
6	2	13	0	0	0
7	4	112	22	3	2
8	4	119	19	3	2
9	5	120	38	0	1
10	5	129	38	0	1
11	7	9	0	0	0
12	9	75	6	0	0
13	10	11	1	1	0
14	11	15	0	0	0
15	11	46	4	4	0
16	11	58	0	0	0
17	11	59	3	3	0

Continued on next page

Table A.1 – *Continued from previous page*

Contingency ID	From Bus	To Bus	No. of violations in base case	No. of violations after MCDO	Is included in cluster
18	15	58	0	0	0
19	16	18	0	0	0
20	17	18	0	0	0
21	18	30	5	5	0
22	18	32	5	5	0
23	19	38	0	0	0
24	20	157	0	0	0
25	21	22	0	0	0
26	22	38	0	0	0
27	22	40	0	0	0
28	22	41	0	0	0
29	23	24	0	0	0
30	24	28	1	0	0
31	24	45	0	0	0
32	25	26	0	0	0
33	25	27	0	0	0
34	26	74	87	0	2
35	26	75	113	28	2
36	28	29	0	0	0
37	29	30	2	2	0
38	29	31	2	2	0
39	30	32	3	3	0
40	32	33	2	2	0
41	33	34	4	4	0
42	33	35	3	3	0

Continued on next page

Table A.1 – *Continued from previous page*

Contingency ID	From Bus	To Bus	No. of violations in base case	No. of violations after MCDO	Is included in cluster
43	33	36	3	3	0
44	34	40	0	0	0
45	34	77	0	0	0
46	35	40	0	0	0
47	36	67	0	0	0
48	37	39	3	3	0
49	37	126	10	9	2
50	37	127	3	3	0
51	39	42	4	4	0
52	40	81	0	0	0
53	40	82	0	0	0
54	41	81	0	0	0
55	41	83	0	0	0
56	41	84	0	0	0
57	42	109	1	1	0
58	43	44	0	0	0
59	44	102	0	0	0
60	44	103	0	0	0
61	45	54	0	0	0
62	46	47	1	0	0
63	47	48	0	0	0
64	47	49	0	0	0
65	48	51	4	0	0
66	48	52	4	0	0
67	49	87	0	0	0

Continued on next page

Table A.1 – *Continued from previous page*

Contingency ID	From Bus	To Bus	No. of violations in base case	No. of violations after MCDO	Is included in cluster
68	50	51	3	0	0
69	51	141	5	0	0
70	52	79	13	5	2
71	52	106	18	9	2
72	52	116	13	6	2
73	52	117	13	6	2
74	53	54	0	0	0
75	53	55	0	0	0
76	54	56	0	0	0
77	55	57	0	0	0
78	55	149	0	0	0
79	55	162	0	0	0
80	56	67	0	0	0
81	57	80	0	0	0
82	58	61	0	0	0
83	59	61	1	1	0
84	61	62	0	0	0
85	61	63	0	0	0
86	64	65	0	0	0
87	64	66	0	0	0
88	67	68	0	0	0
89	68	69	2	2	0
90	69	77	3	0	0
91	69	78	3	0	0
92	69	79	5	0	0

Continued on next page

Table A.1 – *Continued from previous page*

Contingency ID	From Bus	To Bus	No. of violations in base case	No. of violations after MCDO	Is included in cluster
93	70	149	2	0	0
94	70	149	2	0	0
95	71	85	0	0	0
96	71	150	1	0	0
97	74	119	13	0	2
98	75	128	38	0	1
99	78	79	9	4	2
100	78	80	2	0	0
101	82	83	0	0	0
102	84	93	0	0	0
103	85	86	0	0	0
104	86	87	2	2	0
105	86	88	2	2	0
106	88	96	5	3	0
107	88	106	10	9	2
108	89	90	1	0	0
109	90	96	0	0	0
110	91	92	1	1	0
111	91	93	1	1	0
112	91	94	1	1	0
113	92	102	0	0	0
114	94	103	1	1	0
115	94	107	2	1	0
116	95	96	1	1	0
117	95	97	1	1	0

Continued on next page

Table A.1 – *Continued from previous page*

Contingency ID	From Bus	To Bus	No. of violations in base case	No. of violations after MCDO	Is included in cluster
118	95	98	1	1	0
119	96	100	2	2	0
120	98	105	1	1	0
121	100	104	0	0	0
122	106	107	8	5	2
123	107	122	3	3	0
124	109	119	19	1	2
125	109	124	15	1	2
126	109	125	16	1	2
127	110	111	36	4	1
128	110	134	38	0	1
129	110	141	42	0	1
130	111	115	2	2	0
131	112	120	48	12	1
132	115	117	11	2	2
133	116	117	17	2	2
134	116	147	16	2	2
135	117	147	14	2	2
136	120	128	41	0	1
137	120	129	40	0	1
138	122	123	1	0	0
139	135	138	6	0	0
140	138	139	14	0	1
141	138	140	12	0	1
142	138	145	13	0	1

Continued on next page

Table A.1 – *Continued from previous page*

Contingency ID	From Bus	To Bus	No. of violations in base case	No. of violations after MCDO	Is included in cluster
143	142	143	4	0	0
144	142	146	3	0	0
145	149	150	17	3	0
146	149	151	3	0	0
147	149	152	3	0	0
148	151	161	0	0	0
149	153	154	0	0	0
150	153	155	0	0	0
151	154	156	0	0	0
152	154	160	0	0	0
153	155	156	0	0	0
154	156	157	0	0	0
155	157	158	0	0	0
156	158	159	0	0	0
157	159	160	0	0	0
158	161	162	0	0	0
159	2	1	0	0	0
160	3	1	0	0	0
161	4	1	23	3	2
162	5	1	42	0	1
163	7	2	0	0	0
164	13	2	0	0	0
165	112	4	42	0	1
166	119	4	26	5	2
167	120	5	42	0	1

Continued on next page

Table A.1 – *Continued from previous page*

Contingency ID	From Bus	To Bus	No. of violations in base case	No. of violations after MCDO	Is included in cluster
168	129	5	38	0	1
169	9	7	6	0	0
170	75	9	38	0	1
171	11	10	1	1	0
172	15	11	0	0	0
173	46	11	8	8	2
174	58	11	0	0	0
175	59	11	4	4	0
176	58	15	0	0	0
177	18	16	3	3	0
178	18	17	3	3	0
179	30	18	5	5	0
180	32	18	5	5	0
181	38	19	0	0	0
182	157	20	0	0	0
183	22	21	0	0	0
184	38	22	0	0	0
185	40	22	0	0	0
186	41	22	0	0	0
187	24	23	0	0	0
188	28	24	1	1	0
189	45	24	0	0	0
190	26	25	120	0	2
191	27	25	0	0	0
192	74	26	32	0	2

Continued on next page

Table A.1 – *Continued from previous page*

Contingency ID	From Bus	To Bus	No. of violations in base case	No. of violations after MCDO	Is included in cluster
193	75	26	38	0	1
194	29	28	2	2	0
195	30	29	5	5	0
196	31	29	0	0	0
197	32	30	2	2	0
198	33	32	2	2	0
199	34	33	0	0	0
200	35	33	0	0	0
201	36	33	0	0	0
202	40	34	0	0	0
203	77	34	0	0	0
204	40	35	0	0	0
205	67	36	0	0	0
206	39	37	4	4	0
207	126	37	6	6	0
208	127	37	0	0	0
209	42	39	1	1	0
210	81	40	0	0	0
211	82	40	0	0	0
212	81	41	0	0	0
213	83	41	0	0	0
214	84	41	0	0	0
215	109	42	15	1	2
216	44	43	0	0	0
217	102	44	0	0	0

Continued on next page

Table A.1 – *Continued from previous page*

Contingency ID	From Bus	To Bus	No. of violations in base case	No. of violations after MCDO	Is included in cluster
218	103	44	1	1	0
219	54	45	0	0	0
220	47	46	0	0	0
221	48	47	4	0	0
222	49	47	0	0	0
223	51	48	5	0	0
224	52	48	13	5	2
225	87	49	0	0	0
226	51	50	6	0	0
227	141	51	6	0	0
228	79	52	12	0	2
229	106	52	13	10	2
230	116	52	17	3	2
231	117	52	14	3	2
232	54	53	0	0	0
233	55	53	0	0	0
234	56	54	0	0	0
235	57	55	0	0	0
236	149	55	3	0	0
237	162	55	0	0	0
238	67	56	0	0	0
239	80	57	0	0	0
240	61	58	0	0	0
241	61	59	0	0	0
242	62	61	0	0	0

Continued on next page

Table A.1 – *Continued from previous page*

Contingency ID	From Bus	To Bus	No. of violations in base case	No. of violations after MCDO	Is included in cluster
243	63	61	0	0	0
244	65	64	0	0	0
245	66	64	0	0	0
246	68	67	0	0	0
247	69	68	7	3	2
248	77	69	0	0	0
249	78	69	3	0	0
250	79	69	16	0	2
251	149	70	3	0	0
252	149	70	3	0	0
253	85	71	0	0	0
254	150	71	1	0	0
255	119	74	19	4	2
256	128	75	42	0	1
257	79	78	19	0	2
258	80	78	0	0	0
259	83	82	0	0	0
260	93	84	1	1	0
261	86	85	2	2	0
262	87	86	0	0	0
263	88	86	5	2	0
264	96	88	2	2	0
265	106	88	14	9	2
266	90	89	1	0	0
267	96	90	2	2	0

Continued on next page

Table A.1 – *Continued from previous page*

Contingency ID	From Bus	To Bus	No. of violations in base case	No. of violations after MCDO	Is included in cluster
268	92	91	0	0	0
269	93	91	1	1	0
270	94	91	1	1	0
271	102	92	0	0	0
272	103	94	1	1	0
273	107	94	5	5	0
274	96	95	2	2	0
275	97	95	0	0	0
276	98	95	1	1	0
277	100	96	0	0	0
278	105	98	0	0	0
279	104	100	0	0	0
280	107	106	4	4	0
281	122	107	2	2	0
282	119	109	27	5	2
283	124	109	4	1	0
284	125	109	1	1	0
285	111	110	2	2	0
286	134	110	27	0	1
287	141	110	13	0	2
288	115	111	14	3	2
289	120	112	48	0	1
290	117	115	11	2	2
291	117	116	14	2	2
292	147	116	12	0	2

Continued on next page

Table A.1 – *Continued from previous page*

Contingency ID	From Bus	To Bus	No. of violations in base case	No. of violations after MCDO	Is included in cluster
293	147	117	12	0	2
294	128	120	39	0	1
295	129	120	38	0	1
296	123	122	0	0	0
297	138	135	12	0	1
298	139	138	7	0	0
299	140	138	6	0	0
300	145	138	6	0	0
301	143	142	5	0	0
302	146	142	4	0	0
303	150	149	2	2	0
304	151	149	0	0	0
305	152	149	0	0	0
306	161	151	0	0	0
307	154	153	0	0	0
308	155	153	0	0	0
309	156	154	0	0	0
310	160	154	0	0	0
311	156	155	0	0	0
312	157	156	0	0	0
313	158	157	0	0	0
314	159	158	0	0	0
315	160	159	0	0	0
316	162	161	0	0	0

APPENDIX B. SAMPLE COMPOSITE LOAD DYNAMIC DATA

```
3 'USRLOD'  *  'CMLDZNU1'        12    3    0  132   27  146   48

   100.00       0.0000       0.0000      0.50000E-01   0.0000
  0.10000       1.0000       1.0000       0.0000       0.90000
   1.1000      0.63000E-02   1.0200       1.0400        30.000
   5.0000      0.10000E-01   0.11000      0.72000E-01   0.23000
   0.0000      0.35000       0.0000       0.95000       0.0000
   0.0000      0.97980       1.0000       1.0000        2.0000
   0.0000       0.0000       1.0000       0.0000        2.0000
   0.0000       0.0000

   3.0000      0.80000      0.35000E-01   2.8940       0.24800
  0.24800      0.16370      0.16370       1.5000        1.0000
   0.0000       999.00       0.0000       999.00        999.00
   9999.0       9999.0       0.0000       9999.0        9999.0

   3.0000      0.80000      0.35000E-01   2.8940       0.24800
  0.24800      0.16370      0.16370      0.11000        1.0000
   0.0000       999.00       0.0000       999.00        999.00
   9999.0       9999.0       0.0000       9999.0        9999.0

   3.0000       0.0000      -1.0000      -1.0000       -1.0000
  -1.0000      -1.0000      -1.0000      -1.0000       -1.0000
```

```
-1.0000      -1.0000      -1.0000      -1.0000      -1.0000
-1.0000      -1.0000      -1.0000      -1.0000      -1.0000
0.33000E-01   0.60000      0.20000E-01   0.50000E-01
 1.0000       0.97000      0.60000       0.12400
0.11400        0.0000       0.0000        1.0000
 6.0000        2.0000       12.000        3.2000
 11.000        2.5000       0.86000       0.80000
0.70000        1.0000       -3.3000       0.50000
0.40000        0.60000      0.50000        20.000
0.70000        1.3000       0.0000        0.80000
0.20000        0.90000       5.0000      /
```

BIBLIOGRAPHY

[1] P. Kundur, J. Paserba, V. Ajjarapu, G. Andersson, A. Bose, C. Canizares, N. Hatziargyriou, D. Hill, A. Stankovic, C. Taylor, T. Van Cutsem, and V. Vittal, "Definition and classification of power system stability ieee/cigre joint task force on stability terms and definitions," *Power Systems, IEEE Transactions on*, vol. 19, no. 3, pp. 1387–1401, 2004.

[2] N. T. I. Subcommittee, S. Protection, and C. Subcommittee, "A technical reference paper fault-induced delayed voltage recovery," NERC, Tech. Rep., June 2009.

[3] Richard Bravo, Robert Yinger, Dave Chassin, Henry Huang, Ning Lu,Ian Hiskens, Giri Venkataramanan, "Load modeling transmission research," CIEE, Tech. Rep., March 2010.

[4] *Siemens PTI Power Technologies Inc., PSS/E 33, Program Application Guide, Vol. II, May 2011.*

[5] D. Shoup, J. Paserba, and C. Taylor, "A survey of current practices for transient voltage dip/sag criteria related to power system stability," in *Power Systems Conference and Exposition, 2004. IEEE PES*, oct. 2004, pp. 1140 – 1147 vol.2.

[6] Modeling and validation work group, "White paper on modeling and studying FIDVR events," Western Electricity Coordinating Council, Tech. Rep., October 20, 2011.

[7] N. Lu, B. Yang, Z. Huang, and R. Bravo, "The system impact of air conditioner undervoltage protection schemes," in *Power Systems Conference and Exposition, 2009. PSCE '09. IEEE/PES*, march 2009, pp. 1 –8.

[8] J. Shaffer, "Air conditioner response to transmission faults," *Power Systems, IEEE Transactions on*, vol. 12, no. 2, pp. 614 –621, may 1997.

[9] B. Williams, W. Schmus, and D. Dawson, "Transmission voltage recovery delayed by stalled air conditioner compressors," *Power Systems, IEEE Transactions on*, vol. 7, no. 3, pp. 1173 –1181, aug 1992.

[10] L. Taylor and S.-M. Hsu, "Transmission voltage recovery following a fault event in the metro atlanta area," in *Power Engineering Society Summer Meeting, 2000. IEEE*, vol. 1, 2000, pp. 537 –542 vol. 1.

[11] M. Glavic, D. Novosel, E. Heredia, D. Kosterev, A. Salazar, F. Habibi-Ashrafi, and M. Donnelly, "See it fast to keep calm: Real-time voltage control under stressed conditions," *IEEE Power and Energy Magazine*, vol. 10, no. 4, pp. 43–55, 2012.

[12] DOE, "DOE - NERC FIDVR Workshop," [Online]:http://www.nerc.com/files/FIDVR-Conference-Presentations-4-22-08.pdf, April 22 2008.

[13] ——, "DOE-NERC FIDVR Conference," [Online]:http://www.nerc.com/files/FIDVR-Conference-Presentations-9-29-09.pdf, September, 29 2009.

[14] H. Wu and I. Dobson, "Cascading stall of many induction motors in a simple system," *Power Systems, IEEE Transactions on*, vol. 27, no. 4, pp. 2116–2126, Nov 2012.

[15] ——, "Analysis of induction motor cascading stall in a simple system based on the cascade model," *Power Systems, IEEE Transactions on*, vol. 28, no. 3, pp. 3184–3193, Aug 2013.

[16] S. Halpin, K. Harley, R. Jones, and L. Taylor, "Slope-permissive under-voltage load shed relay for delayed voltage recovery mitigation," *Power Systems, IEEE Transactions on*, vol. 23, no. 3, pp. 1211 –1216, aug. 2008.

[17] H. Bai and V. Ajjarapu, "A novel online load shedding strategy for mitigating fault-induced delayed voltage recovery," *Power Systems, IEEE Transactions on*, vol. 26, no. 1, pp. 294 –304, feb. 2011.

[18] S. Halpin, R. A. Jones, and L. Taylor, "The mva-volt index: A screening tool for predicting fault-induced low voltage problems on bulk transmission systems," *Power Systems, IEEE Transactions on*, vol. 23, no. 3, pp. 1205–1210, 2008.

[19] ABB, "Ercot crez reactive power compensation study," FACTS Seminar Presentations, St.Paul Minnesota, March 28 2012.

[20] P. Pourbeik, R. Koessler, W. Quaintance, and W. Wong, "Performing comprehensive voltage stability studies for the determination of optimal location, size and type of reactive compensation," in *Power Engineering Society General Meeting, 2006. IEEE*, 0-0 2006, p. 6 pp.

[21] P. Pourbeik, R. Koessler, and B. Ray, "Addressing voltage stability related reliability challenges of san francisco bay area with a comprehensive reactive analysis," in *Power Engineering Society General Meeting, 2003, IEEE*, vol. 4, 2003, pp. –2639 Vol. 4.

[22] V. Kolluri and S. Mandal, "Determining reactive power requirements in the southern part of the entergy system for improving voltage security - a case study," in *Power Systems Conference and Exposition, 2006. PSCE '06. 2006 IEEE PES*, 2006, pp. 119–123.

[23] A. Meliopoulos, G. Cokkinides, and G. Stefopoulos, "Voltage stability and voltage recovery: Load dynamics and dynamic var sources," in *Power Systems Conference and Exposition, 2006. PSCE '06. 2006 IEEE PES*, 29 2006-nov. 1 2006, pp. 124 –131.

[24] V. Krishnan, H. Liu, and J. McCalley, "Coordinated reactive power planning against power system voltage instability," in *Power Systems Conference and Exposition, 2009. PSCE '09. IEEE/PES*, march 2009, pp. 1 –8.

[25] B. Sapkota and V. Vittal, "Dynamic var planning in a large power system using trajectory sensitivities," *Power Systems, IEEE Transactions on*, vol. 25, no. 1, pp. 461 –469, feb. 2010.

[26] A. Tiwari and V. Ajjarapu, "Optimal allocation of dynamic var support using mixed integer dynamic optimization," *Power Systems, IEEE Transactions on*, vol. 26, no. 1, pp. 305 –314, feb. 2011.

[27] B. Chachuat, A. B. Singer, and P. I. Barton, "Global mixed-integer dynamic optimization," *AIChE Journal*, vol. 51, no. 8, pp. 2235–2253, 2005. [Online]. Available: http://dx.doi.org/10.1002/aic.10494

[28] D. E.Kirk, *Optimal control theory :an introduction.* Englewood Cliffs, New Jersey: Prentice Hall, 1970.

[29] L. T. Biegler and I. E. Grossmann, "Retrospective on optimization," *Computers and Chemical Engineering*, vol. 28, pp. 1169–1192, 2004.

[30] *GE Positive Sequence Load Flow, User Manual Version 18.0, April 2011.*

[31] J. Kueck, "Voltage influence on typical protection and ccontrol for motors, power electronics and other common loads," Western Electricity Coordinating Council, Tech. Rep., February 11, 2011.

[32] J. R. H. Byrd and R. Waltz, "Knitro: An integrated package for nonlinear optimization," in *Large Scale Nonlinear Optimization*, G. di Pillo and M.Roma, Eds. Springer -Verlag, 2006, pp. 35–39.

[33] *KNITRO User Manual. [Online] Available:http:// www.ziena.com/ documentation.htm.*

[34] A. Michel, A. Fouad, and V. Vittal, "Power system transient stability using individual machine energy functions," *IEEE Transactions on Circuits and Systems*, vol. 30, no. 5, pp. 266 – 276, 1983.

[35] A. Darvishi, I. Dobson, A. Oi, and C. Nakazawa, "Threshold-based monitoring of multiple outages with pmu measurements of area angle," *Power Systems, IEEE Transactions on*, vol. 99, no. 4, pp. 1–9, 2015.

[36] ——, "Area angles monitor area stress by responding to line outages," in *North American Power Symposium (NAPS), 2013*, Sept 2013, pp. 1–6.

[37] T. M. Cover and J. A. Thomas, *Elements of Information Theory.* New York: Springer, 1991.

[38] A. M. Kowalski, M. T. Martin, A. Plastino, and G. Judge, "On extracting probability distribution information from time series," *Entropy*, vol. 14, no. 10, pp. 1829–1841, 2012. [Online]. Available: http://www.mdpi.com/1099-4300/14/10/1829

[39] A. Katok and B. Hasselblatt, *Introduction to the modern theory of dynamical systems*, ser. Texts and Monographs in Physics. Berlin: Springer, 1999.

[40] G. Gallavotti, *Statistical mechanics : a short treatise*, ser. Encyclopaedia of mathematics and its applications. Cambridge: Cambridge Univ. Press, 1995.

[41] U. Luxburg, "A tutorial on spectral clustering," *Statistics and Computing*, vol. 17, no. 4, pp. 395–416, Dec. 2007. [Online]. Available: http://dx.doi.org/10.1007/s11222-007-9033-z

[42] M. Meila, "Comparing clusterings by the variation of information," in *Learning Theory and Kernel Machines*, 2003, pp. 173–187. [Online]. Available: http://www.springerlink.com/content/rdda4r5bm9ajlbw3

[43] W. L. Martinez and A. R. Martinez, *Exploratory Data Analysis with MATLAB*. Chapman & Hall/CRC, 2004.

[44] L. Kaufman and P. J. Rousseeuw, *Frontmatter*. John Wiley & Sons, Inc., 2008.

[45] K. Morison, X. Wang, A. Moshref, and A. Edris, "Identification of voltage control areas and reactive power reserve; an advancement in on-line voltage security assessment," in *Power and Energy Society General Meeting - Conversion and Delivery of Electrical Energy in the 21st Century, 2008 IEEE*, 2008, pp. 1–7.

[46] R. H. Byrd, M. E. Hribar, and J. Nocedal, "An interior point algorithm for large scale nonlinear programming," *SIAM Journal on Optimization*, vol. 9, pp. 877–900, 1997.